

https://dspace.org/

Silica and maghemite nanoparticles for the remediation of acid mine drainage-contaminated waters and Nanoparticle modification of metal uptake by a freshwater alga-Scenedesmus sp

Etale, Anita

2015-01-30
http://hdl.handle.net/10539/16817

Downloaded from a DSpace repository. https://dspace.org/

Silica and Maghemite Nanoparticles for the Remediation of Acid Mine Drainage-Contaminated Waters and Nanoparticle Modification of Metal Uptake by a Freshwater Alga - *Scenedesmus sp.*



by

Anita Etale

A thesis submitted to the Faculty of Science in fulfilment of the requirements for the degree of Doctor of Philosophy

September 2014, Johannesburg

DECLARATION

I declare that this thesis is my own unaided work. It is being submitted for the Degree of Doctor of Philosophy at the University of the Witwatersrand, Johannesburg. It has not been submitted before for any degree or examination to any other university.



Ms Anita Etale

This 16th day of September 2014 in Johannesburg

This thesis is submitted after examination and approval by the following supervisors:

Prof. Deanne Drake

School of Animal Plant and Environmental Sciences, University of the Witwatersrand, Johannesburg

Dr. Hlanganani Tutu

Molecular Sciences Institute, School of Chemistry, University of the Witwatersrand, Johannesburg

ABSTRACT

Aims: The adsorptive removal of Cu, Mn, Hg and U by silica and maghemite nanoparticles (NPs) under acid mine drainage (AMD) conditions was investigated with the aim of assessing the applicability of NPs for remediation of AMD-contaminated water. The effect of NPs on metal uptake by algae, an increasingly popular remediation alternative, was also investigated.

Methods: NP and algal metal removal were quantified by batch experiments using commercially prepared, bare and amine-functionalised silica-carbon hybrid NPs characterised for size, surface area, porosity, crystallinity, elemental composition and hydrodynamic size. Metal uptake by algae was quantified in the presence and absence of NPs.

Results: Silica and maghemite NPs can be used for the adsorptive removal of Cu, Mn, Hg and U from AMD-contaminated surface and ground water. NP metal uptake was rapid and equilibria were attained within 5 minutes with silica and maghemite NPs, and within 45 minutes with amine-functionalised hybrid NPs. Adsorption efficiencies for Cu, Mn, Hg and U at pH 3 were 52, 56, 56 and 49%, respectively with silica and 56, 52, 75 and 50%, respectively, with maghemite NPs. Metal removal was enhanced by >10% in solutions containing ferric, manganese or sulphate ions, although Cu removal was inhibited in solutions with a >1 Mn:Cu ratio. Despite the presence of high affinity amine groups in hybrid NPs, Cu removal was only 52% due to the low surface area of the adsorbent. The comparative study with Hg, however, showed that surface area was not the only determinant of adsorption efficiency: maghemite NPs with a specific surface area ~15 times less than silica adsorbed 21% more Hg.

Metal removal by *Scenedesmus sp.* was enhanced by 12-27% in solutions containing NPs due to the greater sorption surface areas. NPs also modified metal partitioning in algal cells: intracellular concentrations were lower and extracellular concentrations higher in solutions containing NPs relative to controls (no NPs).

Conclusion: Silica and maghemite NPs can be applied for the adsorptive removal of Cu, Mn, Hg and U from AMD-contaminated water and to improve the efficiency of phycoremediation by *Scenedesmus sp*. These findings also point to the possibility of retardation of metals by NPs during their transportation from tailings and contaminated sites. Their partitioning to NPs and the strength of the interactions thereof can determine the prevalence of the metals in solution or in the solid phase.

ACKNOWLEDGEMENTS

This work would not have been possible without the support of many people. I would first like to thank my supervisors, Prof. Deanne Drake and Dr. Hlanganani Tutu who gave me the opportunity to conduct this research. Their guidance and encouragement has been unfailing during these last three years. I am also thankful to Prof. Stuart Sym and Dr. Sashnee Raja for accepting to be on my committee. Prof. Sym also provided the algal starter culture and allowed me to use his culturing facility without which part of this work would not have been possible. Prof. Kevin Balkwill's insights during the writing workshops and his support and encouragement all these years have made my experience at the School of APES fulfilling.

Gratitude also goes to Jacques Gerber for the hours spent teaching me how to align the transmission and scanning electron microscopes and to my mates in the lab, the office and at the schools of APES and Chemistry who have been immensely helpful. Kirsten Olsen's help with field sampling, Wendy Foden for always reminding me to take a break and Kathleen Smart and Tammy van Tonder for more kindness than words can tell. Thanks also Sipho Mhlambi for work on identifying the algal species, Hlonipani Mthunzi for help with statistical analyses and Bongani Yalala for mercury analyses.

Support from family and friends has been immense – from my husband who literally put his life on hold to support me, to friends and family members who tried not to feel ignored by me. I am forever indebted to you all; I hope we can now make up for lost time. Finally, special thanks go to the Global Change and Sustainability Research Institute (GCSRI) for financial support and to Prof. Barend Erasmus for his encouragement.

"When I finally arrived at the top, I saw that there was another mountain to climb. That's how life is, once the first goal is achieved, you see better your next adventure."

(*Amelie Whissell*)

CONTENTS

DECLARATION i

ABSTRACT ii

ACKNOWLEDGEMENTS iii

1 Introduction 1

1.1 The formation of acid mine drainage 2

1.2 Ecological impacts of AMD 3

1.3 Rationale for the study 4

1.4 Techniques for the remediation of metal-contaminated water 4

1.5 Nanoparticles for pollution remediation 6

1.6 Research aims and objectives 7

1.7 References 9

2 Application of maghemite nanoparticles as sorbents for the removal of Cu(II), Mn(II) and U(VI) ions from aqueous solution in acid mine drainage conditions 16

3 Mesoporous silica nanoparticles for the adsorptive removal of Cu(II), Mn(II) and U(VI) from acid mine drainage 28

3.1 Introduction 29

3.2 Experimental 30

3.2.1 Adsorbent characterisation 30
3.2.2 Adsorption studies 30
3.2.3 Data analysis 31
Kinetics 31
Isotherms 31
Thermodynamics 32

3.3 Results and discussion 33

3.3.1 Particle characterisation 33
3.3.2 Effect of adsorbent concentration 34
3.3.3 Effect of contact time 35
3.3.4 Effect of initial metal concentrations 37
3.3.5 Effects of Fe^{3+}, Mn^{2+} and SO_4^{2-} ions 38

3.3.6 Effect of pH 40
3.3.7 Effect of temperature 41
3.3.8 Adsorption mechanism 41
3.3.9 Application studies 42
3.4 Conclusions 44

3.5 Acknowledgements 44

3.6 References 45

3.7 Supplementary Information 49

4 Adsorptive removal of mercury from acid mine drainage: A comparison of silica and maghemite nanoparticles 50

4.1 Introduction 51

4.2 Materials and methods 52

4.2.1 Materials 52
4.2.2 Adsorbent characterisation 52
4.2.3 Adsorption studies 52
Application to contaminated surface and ground water 53
4.2.4 Data analyses 53
Kinetics 53
Isotherms 54
Evaluation of adsorbent efficiency 54
Statistical analyses 55
4.3 Results and discussion 55

4.3.1 Adsorbent characterization 55
4.3.2 Adsorption kinetics 57
4.3.3 Effect of pH 59
4.3.4 Effect of sulphate and manganese ions 60
4.3.5 Effect of adsorbent concentration 61
4.3.6 Adsorption isotherms 62
4.3.7 Comparison of NP efficiency 63
4.3.8 Hg adsorption from AMD-contaminated water 64
4.4 Conclusions 65

4.5 Acknowledgements 66

4.6 References 67

4.7 Supplementary information 71

5 Synthesis, characterisation and application of amine functionalised silica-carbon hybrid nanoparticles for the adsorptive removal of Cu(II) from acidic solutions ... 72

5.1 Introduction ... 73

5.2 Materials and methods ... 74

5.2.1 Materials ... 74
5.2.2 Synthesis of amine-functionalized silica-carbon nanoparticle adsorbents ... 74
5.2.3 Characterisation of the adsorbent ... 75
5.2.4 Adsorption studies ... 75
5.2.5 Data analyses ... 76
Kinetics ... *76*
Isotherms ... *76*

5.3 Results and discussion ... 76

5.3.1 Adsorbent characterisation ... 76
5.3.2 Effect of adsorbent concentration ... 80
5.3.3 Effect of contact time ... 81
5.3.4 Effect of Cu concentration ... 81
5.3.5 Effect of pH ... 83
5.3.6 Selectivity ... 83
5.4 Conclusion ... 84

5.5 Acknowledgements ... 85

5.6 References ... 86

6 The effects of silica and maghemite nanoparticles on uptake of Cu(II), Mn(II) and U(VI) from aqueous solutions by a freshwater alga - *Scenedesmus sp.* ... 89

6.1 Introduction ... 90

6.2 Materials and methods ... 91

6.2.1 Materials ... 91
6.2.2 Algal culturing ... 91
6.2.3 Particle characterization ... 92
6.2.4 Metal uptake studies ... 92
Adsorption of Cu, Mn and U by silica and maghemite NPs ... *92*
Metal uptake by Scenedesmus sp. in the presence and absence of NPs ... *93*
Determination of extracellular and intracellular metal concentrations of Scenedesmus sp. ... *94*
6.2.5 Statistical analyses ... 94
6.3 Results ... 94

6.3.1 Particle characterization 94
6.3.2 NP metal adsorption 97
6.3.3 Modification of algal metal removal by NPs 99
Effect on total metal removal *99*
Effect of NPs on algal metal partitioning *101*
6.4 Conclusions 106
6.5 Acknowledgements 106
6.6 References 107
7 Summary and outlook 113
7.1 NP-metal interactions 113
7.2 The effect of NP functionalisation on adsorption efficiency 116
7.3 The effect of NPs on metal uptake by *Scenedesmus sp.* 117
7.4 Reference 117
8 Appendix 118

List of figures

Chapter 3

Figure 3.1: Transmission electron micrograph (a) and FTIR spectra (b) of silica NPs 34
Figure 3.2: The effect of adsorbent concentration on adsorption of Cu, Mn and U to silica NPs at pH 3 (±SD) 35
Figure 3.3: The effect of contact time on the adsorption of Cu, Mn and U by silica NPs (±SD) 36
Figure 3.4: The effect of initial metal concentration on adsorption of Cu (a), Mn (b) and U (c) (±SD) by silica NPs 37
Figure 3.5: The effect of Fe^{3+} (a), SO_4^{2-} (b) and Mn^{2+} (c) ions on the adsorption of Cu, Mn and U by silica NPs (±SD) at pH 3 39
Figure 3.6: The effect of pH on adsorption of Cu, Mn and U to silica NPs (±SD). 40
Figure 3.7: Intraparticle diffusion plot for adsorption of Cu to silica NPs at pH 3 42
Figure 3.8: Removal efficiencies of Cu and Mn from contaminated surface and groundwater by silica NPs. No readings were recorded for U due to below-detection concentrations in water samples 43

Chapter 4

Figure 4.1: Transmission electron micrographs of silica (a) and maghemite (b) NPs 56
Figure 4.2: Powder X-ray diffractograms of maghemite (a) and silica (b) NPs 57
Figure 4.3: The effect of time on adsorption of Hg to silica (a) and maghemite (b) NPs at pH 3. 58
Figure 4.4: The effect of pH on Hg adsorption by silica and maghemite NPs (±SD). Different letters indicate statistically significant differences in adsorption at different pH levels; lower case letters for silica and upper case letters for maghemite. * indicates significant differences in adsorption by NPs at a given pH ($p < 0.05$). 59
Figure 4.5: The effect of sulphates (a) and manganese ions (b) on adsorption of Hg by silica and maghemite NPs (±SD) at pH 3. Different letters indicate statistically significant differences in adsorption at different treatments; lower case letters for silica and upper case letters for maghemite. 60
Figure 4.6: The effect of adsorbent concentrations on Hg removal by silica and maghemite NPs (±SD) at pH 3. Different letters indicate statistical differences in adsorption at different NP concentrations; lower case letters for silica and upper case letters for maghemite. 62
Figure 4.7: The effect of initial Hg concentrations on adsorption efficiency of silica (a) and maghemite (b) NPs 62
Figure 4.8: Adsorption densities of Hg on silica (a) and maghemite (b) NPs at pH 3 64
Figure 4.9: Efficiency of Hg removal from AMD-contaminated surface and ground water by silica and maghemite NPs (±SD). Different letters indicate statistically significant differences in adsorption by silica and maghemite from the same water sample. 65

Chapter 5

Figure 5.1: TEM image of amine-functionalised silica-carbon hybrid NPs 78
Figure 5.2: Nitrogen adsorption-desorption isotherm for the NH-SC adsorbent. 79
Figure 5.3: FTIR spectra of parent silica NPs (a) and the NH-SC hybrid NPs (b) 80
Figure 5.4: The effect of adsorbent concentration on Cu uptake at pH 3. (Experimental conditions: adsorbent mass = 10 mg, contact time = 60 minutes; Cu concentration = 2 mg L^{-1}, sample volume = 10 mL, temperature = ~25°C.) 80
Figure 5.5: (a) The effect of contact time on the uptake of Cu ions by NH-SC hybrid NPs (± SD), and (b) the pseudo-second-order plot for the adsorption. (Adsorbent concentration = 10 mg, Cu concentration = 2 mg L^{-1}, volume of Cu solution = 10 mL, solution pH = 3). 81

Figure 5.6: (a) The effect of metal concentration on adsorption efficiency of NH-SC hybrid NPs and (b) the linearised Freundlich-model plot of adsorption data. (Adsorbent concentration = 10 mg, Cu solution = 10 mL of 2 mg L^{-1}, solution pH =3). 82
Figure 5.7: The effect of pH in Cu adsorption by NH-SC hybrid NPs. (Adsorbent concentration = 10 mg, Cu concentration = 2 mg L^{-1}, volume of Cu solution = 10 mL). 83
Figure 5.8: The effect of competing ions on Cu adsorption by NH-SC hybrid NPs at pH 3. 84

Chapter 6

Figure 6.1: Transmission electron micrographs of silica (a) and maghemite (b) NPs 95
Figure 6.2: Silica and maghemite particle size in the absence of metal ions and in the presence of various concentrations of Cu, Mn and U. to values correspond to aggregate diameters immediately NPs were added to metal solutions, and t4 to diameters after 4 hours. Initial NP concentrations were 3 mg/L and data are mean ± standard deviation (n = 3). Different letters above columns within a concentration indicate statistically significant differences (p <0.05) in the mean hydrodynamic size of NP agglomerates within that particular concentration. 96
Figure 6.3: Adsorption kinetics of Mn (a), Cu (b) and U (c) to silica (A) and maghemite (B) nanoparticles at pH 6.5. Data are mean ± standard deviation (n = 2). 98
Figure 6.4: Removal of Cu (A), Mn (B) and U (C) by *Scenedesmus sp.* in the presence and absence of silica and maghemite NPs after 4 hours. Data are mean ± standard deviation (n = 3). Different letters above columns within a concentration indicate statistically significant differences (p <0.05) in the means of total algal metal content as a result of the different treatments. 101
Figure 6.5: Extracellular (i) and intracellular (ii) concentrations of Cu (A), Mn (B) and U (C) of *Scenedesmus sp.* cells in the presence and absence of silica and maghemite NPs. Legends in (i) are for both graphs in the set and data are mean ± standard deviation (n = 3). Different letters above columns within a concentration indicate statistically significant differences (p <0.05) in the means of intracellular or extracellular metal concentrations of algal cells. 105

List of tables

Chapter 1

Table 1.1: Global inputs of selected trace elements into aquatic ecosystems (thousand tonnes per annum) [a] 1

Chapter 3

Table 3.1: Adsorption rate constants and coefficients of correlation (R^2) for kinetics models fitted to adsorption data.....48

Table 3.2: Parameters of adsorption isotherms fitted to adsorption data.....49

Table 3.3: Thermodynamic parameters for the adsorption of Cu, Mn and U to silica NPs.....52

Table 3.4: Physico-chemical characteristics of contaminated water used in application studies..54

Chapter 4

Table 4.1: Parameters of kinetics models fitted to adsorption data.....69

Table 4.2: Isotherm parameters for the adsorption of Hg to silica and maghemite NPs at pH 3 (±0.1) and 25°C.....74

Table 4.3: Characteristics of AMD-contaminated surface and ground water.....75

Chapter 5

Table 5.1: Physical properties of silica, oxidised silica-carbon composites and aminated silica-carbon composites.....89

Table 5.2: Distribution coefficients Cu and other tested metals on the NH-SC adsorbent.....94

Chapter 6

Table 6.1: Structural properties of silica and maghemite NPs as determined by N_2sorption experiments.....105

Table 6.2: Kinetic and isotherm parameters obtained after fitting adsorption data to the pseudo-second order kinetics model and the Freundlich isotherm model.....109

Nomenclature

AMD – Acid Mine Drainage

BET – Brunauer-Emmett-Teller

CVAAS - Cold Vapour Atomic Absorption Spectroscopy

EC - Electrical Conductivity

FTIR – Fourier Transform Infrared Spectroscopy

GW – Ground Water

ICP-OES – Inductively Coupled Plasma - Optical Emission Spectroscopy

JCPDS - Joint Committee on Powder Diffraction Standards

NH-SC – amine-functionalised Silica-Carbon hybrid nanoparticles

NPs – Nanoparticles

Pers. obs. – Personal observation

pH_{PZC} – pH Point of Zero Charge

PRBs – Permeable Reactive Barriers

SC – Silica-Carbon hybrid nanoparticles

SD – Standard Deviation

SW – Surface Water

TEM – Transmission Electron Microscopy

XRD – X-ray Diffraction

1 Introduction

Industrialization and rapid technological advances since the turn of the last century have greatly increased the exploitation and consumption of metals on a global scale. The seminal works by Nriagu and Pacyna (1988) and Nriagu (1989) revealed the extent of biospheric metal contamination by anthropogenic activities including mining, energy production, manufacturing, and agriculture since the 1930s. These studies which reported 114-, 18-, 5- and 35-fold increases in the production of Al, Cr, Cu and Ni, respectively between 1930 and 1985, also revealed that mining and industrial processes accounted for most of the metal contamination in aquatic ecosystems (Table 1.1). No doubt these figures are much higher and aquatic metal contamination more serious ~30 years on, as has been reported by a number of more recent studies (Boult et al., 1994; Banks et al., 1997; Malm et al., 1995; España et al., 2005; Nieto et al., 2007).

Table 1.1: Global inputs of selected trace elements into aquatic ecosystems (thousand tonnes per annum) [a].

Source	As	Cd	Cu	Cr	Hg	Mn	Ni	Pb	Zn
Domestic wastewater	9.2	1.7	28	46	0.3	110	62	6.8	48
Electric power plants	8.2	0.12	13	5.7	1.8	11	11	0.72	18
Base metal mining and smelting	7.4	2.0	14	12	0.1	40	13	7.0	29
Manufacturing processes	7.0	2.4	34	51	2.1	21	7.4	14	85
Atmospheric fallout	5.6	2.2	11	9.1	2.0	12	10	100	40
Sewage discharges	4.1	0.69	12	19	0.16	69	11	9.4	17
Total	**42**	**9.1**	**112**	**143**	**6.5**	**263**	**114**	**138**	**237**

[a] Source: Nriagu & Pacyna 1988 (Reprinted by permission of Taylor & Francis LLC).

In fact, the extraction of precious and base metals from ores has been the mainstay of economies for millennia. There is evidence, for example, of copper mining in Cyprus from as early as 4000 BC and from the Rio Tinto deposits from 1200-500 BC (Leblanc, 2000). Records also describe the trade of Hg from the vast cinnabar reserves of Almadén in present day Spain by the Phoenicians and Carthagians from 2700 BC (Malm, 1998). Importantly, even in those early days, the negative effects of mining and metals to the environment, humans and animals were recognized. Dioscorides, the Greek physician (40 - 90 AD) remarked that lead, which was so extensively used in Roman aqueducts, "*makes the mind give way*" and Pliny, in his *Natural*

History observed that "*the exhalations of silver mines are dangerous to all animals, but to dogs more particularly*" (Nriagu, 1990).

Present day metal mining occurs on all continents except Antarctica, with reports of its negative impacts on water resources, aquatic organisms and humans emerging from regions as diverse as the Iberian Pyrite Belt of Spain and Portugal (Nieto et al., 2007), the Amazon (Malm et al., 1995), New Zealand (Bray et al., 2008) and Australia (Hogsden & Harding, 2012). In South Africa, gold mining in the Witwatersrand Basin of Johannesburg since 1886 has resulted in considerable contamination of water resources (Naicker et al., 2003; McCarthy, 2011; Tutu et al., 2008). Tailings dumps, which have been a feature of the landscape since mining began, recharge both ground water aquifers and surface water bodies with acidic, metal-contaminated water. Indeed the generation of acid mine drainage (AMD) is now a national concern, eliciting the action of various government and non-governmental institutions (Ramontja et al., 2010).

1.1 The formation of acid mine drainage

Acid mine drainage is formed via a cascade of reactions (Equations 1-4), when ferrous sulphide phases like pyrite (and to a lesser extent pyrrhotite, arsenopyrite and chalcopyrite) are exposed to oxygenated water. In mine tailings, the process begins when rain water percolates through the finely divided tailings leading to the oxidation of pyrite to ferrous iron (Equation 1) and then to ferric iron (Equation 2). Ferric iron which is soluble below pH 3.5 then acts as an additional oxidizing agent for pyrite (Equation 3). These reactions are dependent on such factors as temperature, pH, Eh and pyrite grain size (Singer & Stumm, 1970; Bigham & Nordstrom, 2000). Microorganisms also play an important role in the generation of AMD. Below pH 3.5, reaction 2 is catalysed by chemoautotrophic bacteria like *Leptospirillum ferrooxidans* and *Thiobacillus ferrooxidans* (Rawlings et al., 1999).

$$FeS_2 + {}^{7}/_{2}O_2 + H_2O \rightarrow Fe^{2+} + 2SO_4^{2-} + 2H^+ \quad (1)$$

$$Fe^{2+} + {}^{1}/_{4}\,O_2 + H^+ \rightarrow Fe^{3+} + {}^{1}/_{2}H_2O \quad (2)$$

$$FeS_2 + Fe^{3+} + 12H_2O \rightarrow 12Fe^{2+} + 2SO_4^{2+} + 16H^+ \quad (3)$$

$$Fe^{3+} + 3H_2O \rightarrow Fe(OH)_3 + 3H^+ \quad (4)$$

Above pH 3.5 ferric iron precipitates as $Fe(OH)_3$ (Equation 4); a reaction apparently able to buffer the pH of AMD at 2.5-3.5 (España et al., 2005). This sustained acidity leads to the dissolution of ores that occur alongside pyrite hence the presence of other ions such as Ag, Au, Cd, Co, Mn, Ni, Hg, Mo, Se and Zn in mine drainage (McCarthy, 2011). The result is acidic

metal-laden water that percolates through the tailings heaps to recharge groundwater or emerge at the base of dumps into surface waters (Durand, 2012). Not all mine drainage is acidic though. In host rock with sufficient buffering capacity e.g. from silicate and carbonate minerals, the acid is neutralized and metal ion concentrations in such drainage tends to be lower, although that of sulphates remains high (Banks et al., 1997).

1.2 Ecological impacts of AMD

The mechanisms through which AMD affects the ecology of aquatic systems and species may be broadly classified as either chemical or physical, although both result in diminished ecological stability through species losses, impaired reproduction, decreased biodiversity, impaired ecosystem functioning and simplification of food webs (see review by Byrne et al. (2012). Niyogi et al. (2002), for instance, observed that the biodiversity of primary producers in AMD-receiving streams in the Rocky Mountains of Colorado decreased with increasing concentrations of Al, Fe and Zn. Other studies have also reported reduced populations of benthic invertebrates and fishes (Iwasaki et al., 2009; Greig et al., 2010).

The chemical impacts of AMD include increased acidity, destruction of bicarbonate buffering systems and increased concentrations of dissolved and particulate metals, while physical impacts include deposition of metal oxyhydroxides e.g. $Fe(OH)_3$, which destroys breeding and feeding grounds and smothers stream benthic life (Gray, 1997). All these factors compromise primary and secondary production, nutrient cycling and energy flows, reproduction and community structure, hence the low biodiversity of most AMD-impacted streams (Bray et al., 2008; Byrne et al., 2012).

High metal concentrations are also toxic to primarily terrestrial species including birds, animals and humans (Jackson et al., 2011; Georgopoulos et al., 2011). A number of human diseases including hypertension, Alzheimer's, psychiatric disorders (e.g. intelligence and mood impairments) and congenital birth defects have been linked to metal poisoning (Ekino et al., 2007; Houston, 2011; Yorifuji et al., 2011). Consequently, the WHO has set guidelines for the maximum acceptable concentrations of metals in drinking water (World Health Organization, 2011). However, although metal concentrations in AMD-impacted streams often surpass these standards, there have been reports, particularly in informal settlements and small holder farms, of the consumption AMD-contaminated water by humans and livestock (Lusilao-Makiese, 2012). The remediation of metal-contaminated water is therefore necessary in order to prevent the negative effects of excessive metal concentrations on ecological systems, humans and animals.

1.3 Rationale for the study

In the South African context, remediation of metal-contaminated water is also important because the country is classified as water-scarce, with most regions having a negative water balance i.e. evapotranspiration exceeds precipitation (McCarthy, 2011). Coupled with increasing demand from population growth, agriculture and industry, it is clear that the country's already over allocated water resources will come under significant pressure in future and additional sources will be required. Mine decant from the Witwatersrand goldfields is estimated at 350 ML/day, which is equivalent to 10% of the daily supply of potable water to urban areas in Gauteng (Manders et al., 2009). Treatment of mine drainage therefore presents an opportunity for augmenting current and future water supplies, and may in fact become absolutely essential. Separately, an understanding of NP-metal sequestration can give insights into mechanisms of pollutant retardation in contaminated environments and provide information for *in-situ* treatments techniques.

1.4 Techniques for the remediation of metal-contaminated water

A pump-and-treat facility valued at R 2.2 billion was recently installed in Germiston, Johannesburg, as a short-term measure for the remediation of AMD from the Central Rand (Kolver, 2014). It is expected that this facility will treat mine decant to a standard sufficient for it to be released into the Vaal River, meeting environmental standards set by the Department of Water Affairs and Sanitation (Department of Water Affairs and Forestry, 1996).

Several other techniques that may be classified broadly as either active or passive are also available (Johnson & Hallberg, 2005). Passive treatments, which hinge on raising the pH of AMD and thereby also decreasing bacterial activity, include the use of wetlands, limestone drains and permeable reactive barriers. In general, these options are cheaper than active treatment techniques. They can, however, be less effective in some cases e.g. the effectiveness of limestone as a buffer can be reduced due to "armouring" (the deposition of iron on limestone particles) or its dissolution (Evangelou, 1998).

Active treatment techniques may be biological or non-biological. Biological treatments comprise the use of algae, fungi and higher plants to take up metal ions from contaminated water (Das et al., 2009; Monteiro et al., 2012). Such bioremediation approaches exploit the fact that living organisms are able to sequester metal ions from soil, air or aqueous media in their roots, leaves and stems or cells (algae) (Padmavathiamma & Li, 2007). Higher plants exhibit different metal removal strategies that have been exploited in phytoremediation approaches. These include:

- stabilization – metal uptake and sequestration resulting in reduced bioavailability. This strategy was applied for the management of tailings in the Cartagena-La Union mining district of Spain using *Hyparrhenia hirta* and *Zygophyllum fabago* (Conesa et al., 2007);
- extraction (accumulation) – accumulation of metals in harvestable plant parts e.g. water lettuce (*Pistia stratoites*) (Odjegba & Fasidi, 2004)*;*
- filtration (rhizofiltration) – metal uptake from aqueous media by plant roots. Dushenkov et al. (1995) demonstrated the uptake of Cu, Cd, Cr, Ni, Pb and Zn using sunflower (*Helianthus annus*) and Indian mustard (*Brassica juncea* (L));
- volatilization - e.g. of selenium by *Brassica juncea* (L) (de Souza et al., 2000).

Algae, on the other hand, take up metal ions via sequestration to cell walls, phytochelatins and exopolymeric substances (EPS) produced in response to high metal concentrations (Pistocchi et al., 2000; Howe & Merchant, 1992; Pawlik-Skowrońska, 2001). The carboxyl, hydroxyl, phosphate, sulphydryl and amine functionalities of phytochelatins, EPS and algal cell walls carry net negative charges which confer cation affinity to algal cells. Algal metal binding involves both ionic and covalent bonding in a process that is characterised by an initial rapid stage of surface sequestration followed by slower intra-cellular transport by ion carriers such as cysteine (Crist et al., 1981; Robinson, 1989). Nevertheless, bioremediation has a number of disadvantages including difficulties with harvesting and safe disposal of metal-laden biomass and the fact that growing conditions for plants are not always met, which reduces the efficiency of techniques.

Non-biological active treatment methods include chemical treatment using lime (CaO), calcium carbonate, sodium carbonate and sodium hydroxide. These chemicals are applied to raise AMD pH and precipitate metal ions (Matlock et al., 2002). Other options, which may be classified as physicochemical techniques, include reverse osmosis, nanofiltration (Zhong et al., 2007), electrolysis (Cifuentes et al., 2009), ion exchange (Sprynskyy et al., 2010) and adsorption (Babel & Kurniawan, 2003). However, most of these have disadvantages such as high capital and maintenance costs, high energy consumption, production of large volumes of sludge and membrane failure due to coagulation (Kurniawan et al., 2006; Fu & Wang, 2011). As a result, adsorption is attracting increasing attention, especially for waters with low (ppm and ppb) metal concentrations. Adsorption processes are simple, cost less and can be employed with adsorbents as simple as agricultural wastes like rice husks and coconut coir (Feng et al. 2004; Anirudhan et al. 2008) or more efficient ones e.g. activated carbons (Mohan & Chander, 2001), ion exchangers like clinoptilolite (Cozmuta et al., 2012), zeolites (Moreno et al., 2001; Kosobucki et al., 2008), diatomite (Sprynskyy et al., 2010) and resins (Atia et al., 2008), fly ash (Wang & Wu, 2006) and nanoparticles (Hua et al., 2012).

1.5 Nanoparticles for pollution remediation

A good adsorbent is characterised by such properties as high sorption surface area, high sorption capacities, the ability to be dispersed in solution, stability over a wide pH range, affordability and in some cases, sorbate specificity. Many commonly used adsorbents have low adsorption capacities due to low surface areas, low reactivities and poor specificity for ions of interest. Nanoparticles (NPs), on the other hand, make good adsorbents due to their high specific surface areas and high reactivities (Waychunas & Zhang, 2008). Their surfaces can also be easily modified by the addition of functional groups to target specific ions e.g. grafting of amine groups for targeted removal of Cu. Although nanoparticles may be more expensive compared to agricultural waste adsorbents for example, their high adsorption efficiencies and low waste volumes compensate for this. In addition, the prices of NPs are progressively decreasing due to new production techniques and market competition.

NPs are defined as particles with at least one dimension in the 1-100 nm size range. They may be produced by processes like weathering, microbial activity mining and combustion. NPs are also increasingly being manufactured by photolithography, colloidal aggregation or organic synthesis for applications as varied as catalysis, drug delivery, electronics, cosmetics, energy, materials sciences, environmental analysis and pollution remediation (Biswas & Wu, 2005; Ju-Nam & Lead, 2008). For remediation applications, NPs are preferred over larger-sized adsorbents due to (i) their high surface-area-to-volume ratios which increase uptake per mass of applied adsorbent and also result in less contaminated wastes, (ii) high reactivities and (iii) the potential for surface functionalization to increase specificity for target ions. Indeed, NPs of various parent materials have been extensively applied for the adsorptive removal of organic and inorganic contaminants from water (Mhlanga et al., 2007; Mhlanga et al., 2013; Qu et al., 2013; Masinga et al., 2014). Metal oxide NPs are more widely used, compared to metal NPs. Silica NPs, for example, have been used for the adsorptive removal of Cu, Ni, Cu, Cr, Cd and Hg from synthetic waste water (Lee et al., 2001; Mureseanu et al., 2008; Bois et al., 2003). Other studies have reported similar uses for NPs of titanium (Engates & Shipley, 2011), hematite (Grover et al., 2012), magnetite (Das et al., 2010) and maghemite (Jiang et al., 2013).

However, besides a single study by Wilkin & McNeil (2003) which evaluated use of zero-valent iron for treatment of AMD-contaminated water, there is a dearth of information on the use of NPs under the conditions imposed by AMD such as low pH and high metal and sulphate concentrations. Thus, although society and many technologies are firmly in the ‘nano-age’, much remains unknown with respect to the use of nanoparticles for the treatment of AMD-contaminated

waters. Yet, going by results from other applications, the use of nanotechnology has enormous potential for transforming current AMD-remediation practices.

1.6 Research aims and objectives

The overarching aims of this research were, therefore to conduct initial investigations of NP-metal binding under mine drainage conditions. The effect of NPs on metal uptake by algae, an increasingly popular remediation alternative, was also investigated. Thus, using silica and maghemite nanoparticles, the removal of four metal ions common in AMD *viz.* Cu, Mn, Hg and U was investigated in NP-only treatments and in combination with a selected freshwater alga: *Scenedesmus sp.* Silica NPs were selected because of their low pH_{PZC} (pH 2-3; (Nawrocki & Buszewski, 1998)) which means that particles are negatively charged at the low pH of AMD and primed for cation adsorption. Porous silica NPs with high surface areas were selected in order to ensure high adsorption efficiencies. The choice of maghemite was based on the fact that iron oxides are good metal ion adsorbents, sometimes even better than silica (Kosmulski, 2000). The following specific objectives were set for this study:

(i) to characterise silica and maghemite NPs for size, chemical composition, surface area, porosity and crystallinity by transmission electron microscopy, dynamic light scattering, Fourier Transform Infrared (FTIR) spectroscopy, N_2 adsorption-desorption and X-ray diffraction;

(ii) to investigate the effects of parameters including (i) contact time, (ii) solution pH, (iii) temperature (iv) NP concentrations, (v) metal concentrations and (vi) the presence of ions common in AMD *viz*. manganese, sulphate and ferric ions, on the adsorption of Cu, Mn, Hg and U ions by silica and maghemite NPs;

(iii) to describe adsorption processes by fitting data to selected kinetic, isotherm and thermodynamic models;

(iv) to determine the effect of surface functionalisation by amine moieties on Cu uptake by silica NPs;

(v) to quantify the effect of NPs on metal uptake by algae and partitioning between extracellular and intracellular matrices. *Scenedesmus sp.,* a freshwater green microalga with widespread environmental distribution and high metal removal capacity was used for this study.

The results of these investigations comprise this thesis and are presented as five complete manuscripts (of which one is published and three are under review) as follows:

Chapter 2: Application of maghemite nanoparticles as sorbents for the removal of Cu(II), Mn(II) and U(VI) ions from aqueous solution in acid mine drainage conditions.

(Anita Etale, Hlanganani Tutu, Deanne C. Drake. *Applied Water Science; doi: 10.1007/s13201-014-0217-3*).

Chapter 3: Mesoporous Silica Nanoparticles for the Adsorptive Removal of Cu(II), Mn(II) and U(VI) from Acid Mine Drainage.

(Anita Etale, Hlanganani Tutu, Deanne C. Drake. *Manuscript accepted for publication by Mine Water & the Environment*).

Chapter 4: Adsorptive removal of mercury from acid mine drainage: A comparison of silica and maghemite nanoparticles.

(Anita Etale, Bongani Yalala, Hlanganani Tutu, Deanne C. Drake. *Manuscript under review by Toxicological & Environmental Chemistry*).

Chapter 5: Synthesis, characterisation and application of amine-functionalized silica-carbon hybrid nanoparticles for the adsorptive removal of Cu(II) in acidic environments.

(Anita Etale, Nikita Tavengwa, Deanne C. Drake, Hlanganani Tutu. *Manuscript will be submitted to Colloids & Surfaces A: Physicochemical & Engineering Aspects).*

Chapter 6: The effects of silica and maghemite nanoparticles on uptake of Cu(II), Mn(II) and U(VI) from aqueous solutions by a freshwater alga - *Scenedesmus sp.*

(Anita Etale, Hlanganani Tutu, Deanne C. Drake. *Manuscript under review by Applied Phycology*).

1.7 References

Anirudhan, T.S., Divya, L. & Ramachandran, M. 2008. Mercury(II) removal from aqueous solutions and wastewaters using a novel cation exchanger derived from coconut coir pith and its recovery. *Journal of Hazardous Materials*, 157(2-3): 620–627.

Atia, A.A., Donia, A.M. & Awed, H.A. 2008. Synthesis of magnetic chelating resins functionalized with tetraethylenepentamine for adsorption of molybdate anions from aqueous solutions. *Journal of Hazardous Materials*, 155(1-2): 100–108.

Babel, S. & Kurniawan, T.A. 2003. Low-cost adsorbents for heavy metals uptake from contaminated water: A review. *Journal of Hazardous Materials*, 97(1-3): 219–243.

Banks, D., Younger, P.L., Egil, R.A. & Sheila, R.I. 1997. Mine-water chemistry:The good, the bad and the ugly. *Environmental Geology*, 32(3): 157–174.

Bigham, J.M. & Nordstrom, D.K. 2000. Iron and aluminum hydroxysulfates from acid sulfate waters. *Reviews in Mineralogy and Geochemistry*, 40(1): 351–403.

Biswas, P. & Wu, C. 2005. Nanoparticles and the environment. *Journal of the Air & Waste Management Association*, 55: 708–746.

Bois, L., Bonhommé, A., Ribes, A., Pais, B., Raffin, G. & Tessier, F. 2003. Functionalized silica for heavy metal ions adsorption. *Colloids and Surfaces A: Physicochemical and Engineering Aspects*, 221(1-3): 221–230.

Boult, S., Colins, D.N., N, W.K. & Curtis, C.D. 1994. Metal transport in a stream polluted by acid mine drainage-the Afon Goch, Anglesey, UK. *Environmental Pollution*, 84: 279–284.

Bray, J.P., Broady, P.A., Niyogi, D.K. & Harding, J.S. 2008. Periphyton communities in New Zealand streams impacted by acid mine drainage. *Marine and Freshwater Research*, 59: 1084–1091.

Byrne, P., Wood, P.J. & Reid, I. 2012. The impairment of river systems by metal mine contamination: A review including remediation options. *Critical Reviews in Environmental Science and Technology*, 42(19): 2017–2077.

Cifuentes, L., García, I., Arriagada, P. & Casas, J.M. 2009. The use of electrodialysis for metal separation and water recovery from $CuSO_4$–H_2SO_4–Fe solutions. *Separation and Purification Technology*, 68(1): 105–108.

Conesa, H.M., Faz, A. & Arnaldos, R. 2007. Initial studies for the phytostabilization of a mine tailing from the Cartagena-La Union Mining District (SE Spain). *Chemosphere*, 66(1): 38–44.

Cozmuta, L.M., Cozmuta, A.M., Peter, A., Nicula, C., Nsimba, E.B. & Tutu, H. 2012. The influence of pH on the adsorption of lead by Na-clinoptilolite : Kinetic and equilibrium studies. *Water SA*, 38(2): 269–278.

Crist, R.H., Oberholser, K., Shank, N. & Nguyen, M. 1981. Nature of bonding between metallic ions and algal cell walls. *Environmental Science and Technology*, 15(10): 1212–1217.

Das, B.K., Roy, A., Koschorreck, M., Mandal, S.M., Wendt-Potthoff, K. & Bhattacharya, J. 2009. Occurrence and role of algae and fungi in acid mine drainage environment with special reference to metals and sulfate immobilization. *Water Research*, 43(4): 883–94.

Das, D., Sureshkumar, M.K., Koley, S., Mithal, N. & Pillai, C.G.S. 2010. Sorption of uranium on magnetite nanoparticles. *Journal of Radioanalytical and Nuclear Chemistry*, 285(3): 447–454.

Department of Water Affairs and Forestry. 1996. *South African water quality guidelines. Volume 7: Aquatic ecosystems*. Pretoria.

Durand, J.F. 2012. The impact of gold mining on the Witwatersrand on the rivers and karst system of Gauteng and North West Province, South Africa. *Journal of African Earth Sciences*, 68: 24–43.

Dushenkov, V., Kumar, P.B., Motto, H. & Raskin, I. 1995. Rhizofiltration: The use of plants to remove heavy metals from aqueous streams. *Environmental Science & Technology*, 29(5): 1239–45.

Ekino, S., Susa, M., Ninomiya, T., Imamura, K. & Kitamura, T. 2007. Minamata disease revisited: An update on the acute and chronic manifestations of methyl mercury poisoning. *Journal of the Neurological Sciences*, 262(1-2): 131–44.

Engates, K.E. & Shipley, H.J. 2011. Adsorption of Pb, Cd, Cu, Zn, and Ni to titanium dioxide nanoparticles: effect of particle size, solid concentration, and exhaustion. *Environmental Science and Pollution Research*, 18(3): 386–395.

España, J.S., Pamo, E.L., Santofimia, E., Aduvire, O., Reyes, J. & Barettino, D. 2005. Acid mine drainage in the Iberian Pyrite Belt (Odiel river watershed, Huelva, SW Spain): Geochemistry, mineralogy and environmental implications. *Applied Geochemistry*, 20(7): 1320–1356.

Evangelou, V.P. 1998. Pyrite chemistry: the key for abatement of acid mine drainage. In W. Geller, H. Klapper, & W. Salomons, eds. *Acidic mining lakes: Acid mine drainage, limnology and reclamation*. Berlin Heidelberg: Springer-Verlag, pp. 197–222.

Feng, Q., Lin, Q., Gong, F., Sugita, S. & Shoya, M. 2004. Adsorption of lead and mercury by rice husk ash. *Journal of Colloid and Interface Science*, 278(1): 1–8.

Fu, F. & Wang, Q. 2011. Removal of heavy metal ions from wastewaters: A review. *Journal of Environmental Management*, 92(3): 407–418.

Georgopoulos, P.G., Roy, A., Opiekun, R.E. & Lioy, P.J. 2011. Environmental copper: Its dynamics and human exposure issues. *Journal of Toxicology and Environmental Health , Part B : Critical Reviews*, 4(4): 341–394.

Gray, N.F. 1997. Environmental impact and remediation of acid mine drainage: A management problem. *Environmental Geology*, 30(1/2): 62–71.

Greig, H.S., Niyogi, D.K., Hogsden, K.L., Jellyman, P.G. & Harding, J.S. 2010. Heavy metals: confounding factors in the response of New Zealand freshwater fish assemblages to natural and anthropogenic acidity. *Science of the Total Environment*, 408(16): 3240–3250.

Grover, V.A., Hu, J., Engates, K.E. & Shipley, H.J. 2012. Adsorption and desorption of bivalent metals to hematite nanoparticles. *Environmental Toxicology and Chemistry*, 433(1): 86–92.

Hogsden, K.L. & Harding, J.S. 2012. Anthropogenic and natural sources of acidity and metals and their influence on the structure of stream food webs. *Environmental Pollution*, 162: 466–74.

Houston, M.C. 2011. Role of mercury toxicity in hypertension, cardiovascular disease, and stroke. *Journal of Clinical Hypertension*, 13(8): 621–627.

Howe, G. & Merchant, S. 1992. Heavy metal-activated synthesis of peptides in *Chlamydomonas reinhardtii*. *Plant Physiology*, 98(1): 127–136.

Hua, M., Zhang, S., Pan, B., Zhang, W., Lv, L. & Zhang, Q. 2012. Heavy metal removal from water / wastewater by nanosized metal oxides: A review. *Journal of Hazardous Materials*, 212: 317–331.

Iwasaki, Y., Kagaya, T., Miyamoto, K.-I. & Matsuda, H. 2009. Effects of heavy metals on riverine benthic macroinvertebrate assemblages with reference to potential food availability for drift-feeding fishes. *Environmental Toxicology and Chemistry*, 28(2): 354–363.

Jackson, A.K., Evers, D.C., Etterson, M.A., Condon, A.M., Folsom, S.B., Schmerfeld, J. & Cristol, D.A. 2011. Mercury exposure affects the reproductive success of a free-living terrestrial songbird, the Carolina Wren (*Thryothorus ludovicianus*). *The Auk*, 128(4): 759–769.

Jiang, W., Pelaez, M., Dionysiou, D.D., Entezari, M.H., Tsoutsou, D. & O'Shea, K. 2013. Chromium(VI) removal by maghemite nanoparticles. *Chemical Engineering Journal*, 222: 527–533.

Johnson, D.B. & Hallberg, K.B. 2005. Acid mine drainage remediation options: A review. *Science of the Total Environment*, 338: 3–14.

Ju-Nam, Y. & Lead, J.R. 2008. Manufactured nanoparticles: An overview of their chemistry, interactions and potential environmental implications. *Science of the Total Environment*, 400(1-3): 396–414.

Kolver, L. 2014. AMD pumps installed, operational by end-April. *Mining Weekly*. http://www.miningweekly.com/article/central-basin-amd-treatment-pumps-installed-facility-to-be-operational-end-april-2014-03-14 9 June 2014.

Kosmulski, M. 2000. Sorption of heavy metal cations on silica. In E. Papirer, ed. *Adsorption on silica surfaces*. New York: Marcel Dekker Inc, pp. 399–437.

Kosobucki, P., Kruk, M. & Buszewski, B. 2008. Immobilization of selected heavy metals in sewage sludge by natural zeolites. *Bioresource Technology*, 99(13): 5972–5976.

Kurniawan, T.A., Chan, G.Y.S., Lo, W.-H. & Babel, S. 2006. Physico–chemical treatment techniques for wastewater laden with heavy metals. *Chemical Engineering Journal*, 118(1-2): 83–98.

Leblanc, M. 2000. 4,500-year-old mining pollution in southwestern Spain: Long-term implications for modern mining pollution. *Economic Geology*, 95(3): 655–662.

Lee, B., Kim, Y., Lee, H. & Yi, J. 2001. Synthesis of functionalized porous silicas via templating method as heavy metal ion adsorbents : The introduction of surface hydrophilicity onto the surface of adsorbents. *Microporous and Mesoporous Materials*, 50: 77–90.

Lusilao-Makiese, J.G. 2012. *Characterization and modeling of mercury speciation in industrially polluted areas due to energy production and mineral processing in South Africa*. PhD Thesis, University of the Witwatersrand.

Malm, O. 1998. Gold mining as a source of mercury exposure in the Brazilian Amazon. *Environmental Research*, 77(2): 73–8.

Malm, O., Castroa, M.B., Bastosa, W.R., Fernando, J.P., Guimaresa, J.R.D. & Pfeiffer, W.C. 1995. An assessment of Hg pollution in different goldmining areas, Amazon Brazil. *Science of the Total Environment*, 175: 127–140.

Manders, P., Godfrey, L. & Hobbs, P. 2009. *Acid Mine Drainage in South Africa*. Pretoria.

Masinga, S.P., Nxumalo, E.N., Mamba, B.B. & Mhlanga, S.D. 2014. Microwave-induced synthesis of β-cyclodextrin/N-doped carbon nanotube polyurethane nanocomposites for water purification. *Physics and Chemistry of the Earth, Parts A/B/C*, 67-69: 105–110.

Matlock, M.M., Howerton, B.S. & Atwood, D. a. 2002. Chemical precipitation of heavy metals from acid mine drainage. *Water Research*, 36(19): 4757–64.

McCarthy, T.S. 2011. The impact of acid mine drainage in South Africa. *South African Journal of Science*, 107(5/6): 1–7.

Mhlanga, S.D., Mamba, B.B., Krause, R.W. & Malefetse, T.J. 2007. Removal of organic contaminants from water using nanosponge cyclodextrin polyurethanes. *Journal of Chemical Technology & Biotechnology*, 82: 382–388.

Mhlanga, S.D., Masinga, S.P., Bambo, M.F., Mamba, B.B. & Nxumalo, E.N. 2013. A facile procedure to synthesize a three-component β-cyclodextrin polyurethane nanocomposite matrix containing Ag decorated N-CNTs for water treatment. *Nanoscience and Nanotechnology Letters*, 5(3): 341–348.

Mohan, D. & Chander, S. 2001. Single component and multi-component adsorption of metal ions by activated carbons. *Colloids and Surfaces A: Physicochemical and Engineering Aspects*, 177: 183–196.

Monteiro, C.M., Castro, P.M.L. & Malcata, F.X. 2012. Metal uptake by microalgae: Underlying mechanisms and practical applications. *Biotechnology Progress*, 28(2): 299–311.

Moreno, N., Querol, X., Ayora, C., Pereira, C.F. & Janssen-Jurkovicová, M. 2001. Utilization of zeolites synthesized from coal fly ash for the purification of acid mine waters. *Environmental Science & Technology*, 35(17): 3526–34.

Mureseanu, M., Reiss, A., Stefanescu, I., David, E., Parvulescu, V., Renard, G. & Hulea, V. 2008. Modified SBA-15 mesoporous silica for heavy metal ions remediation. *Chemosphere*, 73(9): 1499–504.

Naicker, K., Cukrowska, E. & McCarthy, T.S. 2003. Acid mine drainage arising from gold mining activity in Johannesburg, South Africa and environs. *Environmental Pollution*, 122(1): 29–40.

Nawrocki, J. & Buszewski, B. 1998. Influence of silica surface chemistry and structure on the properties, structure and coverage of alkyl-bonded phases for high-performance liquid chromatography. *Journal of Chromatography A*, 449: 1–24.

Nieto, J.M., Sarmiento, A.M., Olías, M., Canovas, C.R., Riba, I., Kalman, J. & Delvalls, T.A. 2007. Acid mine drainage pollution in the Tinto and Odiel rivers (Iberian Pyrite Belt, SW Spain) and bioavailability of the transported metals to the Huelva Estuary. *Environment International*, 33(4): 445–55.

Niyogi, D.K., Lewis, W.M. & McKnight, D.M. 2002. Effects of stress from mine drainage on diversity, biomass, and function of primary producers in mountain streams. *Ecosystems*, 5: 554–567.

Nriagu, J.O. 1989. A global assessment of natural sources of atmospheric trace metals. *Nature*, 338: 47–49.

Nriagu, J.O. 1990. Global metal pollution: Poisoning the biosphere? *Environment: Science and Policy for Sustainable Development*, 32(7): 7–33.

Nriagu, J.O. & Pacyna, J.M. 1988. Quantitative assessment of worldwide contamination of air, water and soil by trace metals. *Nature*, 333: 134–139.

Odjegba, V.J. & Fasidi, I.O. 2004. Accumulation of trace elements by *Pistia stratiotes*: Implications for phytoremediation. *Ecotoxicology*, 13(7): 637–46.

Padmavathiamma, P.K. & Li, L.Y. 2007. Phytoremediation technology: Hyper-accumulation metals in plants. *Water, Air, and Soil Pollution*, 184(1-4): 105–126.

Pawlik-Skowrońska, B. 2001. Phytochelatin production in freshwater algae *Stigeoclonium* in response to heavy metals contained in mining water; effects of some environmental factors. *Aquatic Toxicology*, 52(3-4): 241–9.

Pistocchi, R., Mormile, A.M., Guerrini, F., Isani, G. & Boni, L. 2000. Increased production of extra- and intracellular metal-ligands in phytoplankton exposed to copper and cadmium. *Journal of Applied Phycology*, 12: 469–477.

Pliny The Elder. *The Natural History*. G. R. Crane, ed. Perseus digital library, Tufts University.

Qu, X., Alvarez, P.J.J. & Li, Q. 2013. Applications of nanotechnology in water and wastewater treatment. *Water Research*, 47(12): 3931–3946.

Ramontja, T., Coetzee, H., Hobbs, P.J., Burgess, J.E., Thomas, A., Keet, M., Yibas, B., van Tonder, D., Netili, F., Rust, U., Wade, P. & Maree, J. 2010. *Mine water management in the Witwatersrand with special emphasis on acid mine drainage report to the inter-ministerial committee on acid mine drainage.* Pretoria.

Rawlings, D.E., Tributsch, H. & Hansford, G. 1999. Reasons why "*Leptospirillum*"-like species rather than *Thiobacillus ferrooxidans* are the dominant iron-oxidizing bacteria in many commercial processes for the biooxidation of pyrite and related ores. *Microbiology*, 145: 5–13.

Robinson, N.J. 1989. Algal metallothioneins: secondary metabolites and proteins. *Journal of Applied Phycology*, 1(1): 5–18.

Singer, P.C. & Stumm, W. 1970. Acidic mine drainage : The rate-determining step. *Science*, 167(3921): 1121–1123.

De Souza, M.P., Lytle, C.M., Mulholland, M.M., Otte, M.L. & Terry, N. 2000. Selenium assimilation and volatilization from dimethylselenoniopropionate by Indian mustard. *Plant Physiology*, 122(4): 1281–8.

Sprynskyy, M., Kovalchuk, I. & Buszewski, B. 2010. The separation of uranium ions by natural and modified diatomite from aqueous solution. *Journal of Hazardous Materials*, 181(1-3): 700–7.

Tutu, H., McCarthy, T.S. & Cukrowska, E. 2008. The chemical characteristics of acid mine drainage with particular reference to sources, distribution and remediation: The Witwatersrand Basin, South Africa as a case study. *Applied Geochemistry*, 23(12): 3666–3684.

Wang, S. & Wu, H. 2006. Environmental-benign utilisation of fly ash as low-cost adsorbents. *Journal of Hazardous Materials*, 136(3): 482–501.

Waychunas, G.A. & Zhang, H. 2008. Structure, chemistry, and properties of mineral nanoparticles. *Elements*, 4: 381–388.

Wilkin, R.T. & McNeil, M.S. 2003. Laboratory evaluation of zero-valent iron to treat water impacted by acid mine drainage. *Chemosphere*, 53(7): 715–25.

World Health Organization. 2011. *WHO guidelines for drinking-water quality, 4th Edition*. Geneva.

Yorifuji, T., Tsuda, T., Inoue, S., Takao, S. & Harada, M. 2011. Long-term exposure to methylmercury and psychiatric symptoms in residents of Minamata, Japan. *Environment International*, 37(5): 907–13.

Zhong, C.-M., Xu, Z.-L., Fang, X.-H. & Cheng, L. 2007. Treatment of acid mine drainage (AMD) by ultra-low-pressure reverse osmosis and nanofiltration. *Environmental Engineering Science*, 24(9): 1297–1306.

2 Application of maghemite nanoparticles as sorbents for the removal of Cu(II), Mn(II) and U(VI) ions from aqueous solution in acid mine drainage conditions

Appl Water Sci
DOI 10.1007/s13201-014-0217-3

ORIGINAL ARTICLE

Application of maghemite nanoparticles as sorbents for the removal of Cu(II), Mn(II) and U(VI) ions from aqueous solution in acid mine drainage conditions

Anita Etale · Hlanganani Tutu · Deanne C. Drake

Received: 6 April 2014 / Accepted: 20 June 2014
© The Author(s) 2014. This article is published with open access at Springerlink.com

Abstract The adsorptive removal of Cu(II), Mn(II) and U(VI) by maghemite nanoparticles (NPs) was investigated under acid mine drainage (AMD) conditions to assess NP potential for remediating AMD-contaminated water. The effects of time, NP and metal concentration, as well as manganese and sulphate ions were quantified at pH 3. Adsorption of all three ions was rapid, and equilibrium was attained in 5 min or less. 56 % of Cu, 53 % of Mn and 49 % of U were adsorbed. In addition, adsorption efficiencies were enhanced by ≥10 % in the presence of manganese and sulphate ions, although Cu sorption was reduced in 1:2 Cu-to-Mn solutions. Adsorption also increased with pH: 86 % Cu, 62 % Mn and 77 % U were removed from solution at pH 9 and increasing initial metal concentrations. Increasing NP concentrations did not, however, always increase metal removal. Kinetics data were best described by a pseudo-second-order model, implying chemisorption, while isotherm data were better fitted by the Freundlich model. Metal removal by NPs was then tested in AMD-contaminated surface and ground water. Removal efficiencies of up to 46 % for Cu and 54 % for Mn in surface water and 8 % for Cu and 50 % for Mn in ground water were achieved, confirming that maghemite NPs can be applied for the removal of these ions from AMD-contaminated waters. Notably, whereas sulphates may increase adsorption efficiencies, high Mn concentrations in AMD will likely inhibit Cu sorption.

Keywords Copper · Manganese · Uranium · Adsorption · Acid mine drainage

A. Etale (✉) · D. C. Drake
School of Animal Plant and Environmental Sciences, University of the Witwatersrand, Private Bag X3, WITS, 2050 Johannesburg, South Africa
e-mail: aetale@gmail.com

H. Tutu
Molecular Sciences Institute, School of Chemistry, University of the Witwatersrand, Private Bag X3, WITS, 2050 Johannesburg, South Africa

Introduction

The contamination of water bodies by metal and radionuclide ions is a major unintended consequence of mining in many regions of the world. In South Africa, mining of base and precious metals has taken place for more than a century and contributed enormously to the growth of the economy. It has also, however, resulted in significant contamination of surface and groundwater by acid mine drainage (AMD) and a suite of metal and radionuclide ions (Naicker et al. 2003; Tutu et al. 2008; Winde 2010). This contamination is a major concern especially in light of the health risks and negative impacts on ecosystems posed by exposure to excessive metal concentrations (WHO 2011). Cu, for example, is toxic to some algae at sub-ppm (parts per million/mg L^{-1}) concentrations (Franklin et al. 2000); and U has been linked to renal failure and certain cancers in humans (Toens et al. 1998; WHO 2011). Mn, although less toxic, lends undesirable qualities like poor taste and staining to potable water. The World Health Organization (WHO) drinking water standards stipulate upper limits of 2 mg L^{-1}, 0.4 mg L^{-1} and 30 µg L^{-1} for Cu, Mn and U, respectively (WHO 2011). Yet concentrations as high as 7 mg L^{-1} for Cu, 129 mg L^{-1} for Mn and 2.6 mg L^{-1} for U have been reported for ground and surface waters sometimes used for potable purposes (Naicker et al. 2003; Tutu et al. 2008; Winde 2010; Saad et al. 2013). The removal of these ions from AMD-contaminated waters is

Published online: 27 June 2014

therefore necessary to reduce negative effects to humans, aquatic organisms and ecosystems. Remediation is also necessary in light of the scarcity of water as a resource and the growing water scarcity and the increasing pressures on this resource by increasing human population and per capita rates of water use.

A number of techniques exist for the removal of metal and radionuclide ions from wastewater, e.g., ion exchange, reverse osmosis, phytoremediation, electrodialysis and chemical precipitation (Kurniawan et al. 2006). These, however, suffer from limitations like low adsorbent capacities, fouling, high maintenance costs, slow uptake rates and production of large quantities of secondary wastes. Adsorption offers an alternative that is free from some of these limitations and as such, has been extensively studied. Among the many adsorbents investigated, e.g., activated carbon, zeolites, polymers, zero-valent iron and agricultural wastes (Fu and Wang 2011), nanoparticles (NPs) have attracted considerable interest due to the special properties of materials at the nanoscale (1–100 nm). NPs are more reactive than larger materials and offer larger sorption surface areas, thus allowing for faster and more efficient adsorption (Waychunas and Zhang 2008).

NPs of various materials such as carbon (e.g., carbon nanotubes), metals (e.g., zero-valent iron) and metal oxides (e.g., titania, iron oxides) have been investigated for the adsorptive removal of metal ions from water (see review by Khajeh et al. 2013). Of the iron oxides, maghemite nanomaterials have shown good efficiency for the removal of ions including As(V) (Tuutijärvi et al. 2009), Mo(VI) (Afkhami and Norooz-Asl 2009), Cr(VI) (Jiang et al. 2013), Cu, Zn, Pb (Roy and Bhattacharya 2012), Se (Jordan et al. 2013) and U (Madrakian et al. 2011). Hu et al. (2006), for example, reported an adsorption capacity of 27.7 mg g^{-1} for Cu at pH 6.5 and 25.7 mg g^{-1} for Ni at pH 8.5. Less information is, however, available on the adsorptive removal of Mn from wastewater by NPs. Perhaps this is due to the lower toxicity of Mn in comparison to other elements. But concentrations in AMD easily surpass limits for drinking water and organism tolerance, hence the need for its removal.

A review of the literature revealed a paucity of information on metal removal by NPs in mine drainage conditions. The pH in AMD, for example, is often $\leq$3 and adsorption in such extreme pH is different from pH 6 at which many studies are conducted. Further, AMD contains additional ions such as manganese and sulphates that are likely to affect the adsorption efficiency of NPs and any remediation technology applied. Manganese and sulphates are abundant in mine drainage, being the products of pyrite (FeS_2) and MnS oxidation (Schemel et al. 2000). However, unlike ferric ions that are also abundant but precipitate at low pH, manganese persists in solution over a wide range of pH and may therefore have an effect on adsorption of other cations. The successful treatment of AMD using NPs requires that these effects are quantified to improve the optimal functioning of remediation technologies.

We therefore designed a study to investigate the use of NPs for the adsorptive removal of metal ions common in AMD. Herein, we report on the findings of the application of maghemite for the removal of Cu(II), Mn(II) and U(VI) from simulated AMD. The effects of time, adsorbate concentrations, adsorbent concentrations as well as those of sulphate and manganese ions on adsorption of these three ions were investigated. We also quantified the adsorption process at pH 5, 7 and 9 to determine process efficiency in pH-amended systems.

Materials and methods

Materials

All metal salts used for this study were analytical grade. $Cu(NO_3)_2{\cdot}2.5{\cdot}H_2O$ and $Mn(NO_3)_2{\cdot}H_2O$ were purchased from Sigma Aldrich (Germany). $UO_2(NO_3)_2{\cdot}6H_2O$ and Na_2SO_4 were from Ace Chemicals (South Africa), and maghemite NPs from Sigma Aldrich (Germany). Metal salt solutions and NP suspensions were prepared using deionised water. NP suspensions (3 mg L^{-1}) were prepared by 30-min sonication in a water bath (Branson 2500). Adjustments of solution pH were made prior to experiments using 0.01 M HNO_3 and 0.01 M NaOH.

Particle characterisation

The size and morphology of maghemite particles was determined using transmission electron microscopy (FEI Tecnai G^2 Spirit TEM) at an acceleration voltage of 120 kV. Particles (0.1 g) were suspended in 100-mL deionised water and sonicated in a water bath for 30 min. A drop of the suspension was then placed on a copper grid and left to dry for 20 min before analysis. The surface area of particles was determined by the Brunauer–Emmett–Teller (BET) method using a Micrometrics Tristar 3000 (Micrometrics Instruments, USA). NP crystallinity was determined by powder X-ray diffraction on a Bruker D8 diffractometer (Cu-$K\alpha$). The scanning range was 10°–90° (2θ) using a step size of 0.026° and step time of 37 s at room temperature (25 °C $\pm$ 2).

Adsorption studies

Adsorption was quantified in batch experiments using solutions of 14.99 mg L^{-1} Cu, 9.52 mg L^{-1} Mn and 42.18 mg L^{-1} U. Freshly sonicated NP suspensions (10 mL)

were contacted with 10-mL metal nitrate solutions in 50-mL polyethylene terephthalate (PET) jars. Experiments were run in triplicate, for 60 min, at ambient temperature (~25 °C) and unless otherwise stated, at pH 3.3 (±0.2).

The effect of contact time was evaluated for durations ranging from 5 s to 60 min (5, 10, 15, 30, 45, 60, 300, 600, 900, 1,800, 2,700 and 3,600 s). The effects of Mn^{2+} (from $Mn(NO_3)_2{\cdot}H_2O$) and SO_4^{2-} (from Na_2SO_4) were quantified for 1:1 and 1:2 molar ratios to the test ion. The effects of both additional ions were tested for Cu and U, but for Mn, only SO_4^{2-} effects were investigated. The effect of adsorbent concentration on adsorption efficiency was tested using 1, 3 and 10 mg L^{-1} maghemite concentrations while that of pH was tested at pH 3, 5, 7 and 9. Finally, adsorption isotherms were investigated for concentrations ranging from 14.99–136.4 mg L^{-1} for Cu, 9.52–104.6 mg L^{-1} for Mn and 4.46–464.2 mg L^{-1} for U.

At the end of experiments, mixtures were separated using Amicon ultracentrifugal filters (100 kDa molecular weight cut off; Millipore) and filtrates acidified with 3 mL 1 % nitric acid. Metal concentrations in filtrates were determined by Inductively Coupled Plasma-Optical Emission Spectrometry (ICP-OES; Spectro Instruments, Kleve, Germany). Adsorption at the various time intervals and at equilibrium was determined by mass-balance calculations.

The equilibrium adsorption capacities of NPs (q_e; mg g^{-1}) were calculated using Eq. 1. Adsorption efficiency was expressed as a percentage using Eq. 2 (Roy and Bhattacharya 2012). C_i and C_e are the initial and equilibrium metal concentrations (mg L^{-1}), m is the mass of adsorbent applied (g) and V is the volume of the solution used (L).

$$q_e = \frac{(C_i - C_e)V}{m} \tag{1}$$

$$\%\ \text{Adsorption efficiency} = \frac{(C_i - C_e)}{C_i} \times 100 \tag{2}$$

Adsorption from AMD-contaminated ground and surface water samples

Surface water samples were collected from the Tweelopiespruit, a stream west of Johannesburg into which a disused mineshaft decants mine drainage (26°50′21.67″S, 27°42′57.49″E). Two water samples were collected from the stream at locations approximately 1 and 1.5 km downstream of the decant point. Groundwater was collected from a well in the vicinity of the stream (650 m away from sampling point 1). Water samples were collected in 1-L acid-washed polypropylene bottles and the pH, conductivity and redox activity of water was recorded on site using field meters. Samples were then transported to the laboratory over ice where they were filtered through 0.45-μm filter paper before use in adsorption experiments. The adsorption protocol was similar to that used for simulated wastewater, except that water samples were used without pH adjustment. Thus, 10 mL of water sample was reacted with 10 mL of 3 mg L^{-1} NP suspension for 60 min, filtered and filtrate metal concentrations determined by ICP-OES.

Modeling

Kinetics

Kinetics data were fitted into three kinetics models: the pseudo-first-order model (Eq. 3), pseudo-second-order model (Eq. 4) (Ho and Mckay 2004), and the intraparticle diffusion model (Eq. 5) (Weber and Morris 1963).

$$\log(q_e - q_t) = \log q_e - \left(\frac{k_1}{2.303}\right)t \tag{3}$$

$$\frac{t}{q_t} = \left(\frac{1}{k_2}\right) + \left(\frac{1}{q_e}\right)t \tag{4}$$

$$q_t = I_d + k_p \cdot (t^{0.5}) \tag{5}$$

q_e and q_t are the NP-loading capacities (mg g^{-1}) at equilibrium and at time t, respectively, while k_p is the initial rate of intraparticle diffusion (mg (g^{-1} $s^{-0.5}$)). The equations were plotted as follows: log ($q_e - q_t$) versus t for the pseudo-first-order model, t/q_t versus t for the pseudo-second-order model and q_t versus $t^{0.5}$ for the intraparticle diffusion model. Rate constants were determined from the slope (k_1) or intercepts (k_2 and I_d) of respective plots.

Adsorption isotherms

Adsorption isotherms at pH 3 were determined using five different concentrations for each ion. Isotherm data were fitted to the Langmuir and Freundlich models (LeVan and Vermeulen 1981) to determine adsorption capacities and infer the nature of binding of sorbate ions at the sorbent surface. The Langmuir model assumes that adsorption takes place at specific homogenous sites and best describes monolayer adsorption. It is represented in the linear form by Eq. 5 where q_{max} is the maximum concentration of metal ions sorbed per unit weight of NPs (mg g^{-1}), and K_L is the Langmuir constant for the reaction.

The Freundlich model on the other hand, assumes that adsorption takes place on a heterogeneous surface by multi-layer adsorption. Its linear form is as expressed in Eq. 6, where K_F and $1/n$ are constants specific to each reaction. K_F is the relative adsorption capacity of the adsorbent and $1/n$ is related to the adsorption intensity and heterogeneity of the sorbent surface. The more heterogeneous the surface, the closer the $1/n$ value is to 1. $1/n$

values can also be used to infer the nature of adsorption, i.e., values below 1 imply chemisorption and those >1 imply cooperative processes, e.g., adsorption in combination with precipitation (Foo and Hameed 2010).

$$\frac{C_e}{q_e} = \left(\frac{1}{q_{max}}\right) C_e + \left(\frac{1}{K_L q_{max}}\right) \quad (5)$$

$$\log q_e = \left(\frac{1}{n}\right) \log C_e + \log K_F \quad (6)$$

Equations 5 and 6 were plotted as follows: C_e/q_e versus C_e and log q_e versus log C_e. q_{max} and $1/n$ were determined from the slopes of these plots, while K_L and K_F were determined from the intercepts.

The speciation of metal ions at various pH and in the presence of additional ions was determined using MEDUSA software (KTH Royal Institute of Technology 2004).

Results and discussion

Particle characterisation

Transmission electron micrographs revealed polydisperse polyhedral particles with diameters <100 nm (Fig. 1a). The X-ray diffraction pattern (Fig. 1b) is consistent with the database for this iron phase in the JCPDS file. The

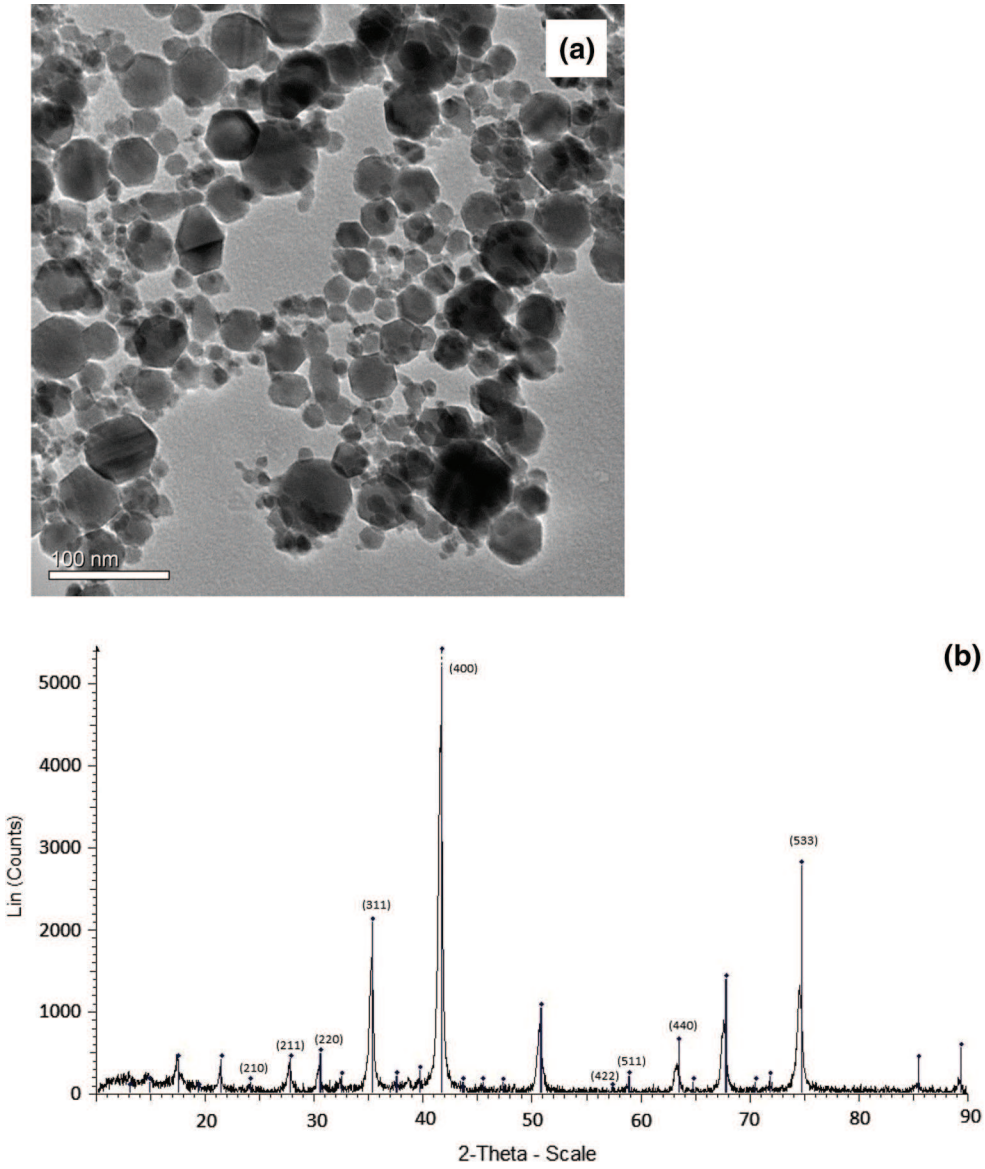

Fig. 1 Transmission electron micrograph (**a**) and powder X-ray diffractogram (**b**) of maghemite nanoparticles. PXRD peaks were as indexed according to JCPDS 39-1346

presence of (2 1 0) and (2 1 1) peaks confirms that the adsorbent was indeed maghemite and not magnetite, both of which have similar X-ray diffractograms (Kim et al. 2012). Thus, although all other wide angle peaks, i.e., from (2 2 0) to (5 3 3) are present in both iron oxide phases, magnetite does not have peaks at (2 1 0) and (2 1 1). The presence of these two peaks in the NP sample therefore confirms that it is maghemite. BET measurements indicated that particles were mesoporous (average pore width was 11.3 nm) with a surface area of 40.8 m^2 g^{-1}.

Effect of contact time

Adsorption was quantified at the following time intervals: 5, 10, 15, 30, 45, 60, 300, 600, 900, 1,800, 2,700 and 3,600 s. Adsorption of all three metal ions was rapid and reactions attained equilibrium within 30 min (Fig. 2). At equilibrium 56 % of Cu, 53 % of Mn and 49 % of U were adsorbed from solutions at pH 3. Similar rapidity of reaction rates was also reported by Chang and Chen (2005) and Banerjee and Chen (2007).

Reaction kinetics were best described by the pseudo-second-order model (Table 1), implying that the binding of metal ions to the maghemite surface was by chemisorption (Ho and Mckay 2004). Further, the fit of data to the intraparticle diffusion model was poor ($R^2 \leq 0.11$). Diffusion to sorption sites within pores was therefore not the rate-limiting step in the adsorption process. This can be explained by the fact that with NP pore diameters of 11.3 nm, hydrated Cu (radius = 0.419 nm), Mn (radius = 0.438 nm) and U (radius = 1.08 nm) ions should have un-impeded access and movement within NP pores (Persson 2010).

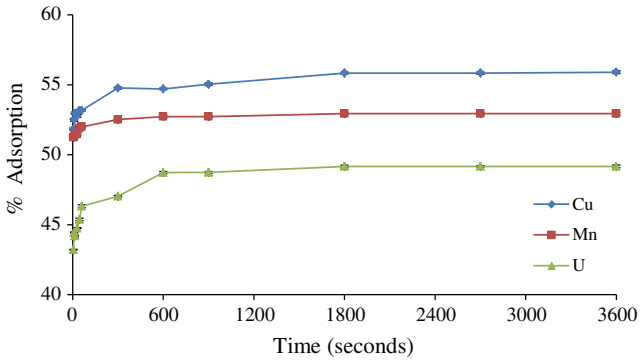

Fig. 2 The kinetics of Cu, Mn and U adsorption to maghemite NPs (±SD) at pH 3 (NP concentration 3 mg L^{-1})

Notably, the adsorption rate was highest for Mn. This was despite the higher initial concentrations hence higher mass transfer drives for Cu and U, as well as the fact that Cu is more electronegative than Mn. Madden et al. (2006) hypothesized that NPs differentially bind metal ions based on their structural configuration. Thus, in their study, adsorption of Cu to hematite increased with decreasing hematite NP size because of the higher incidence, in smaller particles, of sites that stabilized the Jahn–Teller distorted octahedron of Cu. Similarly, the configuration of sorption sites on the maghemite surface may favor the perfect octahedron of Mn relative to the Jahn–Teller distorted Cu, hence the higher adsorption rate of the former. With respect to U, the large ionic size may be responsible for the low-binding rate.

Effects of Mn^{2+} and SO_4^{2-} ions

The adsorption of all three metal ions at pH 3 was enhanced in the presence of Mn^{2+} (Fig. 3a) and SO_4^{2-} ions (Fig. 3b). U adsorption was largely similar in both equimolar and 1:2 U/Mn molar solutions, i.e., adsorption increased by 10 and 11 %, respectively (Fig. 3a). In contrast, Cu sorption increased by 15 % in 1:1 Cu-to-Mn solutions and by only 7 % in 1:2 Cu-to-Mn solutions. Cu adsorption was therefore inhibited by higher Mn concentrations. This leads to the hypothesis that Cu and Mn ions sorb to similar sites on the adsorbent surface (Benjamin and Leckie 1981), resulting in competition in mixed solutions. The high Mn concentrations in AMD may therefore, inhibit adsorption of Cu to maghemite NPs at low pH.

Increases in the presence of sulphate ions were largely similar in both 1:1 and 1:2 metal-to-sulphate solutions (Fig. 3b). The greatest effect of sulphate was on U and Mn, while the least was on Cu. In the treatment of AMD, therefore, the presence of sulphate is likely to have synergistic effects and improve removal efficiency of NPs.

Table 1 Adsorption rate constants and coefficients of correlation (R^2) for kinetics models fitted to adsorption data

Metal	Initial concentration (mg L^{-1})	Pseudo-second order model			Pseudo-first order model			Intraparticle diffusion model
		k_2 (g mg^{-1} s^{-1})	q_e (mg g^{-1})	R^2	k_1 (sec^{-1})	q_e (mg g^{-1})	R^2	R^2
Cu	14.99	0.01	27.93	1	0.002	1.58	0.95	0.14
Mn	9.55	0.04	16.81	1	0.001	2.55	0.78	0.11
U	42.18	0.002	69.44	0.99	0.004	5.57	0.87	0.16

Adsorption at pH 3, adsorbent concentration = 3 mg L^{-1}; volume of adsorbent solution used = 10 mL; volume of metal solution = 10 mL

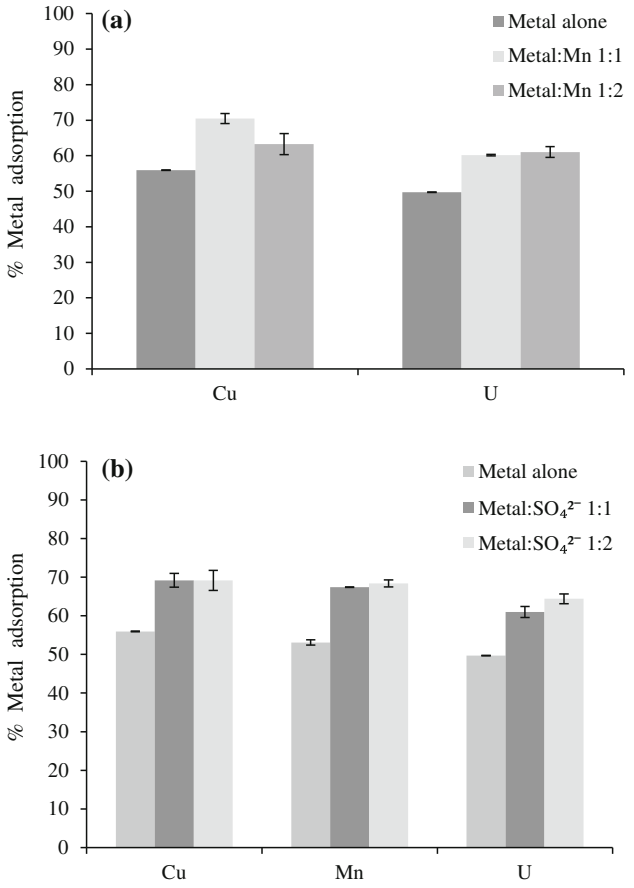

Fig. 3 **a** The effect of manganese ions on adsorption of Cu and U by maghemite NPs (±SD). **b** The effect of sulphate ions on adsorption of Cu, Mn and U by maghemite NPs (±SD)

Mechanisms of adsorption enhancement

Adsorption enhancement in the presence of Mn was likely due to a greater diffusion drive for mass transfer to the adsorbent surface (Ho and Mckay 2004). Driving forces for diffusion of ions towards the adsorbent surface are greater at high ion concentrations, hence increased adsorption.

Enhanced adsorption in the presence of sulphates (and anions like phosphate and arsenate) has been reported previously. Ali and Dzombak (1996), for example, found that the adsorption of Cu at low pH was enhanced in the presence of sulphate. Similarly, arsenate enhanced the sorption of Zn to goethite while phosphate and sulphate ions enhanced sorption of Pb to goethite and boehmite (Weesner and Bleam 1998) and Cd to goethite (Collins et al. 1999).

A number of mechanisms have been proposed to explain these observations. The first is that anions lower the energy barrier for the approach of cations to the adsorbent surface by forming complexes in solution (James and Healy 1972a). Thus, the formation of uncharged complexes such as $CuSO_4$, $MnSO_4$ and UO_2SO_4 can increase adsorption because these complexes experience less repulsion from the maghemite surface than do charged ions. Alternatively, anions may increase adsorption by altering the electrical properties of the adsorbent surface (Benjamin and Leckie 1982). The adsorption of sulphate to maghemite reduces Coulombic repulsions, making the interaction between maghemite sorption sites and cations more favorable. The formation of ternary surface complexes was also suggested by the modeling studies of Ali and Dzombak (1996) and Swedlund and Webster (2001). However, EXAFS (extended x-ray absorption fine structure) and ATR-FTIR (attenuated total reflectance–fourier transform infrared) spectroscopic data by Collins et al. (1999) and Beattie et al. (2008) found no evidence of such structures.

Nonetheless, these and other spectroscopic techniques [EXAFS and X-ray Absorption Spectroscopy (XAS)] resolved U and Cu binding to iron oxides (goethite, schwertmannite and ferrihydrite) as involving the formation of inner sphere complexes (Moyes et al. 2000; Walter et al. 2003). While U complexes may be mononuclear bidentate, binuclear bidentate or mononuclear monodentate, those of Cu are bidentate ($[\equiv FeOH_2)Cu(OH_2)^0]$) or tridentate ($[\equiv Fe_3O(OH_2)Cu_2(OH)_3^0]$) (Peacock and Sherman 2004). With respect to Mn, although we could find no spectroscopic evidence, its adsorption to iron oxides likely also involves formation of inner sphere complexes. This is because adsorption at pH 3, where both maghemite and Mn are positively charged, likely involves specific and not electrostatic interactions (James and Healy 1972b).

Effect of initial metal concentrations

Although percent differences are relatively imperceptible (especially for Cu and Mn), it is clear from Fig. 4a–c that NP loading (q_e) increased with increasing metal concentrations. These increases can be explained by the greater driving force for mass transfer as ion concentrations in solution increase (Ho and Mckay 2004).

As shown in Table 2, the better fit of adsorption data for all three metal ions was given by the Freundlich model, implying that adsorption was to a heterogeneous surface. The $1/n$ values show that adsorption of Cu and Mn was by chemisorption. In addition, the K_F values for these two ions indicate that affinity for sorption sites under the experimental conditions was greater for Mn than Cu. Nevertheless, calculated maximum adsorption capacities for the two metal ions varied little. The removal of U on the other hand, was by cooperative processes, based on the $1/n$ value that was >1. Adsorbent capacity for this ion was, however, lower than that of Cu and Mn. Indeed, a comparison of the adsorption capacity of maghemite NPs and a few other adsorbents is presented in Table 3. From these data, it is clear that at low pH, maghemite NPs have a higher

adsorption capacity for Cu than hematite NPs (Grover et al. 2012). Their capacity for Mn is also almost equal to that of activated carbon (Mohan et al. 2001), but lower than that of reduced graphene oxide with respect to U adsorption (Li et al. 2012). The higher adsorption capacity for maghemite NPs reported by Hu et al. (2006) was due to the larger surface area of the NPs in that study (198 m^2 g^{-1} vs. 40 m^2 g^{-1} for particles in this study), along with the higher pH at which adsorption was conducted. Similarly, the high adsorption efficiency reported by Roy and Bhattacharya (2012) is because of the higher surface area of their nanotubes (111.11 m^2 g^{-1}).

Effect of adsorbent concentration

Adsorbed metal concentrations fluctuated, albeit slightly, with increasing NP concentrations. Cu adsorption went from 52 to 56 % and then 51 % as NP concentrations increased from 1 to 3 and 10 mg L^{-1} (Fig. 5). Mn adsorption went from 50 to 53 % and 52 %, while U adsorption went from 48 to 50 % and 48 % at 1, 3 and 10 mg L^{-1} NP concentrations. The optimal NP concentration was therefore 3 mg L^{-1} in all cases, but differences were small. Decreases in adsorption at 10 mg L^{-1} NP concentrations were likely due to NP agglomeration which increases with, among other things, NP concentrations (He et al. 2008). Particle agglomeration reduces the access of metal ions to sorption sites located in the interior of particles and agglomerates. This, in turn, reduces metal removal efficiency. Care must therefore be exercised in determining the NP concentrations to be used in remediation systems as higher NP concentrations do not always give greater adsorption yields.

Effect of pH

The influence of pH on adsorption was studied at pH 3, 5, 7 and 9. As shown in Fig. 6, removal of all three ions increased with pH. The increase between pH 3 and 9 was least for Mn (9 %) and highest for Cu (31 %). U removal increased by 27 % between pH 3 and 9, with the greatest increase occurring between pH 5 and 7. At this pH range, a hydrolysis product of uranium, schoepite $[(UO_2)_8O_2(OH)_{12}{\cdot}12H_2O]$ is formed hence the increase in adsorption (Tutu 2006). However, because experiments did not exclude CO_2, not all uranium precipitated as schoepite due to the formation of uranyl carbonates and hydrogen carbonates (Waite et al. 1994; Wazne et al. 2006). Indeed, adsorption did not attain maximal efficiencies likely due to the formation of these non-adsorbing species.

Changes in adsorption of ions may be due to any of the following three effects, acting most often, simultaneously: (1) reduced competition from H^+ ions, (2) changes in the adsorbent surface charge and (3) hydrolysis (James and

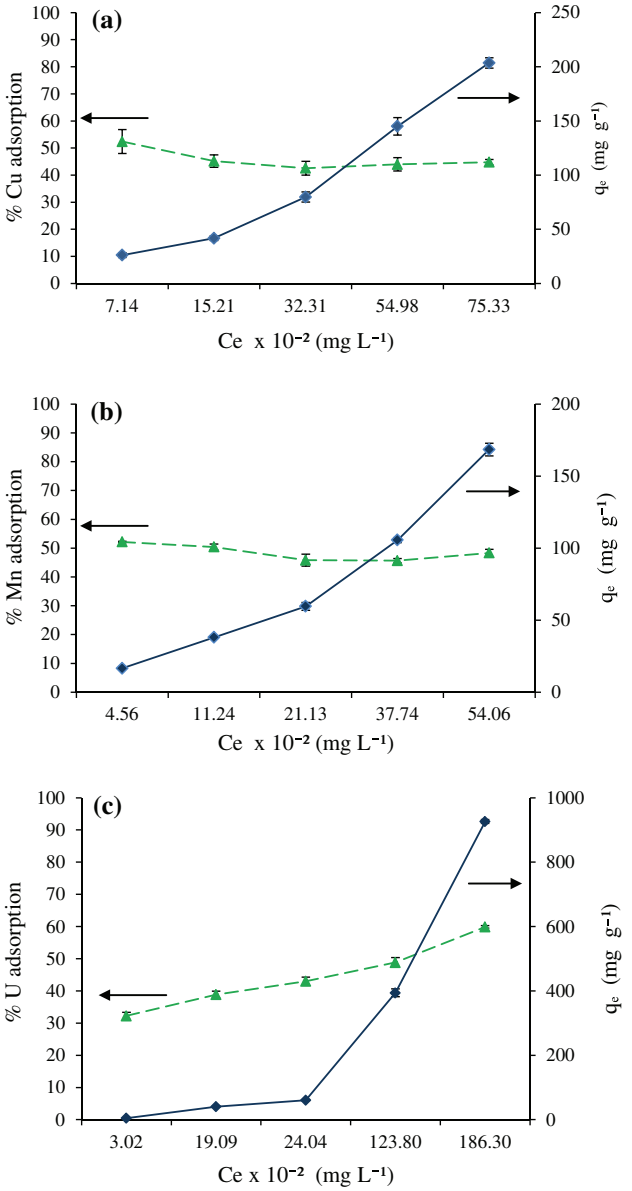

Fig. 4 Adsorption isotherms and percent adsorption efficiencies of Cu (**a**), Mn (**b**) and U (**c**) (±SD)

Table 2 Langmuir and Freundlich isotherm parameters determined for the adsorption of Cu, Mn and U to maghemite NPs

Metal	Freundlich isotherm			Langmuir isotherm		
	R^2	K_F (mg g^{-1})	$1/n$	R^2	q_{max} (mg g^{-1})	K_L
Cu	0.96	4.35	0.83	0.31	108.7	0.03
Mn	0.99	4.03	0.91	0.32	208.3	0.02
U	0.99	1.13	1.25	0.94	20.3	0.07

Adsorption at pH 3, adsorbent concentration = 3 mg L^{-1}; volume of adsorbent solution used = 10 mL; volume of metal solution = 10 mL; equilibration time = 60 min

Table 3 A comparison of the adsorption capacities of maghemite NPs and other adsorbents for Cu, Mn and U

Adsorbent	Metal	Solution pH	Adsorption capacity (mg g^{-1})	References
Maghemite NPs	Cu	3	4.35	This study
Maghemite NPs		6.5	27.7	Hu et al. (2006)
Maghemite nanotubes		6	111.11	Roy and Bhattacharya (2012)
Hematite NPs		4	2.92	Grover et al. (2012)
Magnetite NPs		6	17.6	Banerjee and Chen (2007)
Maghemite NPs	Mn	3	4.03	This study
Activated carbon (wood)		6	4.16	Mohan and Chander (2001)
Activated carbon (coconut shell)		6	16.42	Mohan and Chander (2001)
Lignite		3.5	28.54	Mohan and Chander (2006)
Maghemite NPs	U	3.3	1.13	This study
Magnetite NPs		8.1	5	Das et al. (2010)
Reduced graphene sheets		4	47	Li et al. (2012)

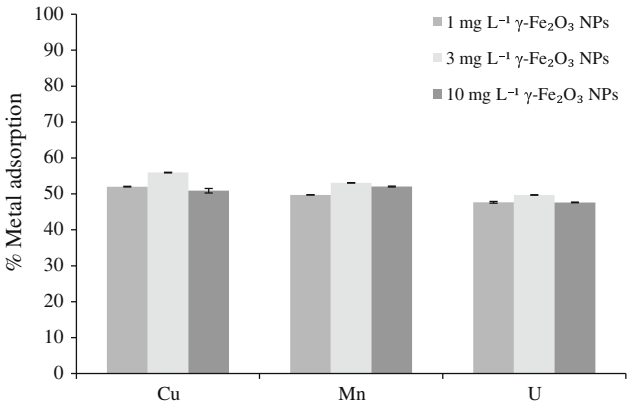

Fig. 5 The effect of adsorbent concentration on adsorption of Cu, Mn and U to maghemite NPs (±SD)

Healy 1972b). As solution pH increases, the concentration of H^+ ions decreases, resulting in less competition between them and cations for sorption sites. pH-related changes to the adsorbent surface also affect the adsorption of cations. Maghemite, with a pH_{PZC} of 6.3–6.9 (Vayssieres 2009) is positively charged below pH 6.3–6.9 but becomes increasingly negatively charged as pH increases. Thus, at low pH, $\equiv FeOH_2^+$ groups dominate the maghemite surface and repulse cations. As pH increases, however, these

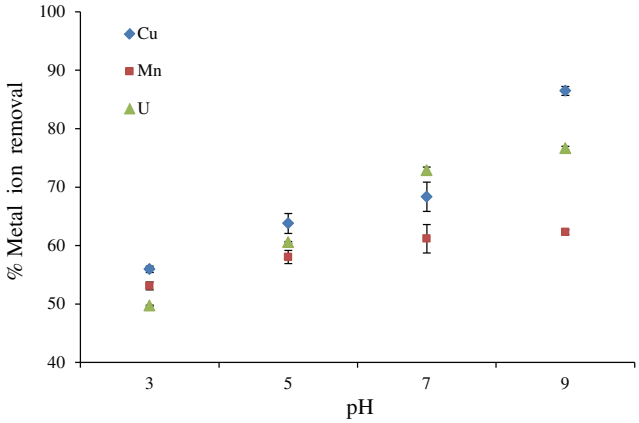

Fig. 6 The effect of pH on adsorption of Cu, Mn and U to maghemite NPs (±SD). Initial concentrations: 14.99 mg L^{-1} for Cu, 9.52 mg L^{-1} for Mn and 42.18 mg L^{-1} for U; NP concentration: 3 mg L^{-1})

moieties are increasingly deprotonated (Eqs. 7, 8) making the approach of cations to the maghemite surface, and subsequently adsorption, more favorable.

$$\equiv FeOH_2^+ \rightarrow \equiv FeOH + H^+ \quad (7)$$

$$\equiv FeOH \rightarrow \equiv FeO^- + H^+ \quad (8)$$

The third factor, hydrolysis, increases adsorption through the formation of more adsorbable species as postulated by James and Healy (1972a). Thus, adsorption of Cu and U increased at higher pH, due to the formation of species such as $CuOH^+$, $Cu(OH)_2$, $(UO_2)_2(OH)_2^{2+}$, and insoluble precipitates. Speciation modeling showed that insoluble $UO_2(OH)_2{\cdot}H_2O$ and CuO form were the dominant species in solutions higher than pH 5 and 5.6, respectively. This explains why the largest increase in U sorption is seen between pH 5 and 7 as well as why Cu removal increased at pH 7 and 9. Mn, on the other hand, does not hydrolyze in the test pH range; hence, the minimal change in adsorption. In fact, Mn adsorption likely increased only due to decreased competition from H^+ ions, and changes on the adsorbent surface.

The pH_{PZC} of particles also has an effect on the nature of adsorption. As particle surfaces are positively charged below the pH_{PZC}, cation adsorption in this pH region likely involves specific interactions. In contrast, adsorption above the pH_{PZC}, where cations and adsorbent surfaces are oppositely charged, involves electrostatic forces. For maghemite, therefore, adsorption across the test pH range was by both specific (ion exchange) and electrostatic interactions.

Another effect that solution pH has on adsorption relates to NP agglomeration. As solution pH approaches the pH_{PZC} of NPs, agglomeration increases due to the decrease in

Table 4 Physical and chemical characteristics of AMD-contaminated surface water (SW) and groundwater (GW) used in application studies

Sample	pH	Conductivity (mS cm^{-1})	Redox potential (mV)	$[Cu]_{tot}$, mg L^{-1} (SD)	$[Mn]_{tot}$, mg L^{-1} (SD)	$[U]_{tot}$, mg L^{-1} (SD)
SW1	3.13	3.52	209.0	1.44 (0.003)	49.74 (0.002)	b.d
SW2	2.79	3.87	227.7	1.22 (0.046)	16.48 (0.006)	b.d
GW	5.62	2.76	6.9	0.24 (0.001)	15.00 (0.140)	b.d

$[\ ]_{tot}$ Total concentration of all species, *b.d* concentration below ICP-OES detection limit

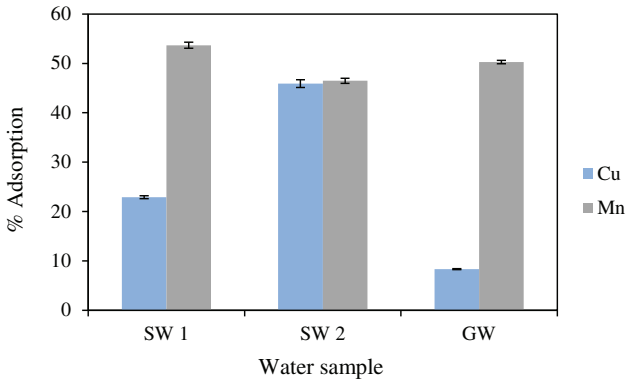

Fig. 7 Removal efficiencies of Cu and Mn from contaminated surface and groundwater by maghemite NPs. U concentrations in both surface and groundwater samples were below detection limits for ICP-OES

repulsive surface charges (He et al. 2008). This, as discussed above ("Effect of adsorbent concentration"), reduces access to sorption sites and decreases adsorption. Although difficult to determine separately from the effects of all other factors mentioned, it is still worth bearing in mind during the determination of operational parameters, that adsorption may decline as solution pH approaches NP pH_{PZC}.

Application studies

Removal of Cu, Mn and U by maghemite NPs was then tested in AMD-contaminated water. Two surface water samples (SW1 and SW2) and one ground water sample (GW) were used. The physical and chemical characteristics of contaminated water samples are presented in Table 4. U concentrations in all three water samples were below ICP-OES detection limits, hence removal could not be quantified.

The results of adsorption experiments are presented in Fig. 7. Of the three water samples, Cu was most efficiently removed from SW2 while Mn was more efficiently adsorbed from SW1. Adsorption of both ions in SW2 was almost equal. Importantly, these data confirm our earlier hypothesis that high Mn concentrations inhibit Cu sorption to maghemite. Thus, although Cu concentrations in SW1 and SW2 were almost similar (Table 4), Cu adsorption from SW2 was double that of SW1, i.e., 46 versus 23 %. This difference may be ascribed to the ratio of Cu:Mn in the two water samples which was 1:35 in SW1 but only 1:14 in SW2. Thus, the much higher Mn concentrations in SW1 limited Cu adsorption from that water sample. The low Cu removal from ground water where the Cu:Mn ratio was 1:63 also corroborates this hypothesis. Nonetheless, these experiments confirm that maghemite NPs can be applied for the remediation of actual AMD-contaminated waters.

Conclusions

Metal contamination of water resources is a growing environmental problem in many mining regions. In addition, increasing pressure on water resources means that demand for technologies for the remediation of contaminated waters will only increase. In this work, the adsorption of Cu, Mn and U ions by maghemite NPs was investigated with the aim of determining NP applicability for the remediation of AMD-contaminated waters. The results show that adsorption at pH 3.3 (±0.2) was rapid and adsorption efficiencies were 56, 53 and 49 % for Cu, Mn and U, respectively.

Adsorption increased in the presence of manganese and sulphate ions, but higher manganese concentrations inhibited Cu sorption. The presence of sulphates, at concentrations similar to those tested here, is therefore likely to increase adsorption of Cu, Mn and U from AMD while manganese may have antagonistic effects on Cu removal by maghemite.

Adsorption was also enhanced at higher pH with removal efficiencies increasing to 86, 62 and 77 % at pH 9 for Cu, Mn and U, respectively. Maghemite NPs can therefore be applied for the removal of Cu, Mn and U from mine drainage both at low and high pH.

Increasing NP concentrations did not, however, always increase adsorbed metal concentrations. Adsorption increased as NP concentration increased from 1 to 3 mg L^{-1} but decreased at 10 mg L^{-1} NP concentrations, likely due to increased agglomeration at higher NP concentrations.

Importantly, work with actual AMD-contaminated surface and groundwater samples confirms that maghemite NPs can indeed be applied for the removal of Cu and Mn from field samples. Although U removal could not be determined due to concentrations below instrument detection capacity, the capability of its removal by maghemite was already established in simulated wastewater. These NPs therefore offer, particularly for Mn, a remediation alternative that does not require pH adjustment or the copious amounts of lime required to achieve this. Low pH waters can, therefore, be directly treated and adjustments to neutral pH would require less time.

The work presented here suggests that metal removal could be optimized based on a combination of pH adjustment and NP concentrations for the treatment of AMD and this is potentially viable for further research. Ongoing work involves quantifying desorption for purposes of re-using NPs in multiple cycles and functionalization of NP surfaces to improve adsorption efficiency.

Acknowledgments A.E. acknowledges funding from the Global Change and Sustainability Research Institute (GCSRI) of the University of the Witwatersrand. We also appreciate the valuable discussions with N. Tavengwa and the contributions of S. Mabaso (ICP analysis) and J. Gerber (Microscopy and Microanalysis Unit).

Open Access This article is distributed under the terms of the Creative Commons Attribution License which permits any use, distribution, and reproduction in any medium, provided the original author(s) and the source are credited.

References

Afkhami A, Norooz-Asl R (2009) Removal, preconcentration and determination of Mo(VI) from water and wastewater samples using maghemite nanoparticles. Colloids Surf A Physicochem Eng Asp 346:52–57. doi:10.1016/j.colsurfa.2009.05.024

Ali MA, Dzombak DA (1996) Interactions of copper, organic acids, and sulfate in goethite suspensions. Geochim Cosmochim Acta 60:5045–5053. doi:10.1016/S0016-7037(96)00311-0

Banerjee SS, Chen D-H (2007) Fast removal of copper ions by gum arabic modified magnetic nano-adsorbent. J Hazard Mater 147:792–799. doi:10.1016/j.jhazmat.2007.01.079

Beattie DA, Chapelet JK, Gräfe M et al (2008) In situ ATR-FTIR studies of SO_4 adsorption on goethite in the presence of copper ions. Environ Sci Technol 42:9191–9196. doi:10.1021/es801767b

Benjamin MM, Leckie JO (1981) Competitive adsorption of Cd, Cu, Zn, and Pb on amorphous iron oxyhydroxide. J Colloid Interface Sci 83:410–419. doi:10.1016/0021-9797(81)90337-4

Benjamin MM, Leckie J (1982) Effects of complexation by Cl, SO_4 and S_2O_3 on adsorption behaviour of Cd on oxide surfaces. Environ Sci Technol 16:162–170. doi:10.1021/es00097a008

Chang Y-C, Chen D-H (2005) Preparation and adsorption properties of monodisperse chitosan-bound Fe_3O_4 magnetic nanoparticles for removal of Cu(II) ions. J Colloid Interface Sci 283:446–451. doi:10.1016/j.jcis.2004.09.010

Collins CR, Vala RK, Sherman DM (1999) Effect of inorganic and organic ligands on the mechanism of cadmium sorption to goethite. Geochim Cosmochim Acta 63:2989–3002. doi:10.1016/S0016-7037(99)00226-4

Das D, Sureshkumar MK, Koley S, et al (2010) Sorption of uranium on magnetite nanoparticles. J Radioanal Nucl Chem 285:447–454. doi:10.1007/s10967-010-0627-0

Foo KY, Hameed BH (2010) Insights into the modeling of adsorption isotherm systems. Chem Eng J 156:2–10. doi:10.1016/j.cej.2009.09.013

Franklin NM, Stauber JL, Markich SJ, Lim RP (2000) pH-dependent toxicity of copper and uranium to a tropical freshwater alga (*Chlorella* sp.). Aquat Toxicol 48:275–289. doi:10.1016/S0166-445X(99)00042-9

Fu F, Wang Q (2011) Removal of heavy metal ions from wastewaters: a review. J Environ Manage 92:407–418. doi:10.1016/j.jenvman.2010.11.011

Grover VA, Hu J, Engates KE, Shipley HJ (2012) Adsorption and desorption of bivalent metals to hematite nanoparticles. Environ Toxicol Chem 31:86–92. doi:10.1002/etc.712

He YT, Wan J, Tokunaga T (2008) Kinetic stability of hematite nanoparticles: the effect of particle sizes. J Nanoparticle Res 10:321–332. doi:10.1007/s11051-007-9255-1

Ho YS, Mckay G (2004) Sorption of copper(II) from aqueous solution by peat. Water Air Soil Pollut 158:77–97. doi:10.1023/B:WATE.0000044830.63767.a3

Hu J, Chen G, Lo IMC (2006) Selective removal of heavy metals from industrial wastewater using maghemite nanoparticle: performance and mechanisms. J Environ Eng 132:709–715. doi:10.1061/(ASCE)0733-9372(2006)132:7(709

James R, Healy T (1972a) Adsorption of hydrolyzable ions at the oxide-water interface. III. A thermodynamic model of adsorption. J Colloid Interface Sci 40:65–81. doi:10.1016/0021-9797(72)90174-9

James R, Healy T (1972b) Adsorption of hydrolyzable ions at the oxide-water interface. I. Co(II) adsorption on SiO_2 and TiO_2 as model systems. J Colloid Interface Sci 40:42–52. doi:10.1016/0021-9797(72)90174-9

Jiang W, Pelaez M, Dionysiou DD et al (2013) Chromium(VI) removal by maghemite nanoparticles. Chem Eng J 222:527–533. doi:10.1016/j.cej.2013.02.049

Jordan N, Ritter A, Foerstendorf H et al (2013) Adsorption mechanism of selenium(VI) onto maghemite. Geochim Cosmochim Acta 103:63–75. doi:10.1016/j.gca.2012.09.048

Khajeh M, Laurent S, Dastafkan K (2013) Nanoadsorbents: classification, preparation, and applications (with emphasis on aqueous media). Chem Rev 113:7728–7768

Kim W, Suh C-Y, Cho S-W et al (2012) A new method for the identification and quantification of magnetite—maghemite mixture using conventional X-ray diffraction technique. Talanta 94:348–352. doi:10.1016/j.talanta.2012.03.001

KTH Royal Institute of Technology (2004) HYDRA/MEDUSA

Kurniawan TA, Chan GYS, Lo W-H, Babel S (2006) Physico-chemical treatment techniques for wastewater laden with heavy metals. Chem Eng J 118:83–98. doi:10.1016/j.cej.2006.01.015

LeVan MD, Vermeulen T (1981) Binary Langmuir and Freundlich isotherms for ideal adsorbed solutions. J Phys Chem 85:3247–3250. doi:10.1021/j150622a009

Li Z, Chen F, Yuan L et al (2012) Uranium(VI) adsorption on graphene oxide nanosheets from aqueous solutions. Chem Eng J 210:539–546. doi:10.1016/j.cej.2012.09.030

Madden AS, Hochella MF, Luxton TP (2006) Insights for size-dependent reactivity of hematite nanomineral surfaces through Cu^{2+} sorption. Geochim Cosmochim Acta 70:4095–4104. doi:10.1016/j.gca.2006.06.1366

Madrakian T, Afkhami A, Rahimi M (2011) Removal, preconcentration and spectrophotometric determination of U(VI) from water samples using modified maghemite nanoparticles. J Radioanal Nucl Chem 292:597–602. doi:10.1007/s10967-011-1453-8

Mohan D, Chander S (2001) Single component and multi-component adsorption of metal ions by activated carbons. Colloids Surf A Physicochem Eng Asp 177:183–196. doi:10.1016/S0927-7757(00)00670-1

Mohan D, Chander S (2006) Single, binary and multicomponent sorption of iron and manganese on lignite. J Colloid Interface Sci 299:76–87. doi:10.1016/j.jcis.2006.02.010

Mohan D, Gupta VK, Srivastava SK, Chander S (2001) Kinetics of mercury adsorption from wastewater using activated carbon derived from fertilizer waste. Coloids Surf A Physicochem Eng Asp 177:169–181

Moyes LN, Parkman RH, Charnock JM et al (2000) Uranium uptake from aqueous solution by interaction with goethite, lepidocrocite, muscovite, and mackinawite: an X-ray absorption spectroscopy study. Environ Sci Technol 34:1062–1068. doi:10.1021/es990703k

Naicker K, Cukrowska E, McCarthy TS (2003) Acid mine drainage arising from gold mining activity in Johannesburg, South Africa and environs. Environ Pollut 122:29–40. doi:10.1016/S0269-7491(02)00281-6

Peacock CL, Sherman DM (2004) Copper(II) sorption onto goethite, hematite and lepidocrocite: a surface complexation model based on ab initio molecular geometries and EXAFS spectroscopy. Geochim Cosmochim Acta 68:2623–2637. doi:10.1016/j.gca.2003.11.030

Persson I (2010) Hydrated metal ions in aqueous solution: how regular are their structures? Pure Appl Chem 82:1901–1917. doi:10.1351/PAC-CON-09-10-22

Roy A, Bhattacharya J (2012) Removal of Cu(II), Zn(II) and Pb(II) from water using microwave-assisted synthesized maghemite nanotubes. Chem Eng J 211–212:493–500. doi:10.1016/j.cej.2012.09.097

Saad DM, Cukrowska EM, Tutu H (2013) Selective removal of mercury from aqueous solutions using thiolated cross-linked polyethylenimine. Appl Water Sci 3:527–534. doi:10.1007/s13201-013-0100-7

Schemel LE, Kimball BA, Bencala KE (2000) Colloid formation and metal transport through two mixing zones affected by acid mine drainage near Silverton, Colorado. Appl Geochem 15:1003–1018. doi:10.1016/S0883-2927(99)00104-3

Swedlund P, Webster J (2001) Cu and Zn ternary surface complex formation with SO_4 on ferrihydrite and schwertmannite. Appl Geochem 16:503–511. doi:10.1016/S0883-2927(00)00044-5

Toens PD, Standler W, Wullschleger NJ (1998) The association of groundwater chemistry and geology with atypical lymphocytes (as a biological indicator) in the Pofadder area. North Western Cape, South Africa 64

Tutu H (2006) Determination and geochemical modelling of the dispersal of uranium in gold-mine polluted land on the Witwatersrand Basin. University of the Witwatersrand

Tutu H, McCarthy TS, Cukrowska E (2008) The chemical characteristics of acid mine drainage with particular reference to sources, distribution and remediation: the Witwatersrand Basin, South Africa as a case study. Appl Geochem 23:3666–3684. doi:10.1016/j.apgeochem.2008.09.002

Tuutijärvi T, Lu J, Sillanpää M, Chen G (2009) As(V) adsorption on maghemite nanoparticles. J Hazard Mater 166:1415–1420. doi:10.1016/j.jhazmat.2008.12.069

Vayssieres L (2009) On the effect of nanoparticle size on water-oxide interfacial chemistry. J Phys Chem C 113:4733–4736. doi:10.1021/jp810721f

Waite TD, Davis JA, Payne TE et al (1994) Uranium(VI) adsorption to ferrihydrite: application of a surface complexation model. Geochim Cosmochim Acta 58:5465–5478. doi:10.1016/0016-7037(94)90243-7

Walter M, Arnold T, Reich T, Bernhard G (2003) Sorption of uranium(VI) onto ferric oxides in sulfate-rich acid waters. Environ Sci Technol 37:2898–2904

Waychunas GA, Zhang H (2008) Structure, chemistry, and properties of mineral nanoparticles. Elements 4:381–388. doi:10.2113/gselements.4.6.381

Wazne M, Meng X, Korfiatis GP et al (2006) Carbonate effects on hexavalent uranium removal from water by nanocrystalline titanium dioxide. J Hazard Mater 166:1415–1420. doi:10.1016/j.jhazmat.2005.11.010

Weber JW, Morris JC (1963) Kinetics of adsorption on carbon from solutions. J Sanit Eng Div Am Soc Civ Eng 89:31–60

Weesner FJ, Bleam WF (1998) Binding characteristics of Pb^{2+} on anion-modified and pristine hydrous oxide surfaces studied by electrophoretic mobility and X-ray absorption spectroscopy. J Colloid Interface Sci 205:380–389. doi:10.1006/jcis.1998.5629

WHO (2011) WHO guidelines for drinking-water quality. WHO Chron 38:564

Winde F (2010) Uranium pollution of the Wonderfonteinspruit, 1997–2008. Part 2: uranium in water—concentrations, loads and associated risks. Water SA 36:257–278

3 Mesoporous silica nanoparticles for the adsorptive removal of Cu(II), Mn(II) and U(VI) from acid mine drainage

Anita Etale[a] *, Hlanganani Tutu[b], Deanne C. Drake[a]

[a] School of Animal Plant and Environmental Sciences, [b] Molecular Sciences Institute, School of Chemistry, University of the Witwatersrand, Private Bag X3, WITS 2050, Johannesburg, South Africa.

The adsorption of Cu(II), Mn(II) and U(VI) ions by mesoporous silica nanoparticles (NPs) was investigated with the aim of assessing the potential of NPs for remediating acid mine drainage (AMD)-contaminated water. Adsorption reactions were found to be rapid, attaining equilibrium within 5 minutes for Cu and less than a minute for Mn and U. Calculated adsorption rates based on the pseudo-second order model (R^2= 0.99) showed that the Mn adsorption was >3 times faster Cu and 7 times faster than U. Adsorption increased with pH and temperature, and $\Delta G°$ and $\Delta H°$ values indicate that the process was spontaneous and endothermic. Isotherm data were best described by the Freundlich and Temkin models (R^2= 0.99), with chemisorption responsible for the removal of Cu and Mn, and adsorption and precipitation for U removal. Importantly, ferric, manganese and sulphate ions increased adsorption from 52, 56 and 49% to 77, 66 and 76% for Cu, Mn and U, respectively. Cu removal was, however, inhibited in 1:2 Cu: Mn solutions. NPs were then applied to actual AMD contaminated ground and surface water. As in simulated wastewater, adsorption was higher for Mn than Cu and removal efficiencies of up to 60% for Mn and 34% for Cu were attained. These NPs can therefore be applied for removal of Cu, Mn and U from AMD-contaminated water. Importantly, they offer an alternative for Mn removal that precludes pH adjustment and the copious amounts of lime required for that.

Key words: adsorption, metal pollution, copper, manganese, uranium

*Corresponding author. Telephone: +27 11 717 6425; Email address: aetale@gmail.com

3.1 Introduction

Mining, despite its economic benefits, often results in significant environmental damage (Nriagu 1988). Gold mining in the Witwatersrand region of South Africa, for example, has resulted in severe contamination of ground and surface water by metal laden acid mine drainage (AMD) (Rösner and van Schalkwyk 2000; Naicker et al. 2003; Tutu et al. 2008; Durand 2012). Metal contamination is of particular concern because of the negative effects of excessive metal concentrations on humans and aquatic organisms (Iwasaki et al. 2009; Georgopoulos et al. 2011), necessitating the remediation of contaminated water. A number of techniques including chemical precipitation, bioremediation, adsorption and ion exchange exist for the removal of metal ions from AMD-contaminated water. Adsorption is widely investigated due to its lower costs and the wide range of adsorbents available including agricultural wastes, fly ash and activated carbon (Babel and Kurniawan 2003). Lately, the use of nanomaterials as adsorbents has garnered much interest because nanomaterials present an alternative free of some of the limitations of other adsorbents such as low adsorption capacity and slow uptake rates. This is because the higher reactivities and large surface area to volume ratios of these materials facilitate greater adsorption rates and efficiencies (Waychunas and Zhang 2008). Engates and Shipley (2011) for example, noted that metal adsorption was >5 times faster with titania NPs (8.3 nm) than with bulk particles (329.8 nm).

Nanoparticles (NPs) of various metal oxides including iron, aluminium, titanium and manganese have been extensively investigated for metal removal (see review by Hua et al. (2012)). Silica NPs are also widely researched (Michard et al. 1996; Bois et al. 2003; Mureseanu et al. 2008; Benhamou et al. 2009; Wu et al. 2009; Ramadan et al. 2010; Lee et al. 2011; Quang et al. 2012). For metal removal from AMD, silica NPs are especially appropriate because their low pH_{PZC} (pH 2-3) (Kosmulski 2009) means particles are negatively charged at the low pH of AMD (often ≤ 3), and thus primed for cation adsorption. Results of many previous studies are, however, not applicable to AMD conditions because of (i) the higher pH at which they were conducted, and (ii) the effects of ions abundant in AMD and with potential to influence adsorption e.g. sulphates, ferric and manganese ions were not studied. Further, despite it being a prevalent contaminant in gold mining regions due to its association with auriferous ores, the removal of U under AMD conditions is less studied. U contamination is particularly significant in the Witwatersrand gold fields with concentrations as high as 72.7 mg L^{-1} reported by Tutu et al. (2008).

The aim of this study was therefore to generate an AMD-relevant understanding of the sorption action of silica NPs for Cu, Mn and U, in order to facilitate an assessment of their

suitability for remediation of AMD-contaminated Witwatersrand waters. Using commercially prepared silica NPs and low pH metal solutions, we quantified the effects of time, metal concentration, NP concentrations, temperature and Fe^{3+}, Mn^{2+} and SO_4^{2-} ions on adsorption of these ions. The process was also studied at higher pH in order to determine process efficiency in pH-amended mine drainage.

3.2 Experimental

3.2.1 Adsorbent characterisation

The size and morphology of silica NPs (Sigma Aldrich; Schnelldorf, Germany) were investigated by transmission electron microscopy (FEI Tecnai G^2 Spirit TEM). 0.1 g of particles was suspended in 100 mL deionised waster and sonicated for 30 minutes. A drop of the suspension was placed on a lacey copper grid and left to dry for 20 minutes before analysis. Fourier Transform Infra Red (FTIR) spectra of NPs were collected in the 4000-500 cm^{-1} frequency range on a Bruker Tensor 27 IR spectrophotometer (Massachussets, USA). The specific surface area and porosity of particles were determined by the BET (Brunauer-Emmett-Teller) and BJH (Barret-Joyner-Halenda) methods using a Micrometrics Tristar 3000 (Micrometrics Instruments, USA).

3.2.2 Adsorption studies

All metal salts used were analytical grade. Copper nitrate ($Cu(NO_3)_2 \cdot 2.5\ H_2O$) and manganese nitrate ($Mn(NO_3)_2 \cdot H_2O$) were from Sigma Aldrich (Schnelldorf, Germany). Uranyl nitrate ($UO_2(NO_3)_2 \cdot 6H_2O$), ferric nitrate ($Fe(NO_3)_3 \cdot 9H_2O$) and disodium sulphate (Na_2SO_4) were from Ace Chemicals (Johannesburg, South Africa).

Stock metal solutions (1000 mg L^{-1}) were prepared by dissolving appropriate masses of metal salts in deionised water. NP suspensions (3 mg L^{-1}) were prepared by 30-minute water bath sonications. Where necessary, the pH of metal solutions and NP suspensions was adjusted prior to experiments using 0.01 M HNO_3 and 0.01 M NaOH. All experiments were carried out in triplicate, at pH 3.0 (± 0.2) and ambient temperature (25 ± 2°C).

Metal adsorption was studied in batch experiments using 13.11 mg Cu L^{-1}, 7.55 mg Mn L^{-1} and 42.18 mg U L^{-1} solutions. Freshly sonicated NP suspensions (10 mL) were reacted with 10 mL metal nitrate solutions in 50 mL polyethylene terephthalate (PET) jars for 60 minutes. A similar procedure was followed for surface and ground water samples except without pH adjustment. Surface water was collected on two occasions from the Tweelopiespruit, a stream into

which a mine shaft decants (26°50'21.67"S, 27°42'57.49"E). The first sampling site was approximately 500 m downstream of the second. Groundwater was from a well 650 m away from the stream (26°05'32.6"S, 27°42'44.6"E).

The effect of contact time was evaluated for durations ranging from 5 seconds to 60 minutes. The effects of Fe^{3+}, Mn^{2+} and SO_4^{2-} ions, introduced as $Fe(NO_3)_3 \cdot 9H_2O$), $Mn(NO_3)_2 \cdot H_2O$ and Na_2SO_4, respectively, were quantified for 1:1 and 1:2 molar ratios to the test ion. At the end of experiments, mixtures were filtered and filtrates acidified with 3 mL 1% HNO_3. Metal concentrations in filtrates were determined by Inductively Coupled Plasma-Optical Emission Spectrometry (ICP-OES; Spectro Instruments, Kleve, Germany). Adsorption efficiencies were determined by mass balance calculations. The equilibrium adsorption capacity of NPs (q_e; mg g^{-1}) was calculated using equation 1 (Lee et al. 2011) where C_i and C_e are the initial and equilibrium metal ion concentrations (mg L^{-1}), m is the mass of adsorbent (g) and V is the volume of adsorbent solution used (L).

$$q_e = \frac{(C_i - C_e)V}{m} \quad (1)$$

3.2.3 Data analysis

Kinetics

Kinetics data were fitted to the pseudo-first-order model (equation 2) and the pseudo-second-order model (equation 3) where q_e and q_t are the NP metal loading capacities (mg g^{-1}) at equilibrium and at time t, respectively (Ho and Mckay 2004). The rate constants, k_1, and k_2 were determined from the slope and intercept of the plots of the equations plotted as follows: log (q_e– q_t) versus t for the pseudo-first-order model and t/q_t versus t for the pseudo-second-order model.

$$\log(q_e - q_t) = \log q_e - \left(\frac{k_1}{2.303}\right)t \quad (2)$$

$$\frac{t}{q_t} = \left(\frac{1}{k_2}\right) + \left(\frac{1}{q_e}\right)t \quad (3)$$

Isotherms

Isotherm data were fitted to the Langmuir, Freundlich and Temkin models (Aharoni and Ungarish 1977; LeVan and Vermeulen 1981). The Langmuir model, which best describes monolayer adsorption, is underlain by assumptions such as the absence of adsorbate interactions. Its linear form is given in equation 4 where q_{max} is the maximum concentration of metal ions

sorbed per unit weight of NPs (mg g^{-1}) and K_L (L mg^{-1}) is the Langmuir constant for the reaction. q_{max} and K_L were determined from the intercept and slope of the plot of C_e/q_e versus C_e.

$$\frac{C_e}{q_e} = \left(\frac{1}{q_{\max}}\right) C_e + \left(\frac{1}{K_L q_{\max}}\right) \quad (4)$$

The Freundlich model on the other hand, accommodates multi-layer adsorption. It is expressed by equation 5, where K_F and $1/n$ are constants specific to each reaction. K_F ((mg g) (L mg)$^{1/n}$) is the adsorption value at unit concentration and $1/n$ is related to the adsorption intensity and heterogeneity of the sorbent surface (Foo and Hameed 2010). These constants were deduced from the intercept and slope, respectively, of a plot of log q_e versus log C_e.

$$\log q_e = \left(\frac{1}{n}\right) \log C_e + \log K_F \quad (5)$$

The Temkin model takes into account the effects of adsorbate interactions excluded by the Langmuir model. It assumes that the heat of adsorption decreases linearly as adsorption increases due to these interactions. It is represented by equation 6 where R is the gas constant (8.3145 J mol^{-1} K^{-1}), T is the absolute temperature, b_T is the variation in adsorption energy (J mol^{-1}) and A_T is the equilibrium binding constant (L mg^{-1}). b_T and A_T were deduced from the slope and intercept of a plot of q_e versus ln C_e.

$$q_e = \frac{RT}{b_T} \ln C_e + \frac{RT}{b_T} \cdot \ln A_T \quad (6)$$

Thermodynamics

The effect of temperature on adsorption at pH 3 was assessed at temperatures ranging from 293-310 K. The standard Gibbs free energy (ΔG^o) was calculated using equation 7 where R is as given above and K is the experimental temperature in Kelvin. K_c was calculated using equation 8 where C_{ads} is the adsorbed metal concentration at equilibrium.

$$\Delta G^o = -RT \ln K_c \quad (7)$$

$$K_c = \frac{C_e}{C_{ads}} \quad (8)$$

The standard enthalpy (ΔH^o) and entropy (ΔS^o) of reactions were then deduced from the slope and intercept of a plot of Van't Hoff's equation (equation 9) i.e. ln K_c versus $1/T$.

$$\ln K_c = -\frac{\Delta H^o}{R} \cdot \frac{1}{T} + \frac{\Delta S^o}{R} \quad (9)$$

3.3 Results and discussion

3.3.1 Particle characterisation

Transmission electron micrographs (Figure 3.1a) revealed polydisperse porous silica particles with diameters in the < 20 - 50 nm range. The average BET surface area of particles was determined as 612 m^2 g^{-1} and the average pore diameter as 4 nm, indicating that particles were mesoporous (Sing et al. 1985). FTIR spectra (Figure 3.1b) consisted of two distinct frequency regions: 4000-2500 nm and 1700-400 nm, which confirmed the silica composition of the NPs i.e. a broad adsorption band in the 4000-2500 nm region due to O-H vibrations from adsorbed or molecular water and one in the 1700-400 nm range due to Si-OH vibration and stretching modes (Swann and Patwardhan 2011).

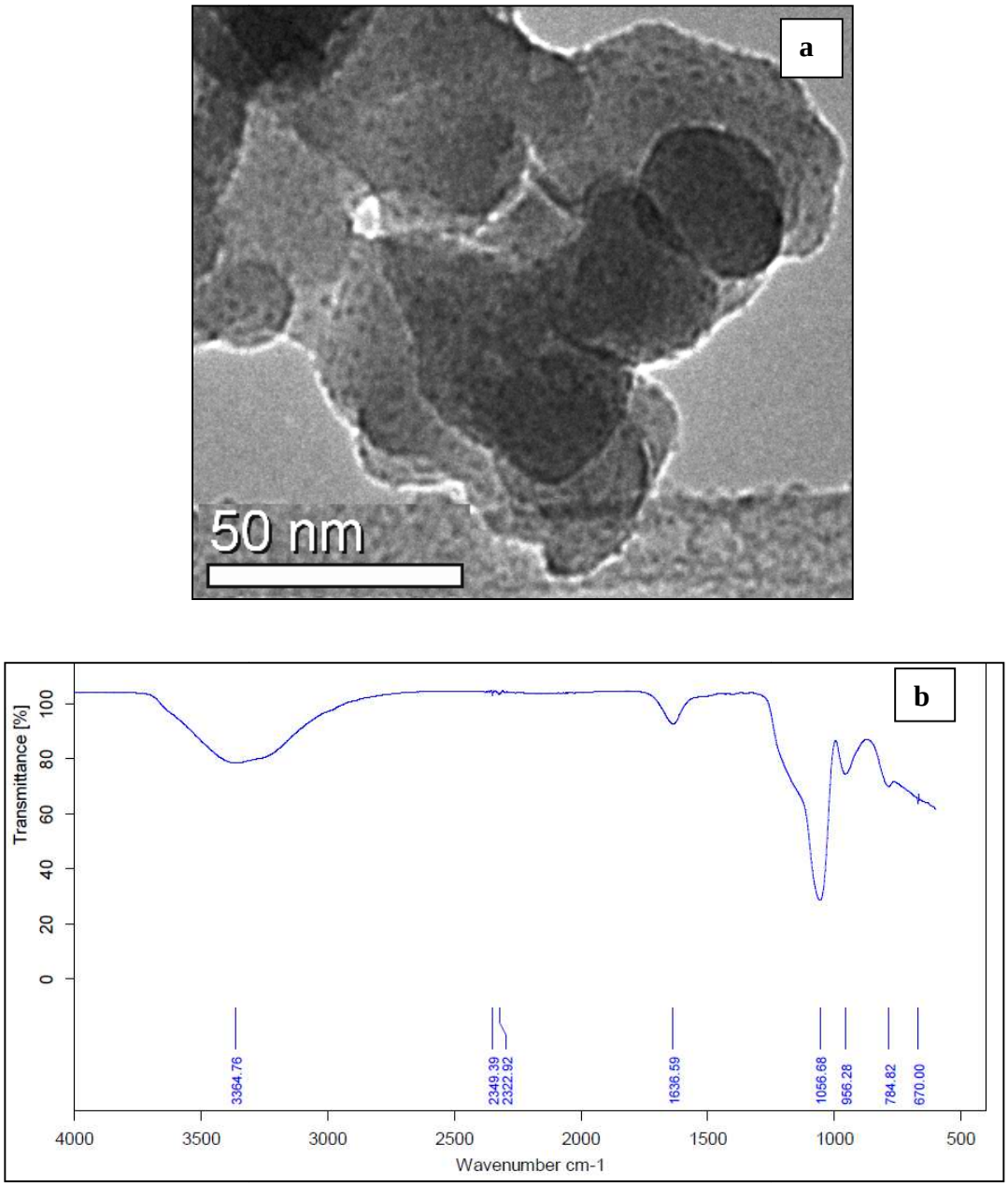

Figure 3.1: Transmission electron micrograph (a) and FTIR spectra (b) of silica NPs

3.3.2 Effect of adsorbent concentration

The optimal adsorbent concentration for experiments was determined by reacting metal solutions with 1, 3, 5 and 9 mg L^{-1} silica NP suspensions for 60 minutes. The results (Figure 3.2) show that adsorbed metal concentrations increased and then decreased, albeit slightly, with

increasing adsorbent concentrations. Peak adsorption for all three metals corresponded with a 3 mg L^{-1} NP concentration. This NP concentration was therefore used for subsequent experiments.

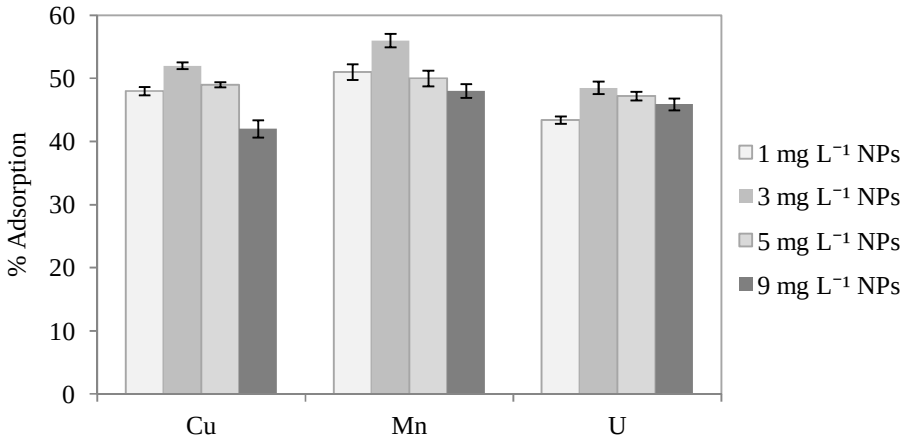

Figure 3.2: The effect of adsorbent concentration on adsorption of Cu, Mn and U to silica NPs at pH 3 (±SD)

Reduced adsorption at higher NP concentrations was likely the result of NP agglomeration which reduces access to sorption sites. Agglomeration is affected by, among other things, (i) high NP concentrations which increases NP collisions (Handy et al. 2008) and (ii) solution pH (Guzmán et al. 2006). As solution pH approaches pH_{PZC}, repulsive surface charges decrease, thus increasing NP coalescence.

3.3.3 Effect of contact time

The effect of contact time on adsorption was studied at time durations ranging from five seconds to 60 minutes. As shown in Figure 3.3, reactions were rapid and equilibrium was attained in five minutes for Cu and within a minute for Mn and U. Rapid adsorption rates were also reported in other investigations including those of Lee and Yi (2007), Xue and Li (2008) and Akhbarizadeh et al. (2013). Brown et al. (1999) proposed that the phenomenon is due to the higher number of surface atoms and defects such as kinks and edges that are more reactive.

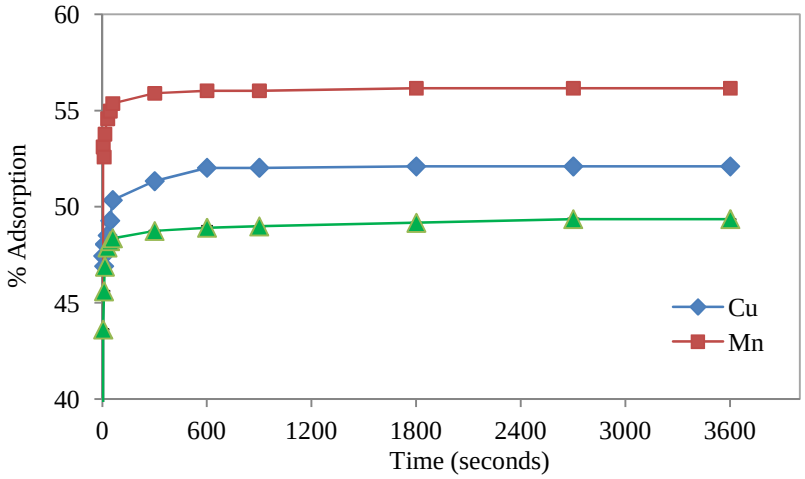

Figure 3.3: The effect of contact time on the adsorption of Cu, Mn and U by silica NPs (±SD)

Kinetics data were better described by the pseudo second-order model than the pseudo-first-order model (Table 3.1). The highest initial adsorption rate (h) and equilibrium adsorption concentration (q_e) were recorded for U due to greater mass transfer action from higher initial concentrations (Ho and Mckay 2004). However, the overall adsorption rate (k_2), was highest for Mn, despite the fact that higher concentrations of Cu and U should have resulted in greater driving forces and faster rates for Cu and U. Indeed, the Mn adsorption rate was >3 times faster than that of Cu and 7 times faster than that of U. We surmise that the structural configuration of sorption sites on NP surfaces was more favourable to Mn ions than Cu and U. This hypothesis was put forward by Madden and Hochella (2005) who found that certain binding environments stabilized the distorted octahedron of Mn^{3+} relative to the perfect octahedron of Mn^{2+}. Thus, steric hindrances and configurational disadvantages may have slowed down the adsorption of Cu and U to sorption sites, and eventually reduced their equilibrium adsorption efficiencies.

Table 3.1: Adsorption rate constants and coefficients of correlation (R^2) for kinetics models fitted to adsorption data.

Metal	Initial concentration (mg L^{-1})	Pseudo-second order model				Pseudo-first order model
		R^2	k_2 (mg g^{-1} sec^{-1})	h (mg $g^{-1}sec^{-1}$)	q_e (mg g^{-1})	R^2
Cu	13.11	1	0.02	11.99	22.78	0.75
Mn	7.55	1	0.07	14.04	14.14	0.74
U	42.18	1	0.01	28.57	69.44	0.89

3.3.4 Effect of initial metal concentrations

The adsorption capacity of silica NPs for the three test ions at pH 3 was studied using metal concentrations ranging from 13.11 - 127 mg L^{-1} for Cu, 7.55 – 84 mg L^{-1} for Mn and 4.46-464 mg L^{-1} for U. for all three metal ions, equilibrium NP loading (q_e) increased with initial metal concentrations (Figure 3.4). This, as noted earlier, was due to greater driving forces at higher initial concentrations, for mass transfer to the adsorbent surface (Ho and Mckay 2000).

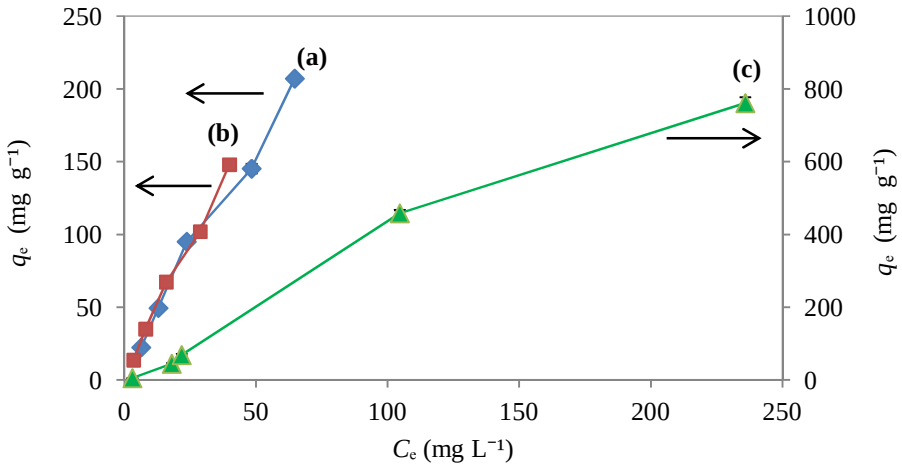

Figure 3.4: The effect of initial metal concentration on adsorption of Cu (a), Mn (b) and U (c) (±SD) by silica NPs

Isotherm data were better described by the Freundlich and Temkin models (Table 3.2). The following conclusions can therefore be made concerning the adsorption of test ions to silica NPs: (i) sorption sites on the silica surface were energetically heterogeneous (ii) metal ions formed more than one layer on the silica surface (iii) adsorbate-adsorbate interaction influenced

adsorption (iv) the adsorption energy decreased linearly with increasing adsorption. In addition, K_F values revealed that, under the experimental conditions, the sorption capacity of silica NPs was much lower for U than Cu and Mn. This is largely a factor of space utilization by adsorbed ions. With a diameter of 6.5 Å (Krestou et al. 2003), the hydrated U ion occupies more space than Cu (4.19 Å) and Mn (4.38 Å) ions (Nightingale 1959). It is also noteworthy that adsorption of Mn exceeds that of Cu, the smaller size of the latter ion notwithstanding. A possible explanation for this has been put forward in section 3.3.2.

With respect to 1/*n* values, the <1 values for Cu and Mn imply chemisorption processes for these ions. The >1 1/*n* value for U, in contrast, is indicative of a cooperative removal processes i.e. adsorption and precipitation (Foo and Hameed 2010); a conclusion corroborated by the findings of Michard et al. (1996).

Table 3.2: Parameters of adsorption isotherms fitted to adsorption data.

Metal	Freundlich isotherm			Temkin isotherm			Langmuir isotherm
	R^2	K_F (mg g^{-1}) (L $mg^{-1})^{1/n}$	1/*n*	R^2	A_T (L g^{-1})	b_T (MJ mol^{-1})	R^2
Cu	0.99	4.06	0.95	0.95	1.58×10^4	1.9	0.60
Mn	0.99	4.45	0.95	0.92	2.46×10^4	2.5	0.44
U	0.99	1.44	1.19	0.83	6.91×10^4	3.2	0.28

3.3.5 Effects of Fe^{3+}, Mn^{2+} and SO_4^{2-} ions

The effects of Fe^{3+}, Mn^{2+} and SO_4^{2-} ions on the adsorption of Cu, Mn and U were investigated at pH 3. The effects of all three additional ions were tested for Cu and U, but only Fe^{3+} and SO_4^{2-} effects were investigated for Mn. As shown in Figure 3.5a and b, ferric and sulphate ions increased the adsorption of all three test ions in the order U > Cu > Mn. The effect of manganese ions was, however, varied i.e. increasing U adsorption increased in both equimolar and 1:2 systems, but inhibiting Cu adsorption in 1:2 Cu/Mn systems (Figure 3.5c).

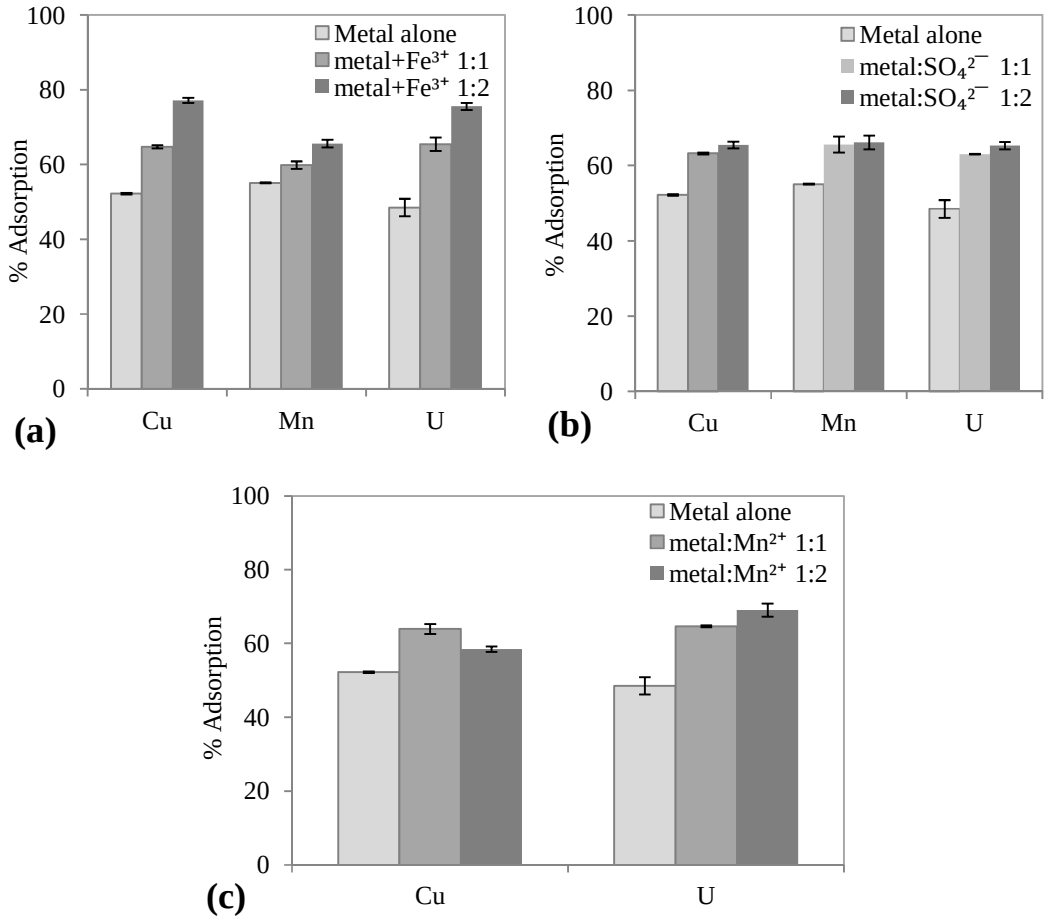

Figure 3.5: The effect of Fe^{3+} (a), SO_4^{2-} (b) and Mn^{2+} (c) ions on the adsorption of Cu, Mn and U by silica NPs (±SD) at pH 3

To explain these observations, metal speciation at variable pH was deduced using MEDUSA software (KTH Royal Institute of Technology 2004). Results indicated that Cu formed a $CuFe_2O_4$ precipitate in the presence of ferric ions (Supplementary Figure 1a), to which the increase in Cu removal may be ascribed. However, no complex was formed with Mn and U. The slight increases in adsorption may be due to additional sorption sites availed by the Fe_2O_3 phase (Supplementary Figure 1b). Sulphates, on the other hand, likely enhanced adsorption by lowering the energy barrier for the approach of ions to the adsorbent surface (James and Healy 1972b) or the formation of more adsorbable species (Benjamin and Leckie 1982). Kosmulski (1999) also suggested that where anion concentration was higher than metal concentrations, adsorption may be enhanced by the formation of ternary surface complexes.

With respect to manganese and its concentration-dependent effects on Cu sorption, we surmise that both ions sorb to similar sites on the silica surface (Benjamin and Leckie 1981). Competition for sorption sites thus ensued in mixed solutions and Cu sorption was inhibited due to the faster sorption rate and possible configurational advantages of Mn (see discussion in section 3.3.2 above). Inhibition is, however, not evident in equimolar solutions due to availability of sorption sites.

3.3.6 Effect of pH

Adsorption was studied at higher pH in order to determine the efficiency of the process in contaminated waters whose pH has been amended intentionally or by natural processes like precipitation. As shown in Figure 3.6, adsorption of all three ions increased with solution pH. Copper adsorption increased from 52% at pH 3 to 94 and 99% at pH 7 and 9, respectively. Increases in manganese adsorption, on the other hand, were modest: only 5.7% across the test pH range. The maximum adsorption of U (77%) was recorded at pH 7 and 9 due to the dominance of $(UO_2)_2(OH)_2^{2+}\cdot H_2O$ in solution from pH 6.

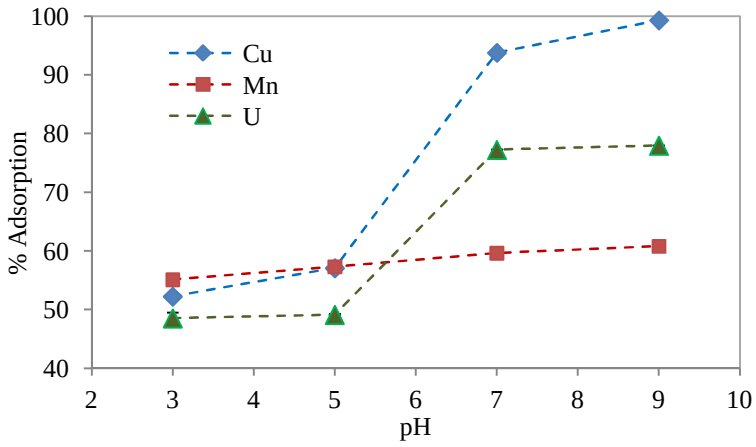

Figure 3.6: The effect of pH on adsorption of Cu, Mn and U to silica NPs (±SD).

Just as reported by James and Healy (1972a) and Krestou et al. (2003), increases in adsorption coincided with the onset of hydrolysis and the formation of more adsorbable species like $Cu(OH)_2$ and $UO_2(OH)_2$. Removal of all three ions was also influenced by declining competition from H^+ ions as pH increased. Solution pH also influenced adsorbent properties i.e. (i) the silica surface became more negatively charged and thus favourable for cation adsorption (ii) NPs experienced less aggregation resulting in greater access to sorption sites (Guzmán et al. 2006); (iii) increased silica dissolution increased the population of available sorption sites (Kosmulski 2000). Indeed,

changes in adsorbent surface properties may be responsible for the slight increases in Mn adsorption since it did not hydrolyze in the test pH range. Hydrolysis does not, however, guarantee maximum adsorption. Krestou et al. (2003) suggested that U adsorption may not attain high efficiencies due to the non-adsorption of (i) poly-nuclear species like $(UO_2)_2(OH)_2^{2+}$ and $(UO_2)_3(OH)_5^{+}$ (ii) uranyl carbonate species. Sorption efficiencies presented here are similar to those reported by Štamberg et al. (2003) in the presence of carbonates (75%) and although they do not attain the 95% removal efficiencies of carbonate-free systems, they provide a more accurate picture for *in-situ* operations.

3.3.7 Effect of temperature

The effect of temperature on adsorption was investigated at 293, 298, 303 and 310 K. Adsorption increased with temperature from 49 to 58% for Cu, 54 to 61% for Mn and 45 to 56% for U; implying that adsorption of these ions to sites on the silica surface was an endothermic process (Table 3.3). $\Delta G°$ values were negative; indicating that adsorption was spontaneous and thermodynamically favourable. Increasing negativity of $\Delta G°$ with temperature also indicates increased adsorption at higher temperatures. With respect to $\Delta S°$ and $\Delta H°$, their positive values corroborate the findings on the spontaneity and endothermic nature of adsorption reactions. Similar results were reported for Cu and Mn to kaolinite (Yavuz et al. 2003) and U to tin oxide NPs (Nilchi et al. 2013).

Table 3.3: Thermodynamic parameters for the adsorption of Cu, Mn and U to silica NPs.

Metal	$\Delta G°$ (kJ mol^{-1})				$\Delta H°$ (kJ mol^{-1})	$\Delta S°$ (J mol^{-1} K^{-1})	R^2
	293K	298K	303K	310K			
Cu	-3.38	-3.69	-3.91	-4.33	18.32	9.01	0.99
Mn	-4.17	-4.39	-4.61	-4.95	15.26	8.09	0.99
U	-0.02	-0.42	-0.73	-1.15	21.95	9.03	0.99

3.3.8 Adsorption mechanism

Adsorption takes place in a number of stages including the transfer of solute molecules from the bulk solution to the exterior of the adsorbent surface, film diffusion, adsorption to sites on the exterior surface and within pores. Solute transfer in bulk solution is generally a rapid process while film diffusion likely controls the adsorption rate only in the early stages of the reaction. In porous sorbents such as the one applied here, transport to sorption sites within pores controls the

adsorption rate. To investigate the possibility of this, kinetics data were fitted to the intraparticle diffusion model of Weber and Morris (1963) (equation 10) where the intraparticle diffusion rate, k_{ipd} (mg g^{-1} $sec^{0.5}$) is determined from the slope of a plot of q_t versus $t^{0.5}$. If intraparticle diffusion is the only rate controlling step, the intercept (C) is at the origin. Where $C > 0$, both external mass transfer and pore-diffusion control the adsorption rate.

$$q_t = k_{ipd} \cdot (t^{0.5}) + C \qquad (10)$$

Figure 3.7 shows the plot for Cu; Mn and U plots were similar. A tri-linearity is evident, indicating a three-step adsorption. The first steep linearity can be assigned to external surface adsorption, the second to intraparticle diffusion and the third to the equilibrium stage (Ramadan et al. 2010). As the second line does not pass through the origin, intraparticle diffusion is not the sole rate controlling step. Such a conclusion is plausible because NP pores, with diameter of 4 nm, access of the hydrated test ions would not be impeded. Overall therefore, adsorption rates were determined both by external mass transfer and intraparticle diffusion.

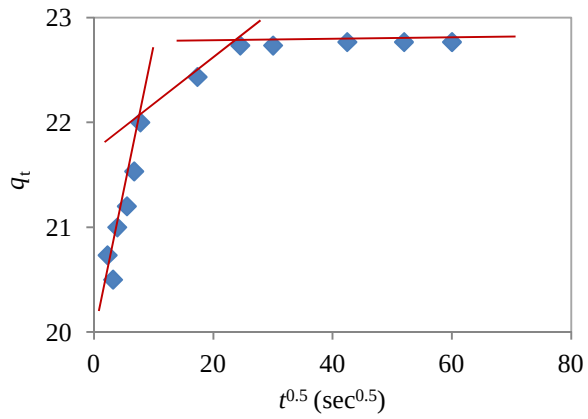

Figure 3.7: Intraparticle diffusion plot for adsorption of Cu to silica NPs at pH 3

3.3.9 Application studies

Silica NPs were then applied for the removal of these three ions from fields samples of AMD-contaminated surface and ground water. The physical and chemical characteristics of the surface water samples (SW1 and SW2) and groundwater sample (GW) are presented in Table 3.4. The chemical signatures of the two surface water samples are variable likely due to a dilution effect from rainfall events shortly before the SW2 sample was collected.

Table 3.4: Physico-chemical characteristics of contaminated water used in application studies.

Sample	pH	Conductivity (mS cm^{-1})	Redox potential (mV)	$[Cu]_{tot}$ (mg L^{-1}) (SD)	$[Mn]_{tot}$ (mg L^{-1}) (SD)	$[U]_{tot}$ (mg L^{-1})
SW1	3.13	3.52	209.0	1.44 (0.003)	49.74 (0.002)	b.d
SW2	2.79	3.87	227.7	1.22 (0.046)	16.48 (0.006)	b.d
GW	5.62	2.76	6.9	0.24 (0.001)	15.00 (0.140)	b.d

The results of adsorption experiments are shown in Figure 3.8. Just as with experiments using simulated wastewater, more Mn than Cu was adsorbed. This further strengthens the hypothesis that Cu and Mn bind to similar sites on silica. Competition for sorption sites, however, also depends on aqueous concentrations and therefore more Mn was adsorbed due to its higher concentrations. Cu adsorption was higher in the SW2 than SW1sample due to the lower Cu:Mn ratio in the former (Table 3.4). The lowest Cu adsorption was in the groundwater sample where the Mn concentration was 63 times that of Cu.

Mn removal is often challenging because its late hydrolysis necessitates copious amounts of lime (CaO) for pH adjustment (Johnson and Hallberg 2005). Silica NPs therefore offer an alternative that circumvents the need for prior pH adjustment; and, depending on the initial concentrations, low Mn concentrations may be achieved in a few adsorption cycles.

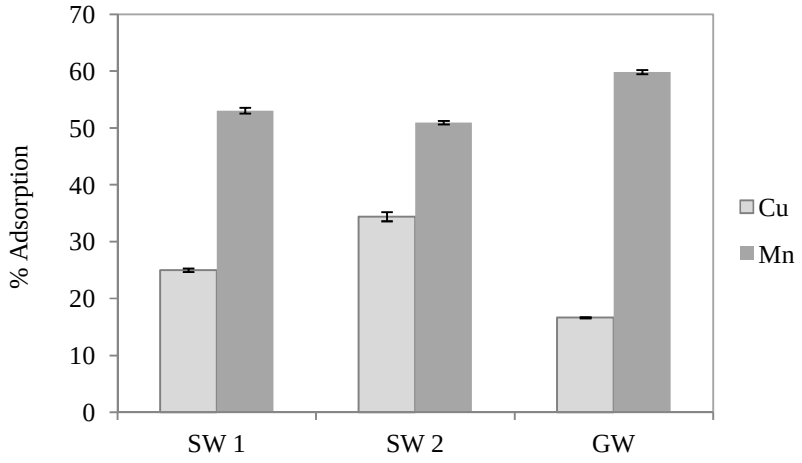

Figure 3.8: Removal efficiencies of Cu and Mn from contaminated surface and groundwater by silica NPs. No readings were recorded for U due to below-detection concentrations in water samples

3.4 Conclusions

We studied the adsorption of Cu, Mn and U by mesoporous silica NPs with the aim of determining their applicability for the remediation of AMD contaminated waters. The adsorption of metal ions was rapid and overall adsorption rates were fastest for Mn than Cu or U. Notably, metal removal did not always increase with adsorbent concentrations as is usually the case with larger-sized adsorbents. The effects of agglomeration on process efficiency were evident in solutions with 5 and 9 mg L^{-1} NP concentrations.

Metal adsorption increased with temperature and initial metal concentrations, and isotherms were better described by the Freundlich and Temkin isotherms. Ferric, manganese and sulphate ions increased process efficiencies although Cu removal was inhibited in solutions with a 1:2 Cu:Mn ratios. Metal removal from contaminated field samples was similar to that in simulated wastewater with respect to Cu and Mn removal i.e. more Mn than Cu was removed from solution, thus supporting the hypothesis that these ions bind to similar sites on the silica surface. Adsorption increased with pH, with Cu exhibiting the highest increase followed by U and then Mn. Removal at pH 3 will therefore yield better results for Mn and U than Cu, but the opposite will apply for higher pH waters where hydrolysis and precipitation will facilitate greater removal of Cu and U.

3.5 Acknowledgements

Funding for this work was provided by the Global Change and Sustainability Research Institute (GCSRI) of the University of Witwatersrand in the form of a PhD fellowship to AE. We also acknowledge the contributions of Kirstin Olsen with field sampling, Siyethemba Mabaso with ICP-OES analyses and Jacques Gerber of the Microscopy and Microanalysis Unit.

3.6 References

Aharoni, C. & Ungarish, M. 1977. Kinetics of activated chemisorption. Part 2.-Theoretical models. *Journal of the Chemical Society, Faraday Transactions 1*. 73:456–464.

Akhbarizadeh, R., Shayestefar, M.R. & Darezereshki, E. 2013. Competitive removal of metals from wastewater by maghemite nanoparticles: A comparison between simulated wastewater and AMD. *Mine Water and the Environment*. 33(1):89–96.

Babel, S. & Kurniawan, T.A. 2003. Low-cost adsorbents for heavy metals uptake from contaminated water: a review. *Journal of Hazardous Materials*. 97(1-3):219–243.

Benhamou, A., Baudu, M., Derriche, Z. & Basly, J.P. 2009. Aqueous heavy metals removal on amine-functionalized Si-MCM-41 and. *Journal of Hazardous Materials*. 171:1001–1008.

Benjamin, M.M. & Leckie, J. 1982. Effects of complexation by Cl, SO_4 and S_2O_3 on adsorption behaviour of Cd on oxide surfaces. *Environmental Science & Technology*. 16(3):162–170.

Benjamin, M.M. & Leckie, J.O. 1981. Competitive adsorption of Cd, Cu, Zn, and Pb on amorphous iron oxyhydroxide. *Journal of Colloid and Interface Science*. 83(2):410–419.

Bois, L., Bonhommé, A., Ribes, A., Pais, B., Raffin, G. & Tessier, F. 2003. Functionalized silica for heavy metal ions adsorption. *Colloids and Surfaces A: Physicochemical and Engineering Aspects*. 221(1-3):221–230.

Brown, G.E., Henrich, V.E., Casey, W.H., Clark, D.L., Eggleston, C., Felmy, A., Goodman, D.W., Grätzel, M., et al. 1999. Metal oxide surfaces and their interactions with aqueous solutions and microbial organisms. *Chemical Reviews*. 99(1):77–174.

Durand, J.F. 2012. The impact of gold mining on the Witwatersrand on the rivers and karst system of Gauteng and North West Province, South Africa. *Journal of African Earth Sciences*. 68:24–43.

Engates, K.E. & Shipley, H.J. 2011. Adsorption of Pb, Cd, Cu, Zn, and Ni to titanium dioxide nanoparticles: effect of particle size, solid concentration, and exhaustion. *Environmental Science and Pollution Research*. 18(3):386–395.

Foo, K.Y. & Hameed, B.H. 2010. Insights into the modeling of adsorption isotherm systems. *Chemical Engineering Journal*. 156:2–10.

Georgopoulos, P.G., Roy, A., Opiekun, R.E. & Lioy, P.J. 2011. Environmental copper: Its dynamics and human exposure issues. *Journal of Toxicology and Environmental Health , Part B : Critical Reviews*. 4(4):341–394.

Guzman, K.A.D., Finnegan, M.P. & Banfield, J.F. 2006. Influence of surface potential on aggregation and transport of titania nanoparticles. *Environmental Science & Technology*. 40(24):7688–7693.

Handy, R.D., von der Kammer, F., Lead, J.R., Hassellöv, M., Owen, R. & Crane, M. 2008. The ecotoxicology and chemistry of manufactured nanoparticles. *Ecotoxicology*. 17(4):287–314.

Ho, Y.S. & Mckay, G. 2000. The kinetics of sorption of divalent metal ions onto sphagnum moss peat. *Water Research*. 34(3):735–742.

Ho, Y.S. & Mckay, G. 2004. Sorption of copper(II) from aqueous solution by peat. *Water Air and Soil Pollution*. 158:77–97.

Hua, M., Zhang, S., Pan, B., Zhang, W., Lv, L. & Zhang, Q. 2012. Heavy metal removal from water / wastewater by nanosized metal oxides: A review. *Journal of Hazardous Materials*. 212:317–331.

Iwasaki, Y., Kagaya, T., Miyamoto, K.-I. & Matsuda, H. 2009. Effects of heavy metals on riverine benthic macroinvertebrate assemblages with reference to potential food availability for drift-feeding fishes. *Environmental Toxicology and Chemistry*. 28(2):354–363.

James, R.O. & Healy, T.W. 1972a. Adsorption of hydrolyzable metal ions at the oxide—water interface. III. A thermodynamic model of adsorption. *Journal of Colloid and Interface Science*. 40(1):65–81.

James, R.O. & Healy, T.W. 1972b. Adsorption of hydrolyzable metal ions at the oxide—water interface. I. Co(II) adsorption on SiO_2 and TiO_2 as model systems. *Journal of Colloid and Interface Science*. 40(1):42–52.

Kosmulski, M. 1999. Adsorption of trivalent cations on silica. *Journal of Colloid and Interface Science*. 211(2):410–412.

Kosmulski, M. 2000. Sorption of heavy metal cations on silica. In *Adsorption on silica surfaces*. E. Papirer, Ed. New York: Marcel Dekker Inc. 399–437.

Kosmulski, M. 2009. pH-dependent surface charging and points of zero charge. IV. Update and new approach. *Journal of Colloid and Interface Science*. 337:439–448.

Krestou, A., Xenidis, A. & Panias, D. 2003. Mechanism of aqueous uranium (VI) uptake by natural zeolitic tuff. *Minerals Engineering*. 16(12):1363–1370.

KTH Royal Institute of Technology. 2004.

Lee, H. & Yi, J. 2007. Removal of copper ions using functionalised mesoporous silica in aqueous solution. *Separation Science and Technology*. 36(11):2433–2448.

Lee, H.W., Cho, H.J., Yim, J.H., Kim, J.M., Jeon, J.K., Sohn, J.M., Yoo, K.S., Kim, S.S., et al. 2011. Removal of Cu(II)-ion over amine-functionalized mesoporous silica materials. *Journal of Industrial and Engineering Chemistry*. 17(3):504–509.

LeVan, M.D. & Vermeulen, T. 1981. Binary Langmuir and Freundlich isotherms for ideal adsorbed solutions. *Journal of Physical Chemistry*. 85(22):3247–3250.

Madden, A. & Hochella, M. 2005. A test of geochemical reactivity as a function of mineral size: Manganese oxidation promoted by hematite nanoparticles. *Geochimica et Cosmochimica Acta*. 69(2):389–398.

Michard, P., Guibal, E., Vincent, T. & Le Cloirec, P. 1996. Sorption and desorption of uranyl ions by silica gel: pH, particle size and porosity effects. *Microporous Materials*. 5(5):309–324.

Mureseanu, M., Reiss, A., Stefanescu, I., David, E., Parvulescu, V., Renard, G. & Hulea, V. 2008. Modified SBA-15 mesoporous silica for heavy metal ions remediation. *Chemosphere*. 73(9):1499–504.

Naicker, K., Cukrowska, E. & McCarthy, T.S. 2003. Acid mine drainage arising from gold mining activity in Johannesburg, South Africa and environs. *Environmental Pollution*. 122(1):29–40.

Nightingale, E.R. 1959. Phenomenological theory of ion solvation. Effective radii of hydrated ions. *The Journal of Physical Chemistry*. 63(9):1381–1387.

Nilchi, A., Dehaghan, T. & Garmarodi, S. 2013. Kinetics, isotherm and thermodynamics for uranium and thorium ions adsorption from aqueous solutions by crystalline tin oxide nanoparticles. *Desalination*. 321:67–71.

Quang, D.V., Kim, J.K., Sarawade, P.B., Tuan, D.H. & Kim, H.T. 2012. Preparation of amino-functionalized silica for copper removal from an aqueous solution. *Journal of Industrial and Engineering Chemistry*. 18(1):83–87.

Ramadan, H., Ghanem, A. & El-rassy, H. 2010. Mercury removal from aqueous solutions using silica , polyacrylamide and hybrid silica – polyacrylamide aerogels. *Chemical Engineering Journal*. 159(1-3):107–115.

Rösner, T. & van Schalkwyk, A. 2000. The environmental impact of gold mine tailings footprints in the Johannesburg region, South Africa. *Bulletin of Engineering Geology and the Environment*. 59(2):137–148.

Sing, K.S.W., Everett, D.H., Haul, R.A., Moscou, L., Pierotti, R.A., Rouquerol, J. & Siemieniewska, T. 1985. Reporting physisorption data for gas/solid systems. *Pure and Applied Chemistry*. 57(4):603–619.

Štamberg, K., Venkatesan, K. & Vasudeva Rao, P. 2003. Surface complexation modeling of uranyl ion sorption on mesoporous silica. *Colloids and Surfaces A: Physicochemical and Engineering Aspects*. 221(1-3):149–162.

Swann, G.E.A. & Patwardhan, S. V. 2011. Application of Fourier Transform Infrared Spectroscopy (FTIR) for palaeoenvironmental research. *Climate of the Past*. (7):65–74.

Tutu, H., McCarthy, T.S. & Cukrowska, E. 2008. The chemical characteristics of acid mine drainage with particular reference to sources, distribution and remediation: The Witwatersrand Basin, South Africa as a case study. *Applied Geochemistry*. 23(12):3666–3684.

Waychunas, G.A. & Zhang, H. 2008. Structure, chemistry, and properties of mineral nanoparticles. *Elements*. 4:381–388. DOI: 10.2113/gselements.4.6.381.

Weber, J.W. & Morris, J.C. 1963. Kinetics of adsorption on carbon from solutions. *Journal of the Sanitary Engineering Division.* 89: 31–60.

Wu, S., Li, F., Xu, R., Wei, S. & Li, G. 2009. Synthesis of thiol-functionalized MCM-41 mesoporous silicas and its application in Cu(II), Pb(II), Ag(I), and Cr(III) removal. *Journal of Nanoparticle Research*. 12(6):2111–2124.

Xue, X. & Li, F. 2008. Removal of Cu(II) from aqueous solution by adsorption onto functionalized SBA-16 mesoporous silica. *Microporous and Mesoporous Materials.* 116(1-3):116–122.

Yavuz, O., Altunkaynak, Y. & Güzel, F. 2003. Removal of copper, nickel, cobalt and manganese from aqueous solution by kaolinite. *Water Research.* 37(4):948–52.

3.7 Supplementary Information

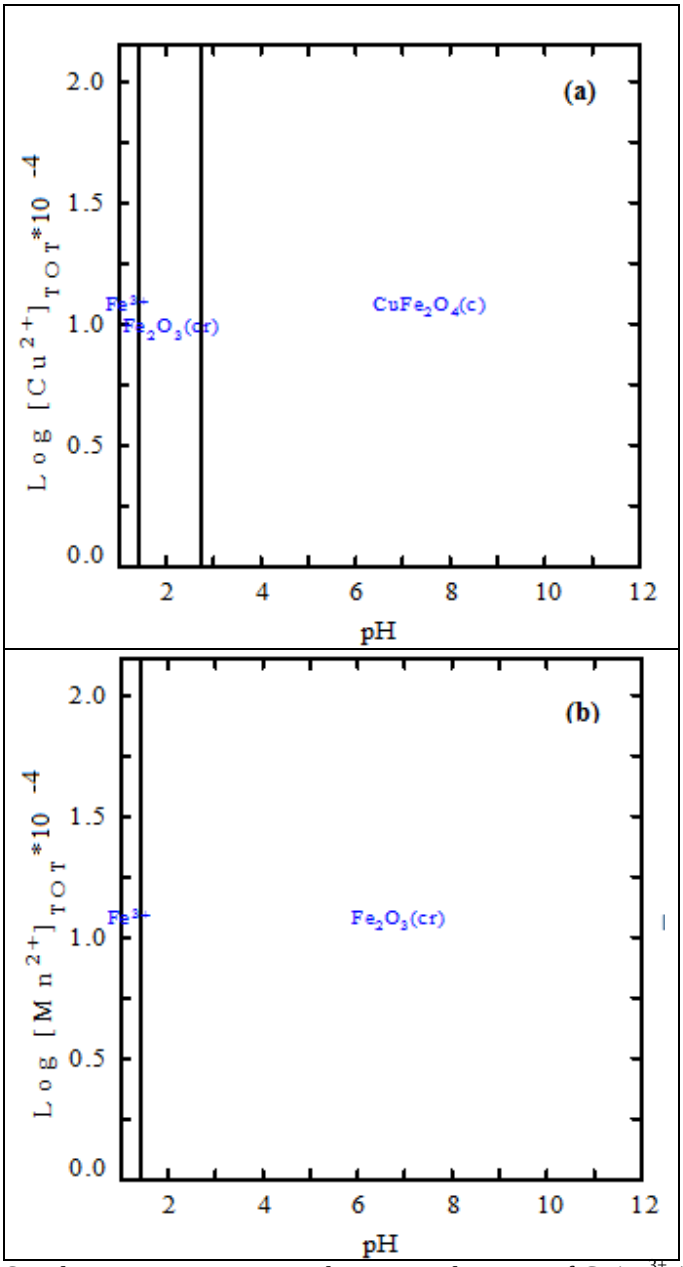

Supplementary Figure 1: Predominance diagrams of Cu/Fe^{3+} (a) and Mn/Fe^{3+} (b) adsorption systems. The U/Fe^{3+} system is similar to the Mn/Fe^{3+} system.

4 Adsorptive removal of mercury from acid mine drainage: A comparison of silica and maghemite nanoparticles

Anita Etale[a] *, Bongani Yalala[b], Hlanganani Tutu[b], Deanne C. Drake[a]

[a] School of Animal Plant and Environmental Sciences; [b] Molecular Sciences Institute, School of Chemistry, University of the Witwatersrand, Private Bag X3, WITS 2050, Johannesburg, South Africa.

Mercury adsorption by silica and maghemite nanoparticles (NPs) was studied with the aim of comparing their performance in the remediation of Acid Mine Drainage (AMD)-contaminated water. Calculated distribution coefficients showed that both NPs are exceptional adsorbents. However, adsorbate coverage per unit area was 30 times higher for maghemite than silica NPs, despite the latter having a surface area ~15 times greater. Maghemite adsorbed 75% of available Hg compared to 56% by silica, making it a more efficient sorbent than silica under AMD conditions. Kinetics data for both adsorbents were fitted by the pseudo-second order model (R^2 = 1) and isotherm data by the Freundlich ($R^2 \geq 0.98$) and Temkin models ($R^2 \geq 0.88$), implying that adsorption to both NPs was by chemisorption. Adsorption increased with NP concentrations and pH: Hg removal was maximal at pH 5 and 7 for both NPs. Efficiencies were also enhanced by manganese and sulphate ions although adsorption to silica was inhibited in 1:2 Hg-to-Mn systems. Importantly, trends in simulated wastewater were replicated in actual AMD-contaminated water samples. This study highlights the fact that properties besides surface area and charge of adsorbents determine adsorbent performance, and superior attributes may not always lead to higher efficiency.

Key words: adsorption, mine water remediation, mesoporous silica, adsorption density.

*Corresponding author. Telephone: +27 11 717 6425; Email address: aetale@gmail.com

4.1 Introduction

Despite considerable effort in recent years to limit environmental mercury releases, mercury pollution in surface water remains a serious environmental concern globally (Pirrone et al., 2010). In regions of mining activity like the Witwatersrand gold fields of Johannesburg, South Africa, the historic use of mercury in gold amalgamation has contributed significantly to the mercury load in tailings and acid mine drainage (AMD) that commonly contaminate surface and ground water (Tutu et al., 2008; Naicker et al., 2003). As early as 1977, Wittmann & Förstner reported concentrations as high as 8.5 mg Hg kg^{-1} in the pelitic sediments of a slimes dam; evidence of the scale of mercury losses from the amalgamation technique.

Aquatic mercury contamination is of concern because of the element's high toxicity to humans and aquatic organisms (Dietz et al., 2013; Houston, 2011). Current treatment of Witwatersrand mine drainage frequently involves the addition of lime to raise its pH which facilitates the hydrolysis and precipitation of metal ions including Cu, Fe, Zn, Pb, Mn and Ni. Although Hg also hydrolyses to $Hg(OH)_2$, this phase has a high intrinsic solubility (5.37×10^{-4} M) and only precipitates if the Hg concentration is above 108 mg L^{-1} (Hahne & Kroontje, 1972). Thus, at the current 18 µg L^{-1} concentrations of mine drainage (Naicker et al., 2003), precipitation may not significantly reduce Hg concentrations and alternative techniques are required.

Techniques such as bioreduction (Oehmen et al., 2009), ion exchange (Anirudhan et al., 2008), electrolysis (Barron-Zambrano et al., 2004)and adsorption (Ramadan et al., 2010) have been investigated. Adsorption has advantages including cost, efficiency and the availability of a broad range of adsorbents like polymers (Saad et al., 2012), fly ash (López-Antón et al., 2009), aluminosilicates (Wu et al., 2007) and nanomaterials (Song et al., 2011). Nanomaterials are considered superior adsorbents because of their higher reactivities and large surface area to volume ratios which allow for faster and higher sorption by small sorbent volumes. Also, less contaminated wastes are generated (Engates & Shipley, 2011).

For adsorption at low pH, silica nanoparticles (NPs) have the added advantage of a low pH_{PZC} (pH 2-3; (Kosmulski, 2009)). This means that NPs are negatively charged under AMD conditions and are therefore primed for cation adsorption. Various studies have applied silica NPs for the adsorption of metals including Cu, Pb, Ag, Cr, Zn and Ni (Mureseanu et al., 2008; Wu et al., 2009; Xue & Li, 2008). None, however, have quantified adsorption under conditions imposed by AMD such as low pH or high sulphate and manganese concentrations. Maghemite NPs are also attractive as adsorbents in AMD-contaminated water because of the high adsorption capacity of iron oxides (Brown & Calas, 2011). Kosmulski (2000) even suggested that their cation sorption capacities were higher than that of silica; the positive charges at low pH notwithstanding i.e. the

pH_{PZC} of maghemite is pH 6.3 (Vayssieres, 2009). To our knowledge, however, no study has assessed this disparity in the nanoparticulate forms of these oxides under mine drainage conditions.

The aim of this work was therefore to assess the efficiency of silica and maghemite NPs in order to inform decisions on their use in the adsorptive removal of Hg from AMD-impacted waters. To do this, the effects of time, adsorbate and adsorbent concentrations, common ions in AMD like manganese and sulphates were quantified in simulated wastewater and actual AMD. The efficiency of NPs was then compared using computed distribution coefficients and adsorption densities.

4.2 Materials and methods

4.2.1 Materials

All metal salts used were analytical grade and used without further purification. Mercury nitrate ($Hg(NO_3)_2{\cdot}H_2O$), manganese nitrate ($Mn(NO_3)_2{\cdot}H_2O$) and commercially prepared silica and maghemite NPs were from Sigma Aldrich (Schnelldorf, Germany). Na_2SO_4 (sulphate ion source) was from Ace Chemicals (Johannesburg, South Africa). Metal solutions and NP suspensions were prepared using deionised water. NP suspensions were prepared by sonicating NPs in a water bath for 30 minutes in a Branson 2500 sonicator (Connecticut, USA). The pH of solutions and suspensions was measured using an Orion Star A211 pH meter (Thermo Scientific) and adjustments made prior to experiments using 0.01 M HNO_3 and 0.01 M NaOH.

4.2.2 Adsorbent characterisation

The size and morphology of nanoparticles were determined by transmission electron microscopy (FEI Tecnai G^2 Spirit TEM) at an acceleration voltage of 120 kV. The surface area, pore volume and pore size of particles was determined by the Brunauer-Emmett-Teller (BET) and BJH (Barret-Joyner-Halenda) methods using a Micrometrics Tristar 3000 (Micrometrics Instruments, USA). The X-ray diffractograms of NPs were collected using a Bruker D8 diffractometer (Cu-$K\alpha$) at a scanning range of 10 - 90° (2θ), a step size of 0.026° and step time of 37 seconds.

4.2.3 Adsorption studies

The adsorption of Hg ions by silica and maghemite NPs was studied in triplicates at ambient temperature (25 ± 2°C) and unless otherwise stated, at pH 3 (± 0.1). Ten millilitres of freshly sonicated NP suspension (3 mg L^{-1}) and 10 mL Hg solutions were contacted in 50 mL PET jars

for 30 minutes. NPs were then separated by centrifugation using Amicon 100 kDa ultracentrifugal filters and supernatants acidified with 3% nitric acid. Mercury concentrations in filtrates were measured by cold vapour atomic absorption spectroscopy (CVAAS) on a Perkin Elmer FIMS 400 mercury analyzer (Connecticut, USA). The operational specifications for the flow injection analysis-mercury hydride system (FI-MH-AAS) were as shown in supplementary table 1.

Mercury adsorption after specific time durations and at equilibrium was determined from mass balance calculations. The NP adsorption capacity at equilibrium (q_e; mg g^{-1}) was calculated using Equation 1 (Xue and Li 2008) where C_i and C_e are the initial and equilibrium metal concentrations (mg L^{-1}), m is the mass of adsorbent applied (g) and V is the volume of solution used (L).

$$q_e = \frac{(C_i - C_e)V}{m} \quad (1)$$

Application to contaminated surface and ground water

Silica and maghemite NPs were also applied for the removal of Hg from AMD-impacted surface and ground water samples. Surface water was collected from the Tweelopiespruit (west of Johannesburg) at locations approximately 2.4 and 2.9 km downstream of a mine decant point (26°50'21.67"S, 27°42'57.49"E). Ground water was sourced from a borehole 650 m southeast of the first stream sampling point (26°05'32.6"S 27°42'44.6"E).

Sampling of AMD-contaminated water was carried out according to standard protocols (Clesceri, Greenberg, and Eaton 1998) and the pH and conductivity of water measured on site using field meters: a Hanna HI9210N pH meter (Hanna instruments) for pH and an Orion 3 Star conductivity meter (Thermo Scientific) for conductivity. Water samples were then transported to the laboratory over ice where they were filtered through 0.45µm filter paper prior to adsorption experiments. A 10 mL volume of filtered water sample was reacted with an equal volume of 3 mg L^{-1} NP suspension for 30 minutes at 25°C. Water samples were used without pH adjustment. The concentration of Hg in filtered samples before and after adsorption was determined by CVAAS.

4.2.4 Data analyses

Kinetics

Kinetics data were fitted to three kinetics models: the pseudo-first order model (Equation 2), the pseudo-second order model (Equation 3) (Ho & Mckay, 2004) and the Elovich model (Equation 4) (Low, 1960).

$$\log(q_e - q_t) = \log q_e - \left(\frac{k_1}{2.303}\right)t \quad (2)$$

$$\frac{t}{q_t} = \left(\frac{1}{k_2}\right) + \left(\frac{1}{q_e}\right)t \quad (3)$$

$$q_t = \frac{1}{\beta}\ln(\alpha\beta) + \frac{1}{\beta}\ln(t) \quad (4)$$

q_e and q_t are the NP loading capacities (mg g^{-1}) at equilibrium and at time t, respectively, while α is the initial sorption rate and β is the desorption constant. k_1 (sec^{-1}) was determined from the slope of a plot of log (q_e - q_t) versus t, and k_2 (mg g^{-1} sec^{-1}) and α (mg g^{-1} sec^{-1}) from the intercepts of the plots of t/q_t versus t and q_t versus ln(t), respectively.

Isotherms

Adsorption isotherm data were fitted to the Langmuir, Freundlich and Temkin isotherm models (Aharoni & Ungarish, 1977; LeVan & Vermeulen, 1981). The Langmuir isotherm best fits data where adsorbate molecules bind to specific sites on an energetically homogenous adsorbent surface in a monolayer. It precludes adsorbate-adsorbate interactions and is expressed in the linear form by Equation 5. q_{max} (mg g^{-1}), the monolayer capacity of the adsorbent and K_L (L mg^{-1}), the Langmuir constant, were determined from the slope and intercept of a plot of C_e/q_e versus C_e.

$$\frac{C_e}{q_e} = \left(\frac{1}{q_{max}}\right)C_e + \left(\frac{1}{K_L q_{max}}\right) \quad (5)$$

The Freundlich model on the other hand, best describes adsorption to heterogeneous surfaces by multi-layer adsorption. Its linear form is as expressed in Equation 6. $1/n$, the heterogeneity factor, and K_F [(mg g) (L mg)$^{1/n}$], the Freundlich constant were deduced from the slope and intercept of a plot of log q_e versus log C_e.

$$\log q_e = \left(\frac{1}{n}\right)\log C_e + \log K_F \quad (6)$$

The Temkin model, unlike the Langmuir model, takes into account the effects of adsorbate-adsorbate interactions on adsorption. It is expressed as in Equation 7 where R is the gas constant (8.3145 J mol^{-1} K^{-1}), T is the absolute temperature, b_T (J mol^{-1}) is the variation in adsorption energy and A_T (L mg^{-1}) is the equilibrium binding constant. b_T and A_T were deduced from the slope and intercept of a plot of q_e versus lnC_e.

$$q_e = \frac{RT}{b_T}\ln C_e + \frac{RT}{b_T}\cdot \ln A_T \quad (7)$$

Evaluation of adsorbent efficiency

The adsorption efficiency of NPs was evaluated based on (i) the distribution coefficient, K_d (mL g^{-1}) and (ii) the adsorption density Γ (mg m^{-2}). The former is simply a measure of the

partitioning of adsorbate molecules between the liquid and solid (sorbent) phase. The higher the K_d value, the greater the sorption ability of the sorbent for the sorbate. A good sorbent has a K_d value ~1 x 10^3 mL g^{-1} and values >10^4 mL g^{-1} correspond to exceptional sorbents (Fryxell et al., 2005). K_d was calculated using Equation 8 where r_{ws} is the water to solid ratio (mL g^{-1}).

$$K_d = \frac{(C_i - C_e)}{C_e} \times r_{ws} \quad (8)$$

The adsorption density, on the other hand, evaluates surface area coverage by adsorbate molecules, providing a measure of the concentration of adsorbate molecules per unit area of the sorbent. It was calculated using Equation 9 where S is the surface area (m^2 g^{-1}) of the adsorbent.

$$\Gamma = \frac{q_e}{S} \quad (9)$$

Statistical analyses

Adsorption efficiencies of silica and maghemite NPs following the different treatments applied were analyzed for statistical differences using Tukey's *post hoc* test at $\alpha < 0.05$.

4.3 Results and discussion

4.3.1 Adsorbent characterization

Transmission electron micrographs revealed that both silica and maghemite NPs were polydisperse with diameters <100 nm (Figure 4.1). NPs of maghemite were polygonal while those of silica were more rounded and porous. The specific surface area and pore volume of silica NPs were 612 m^2 g^{-1} and 0.63 cm^3 g^{-1}, respectively, while those of maghemite was 40.8 m^2 g^{-1} and 0.11 cm^3 g^{-1}. Despite being both nanoparticulate therefore, silica NPs had a surface area ~15x greater than maghemite, likely due to its greater porosity. Both NPs were mesoporous; the average pore size was 4.12 nm for silica and 11.27 nm for maghemite.

X-ray diffractograms (Figure 4.2) revealed that maghemite particles were crystalline while those of silica were amorphous. The (2 1 1) and (2 1 0) peaks of the maghemite spectra were consistent with the database in the JCPDS file for this iron oxide.

FTIR analyses of the NPs (data not shown) revealed bands that corresponded to a number of structural units in these materials. For silica, in addition to the band appearing at 3364 and 1637 cm^{-1} which corresponds to adsorbed water, bands appeared at 1057, 956 and 784 cm^{-1} due to the asymmetric motion of Si-O-Si bonds, Si-OH stretching and Si-O-Si symmetric motion, respectively (Fidalgo & Ilharco, 2001). Maghemite spectra had bands corresponding to O-H

bending and vibrational modes at 3342 and 1622 cm^{-1}, as well as Fe-O stretching bands at 540 and 525 cm^{-1} (Jiang et al., 2013).

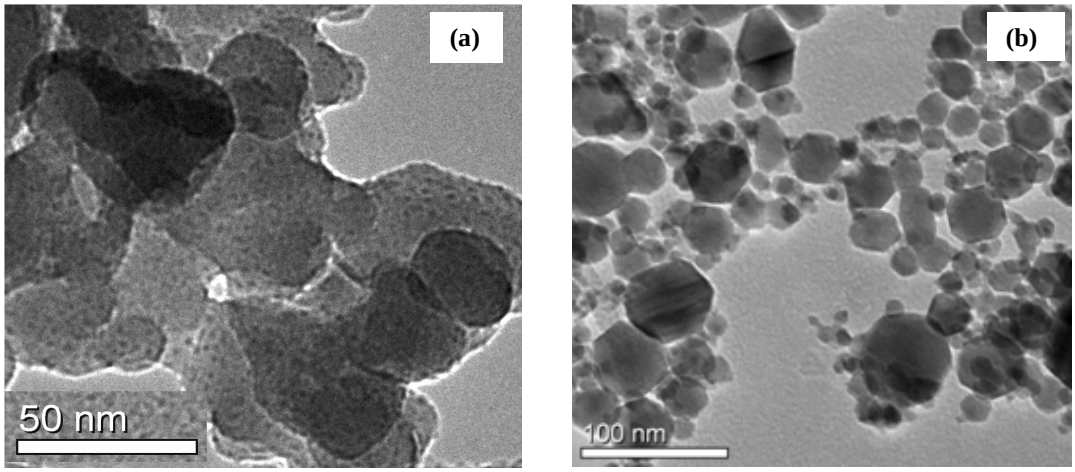

Figure 4.1: Transmission electron micrographs of silica (a) and maghemite (b) NPs

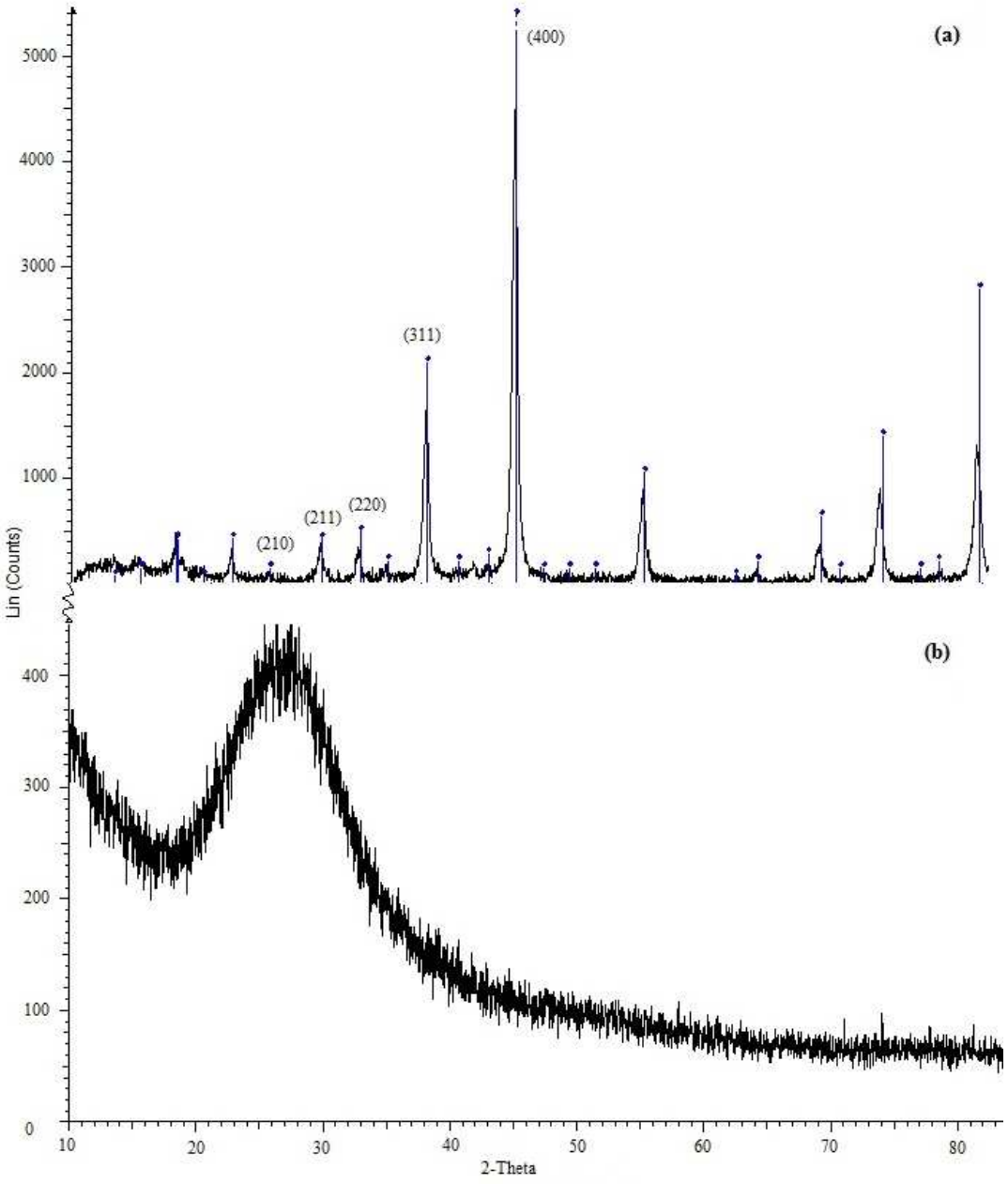

Figure 4.2: Powder X-ray diffractograms of maghemite (a) and silica (b) NPs

4.3.2 Adsorption kinetics

The kinetics of Hg adsorption to silica and maghemite NPs were investigated at time durations ranging from 10 seconds to 60 minutes. Adsorption to both types of NPs was rapid, with most it taking place within 10 seconds, and achieving equilibrium within five minutes of exposure.

Efficiencies at equilibrium were 56% and 75% for silica and maghemite NPs, respectively (Figure 4.3).

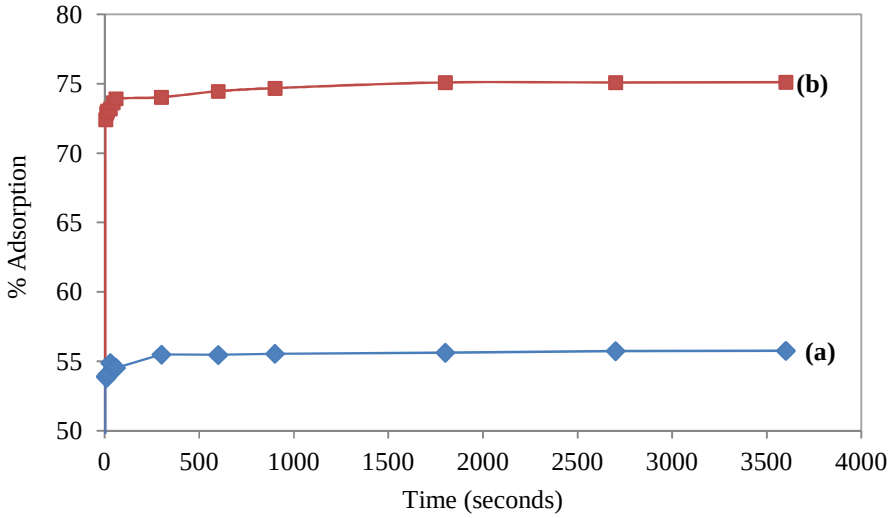

Figure 4.3: The effect of time on adsorption of Hg to silica (a) and maghemite (b) NPs at pH 3.

Table 4.1: Parameters of kinetics models fitted to adsorption data.

Model	Parameters	Silica NPs	Maghemite NPs
Pseudo-first order model	R^2	0.95	0.96
	k_1 (sec^{-1})	0.002	0.002
	q_e (mg g^{-1})	0.020	0.030
Pseudo-second order model	R^2	1	1
	k_2 (g mg^{-1} sec^{-1})	0.80	0.44
	q_e (mg g^{-1})	0.91	1.234
	h (mg $g^{-1}sec^{-1}$)	0.67	0.75
Elovich model	R^2	0.92	0.97
	α (mg $g^{-1}sec^{-1}$)	5.11	5.17
	β (g mg^{-1})	196.08	153.85

Adsorption at pH 3 (± 0.1), adsorbent concentration = 3 mg L^{-1}; volume of adsorbent solution used = 10 mL; volume of Hg solution = 10 mL.

As shown in Table 4.1, kinetics data were better described by the pseudo-second-order model (R^2 = 1) and Elovich model ($R^2 \geq 0.92$), implying that chemisorption was the main mode of Hg adsorption. This conclusion is validated by the speciation of adsorbed Hg at the experimental pH.

Three species exist in solution at pH 3: Hg^{2+}, $HgOH^{+}$ and $Hg(OH)_2$. However, according to MacNaughton and James (1974), Hg^{2+} and $HgOH^{+}$ ions are either not adsorbed at all or are only weakly adsorbed. Hg^{2+} is less adsorbable because the ion is not hydrolysed while for $HgOH^{+}$, the strong covalency of the metal-OH inhibits the sharing of the hydroxo ligand with the adsorbent surface (Schuster, 1991). The main adsorbed species was therefore the uncharged $Hg(OH)_2$ ion and specific interactions (chemisorption) must be invoked to explain adsorption. Notably, the initial adsorption rate and equilibrium adsorption capacity were higher for maghemite than silica, despite a much lower surface area per unit weight.

4.3.3 Effect of pH

The effect of pH on Hg adsorption was investigated at pH 3, 5, 7 and 9. Maximum adsorption occurred at pH 5 and 7 for both NPs: 68% for silica and 82% for maghemite. Indeed, statistical analyses indicated that adsorption efficiencies, for both NPs at pH 5 and 7 were not significantly different (Figure 4.4). Adsorption was, however, higher at pH 9 than at pH 3, although this difference was significant for silica but not maghemite. In addition, adsorption was significantly more efficient for maghemite than silica at all pH levels.

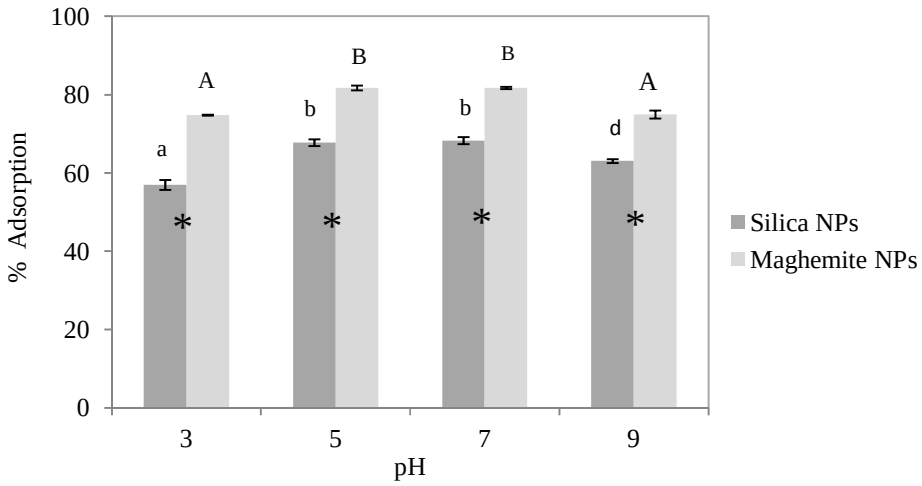

Figure 4.4: The effect of pH on Hg adsorption by silica and maghemite NPs (±SD). Different letters indicate statistically significant differences in adsorption at different pH levels; lower case letters for silica and upper case letters for maghemite. * indicates significant differences in adsorption by NPs at a given pH ($p < 0.05$).

These results compare favourably to those of Barrow & Cox (1992) and Sarkar et al. (2000). Both reported maximum adsorption at pH 4.4, the former to goethite and the latter to kaolinite.

Variations in Hg adsorption efficiency with pH can be explained in terms of pH-related speciation changes thus: it is sub-optimal at pH 3 because a major fraction of Hg ions is present as the less adsorbable Hg^{2+} and $HgOH^{+}$ moieties, is at its peak at pH 5 where all Hg is hydrolysed to the most adsorbable species, $Hg(OH)_2$.

4.3.4 Effect of sulphate and manganese ions

The effects of sulphate and manganese ions on adsorption of Hg were investigated using equimolar and 1:2 Hg-to-SO_4^{2-} and Hg-to-Mn^{2+} concentrations. Mercury removal by both types of NPs was significantly higher in the presence of equimolar sulphate and manganese ions. Adsorption did not, however, increase further in 1:2 Hg-to-SO_4^{2-} solutions (Figure 4.5a). With respect to manganese, adsorption was significantly different across all three treatments for both NPs and was inhibited in 1:2 Hg-to-Mn solutions (Figure 4.5b).

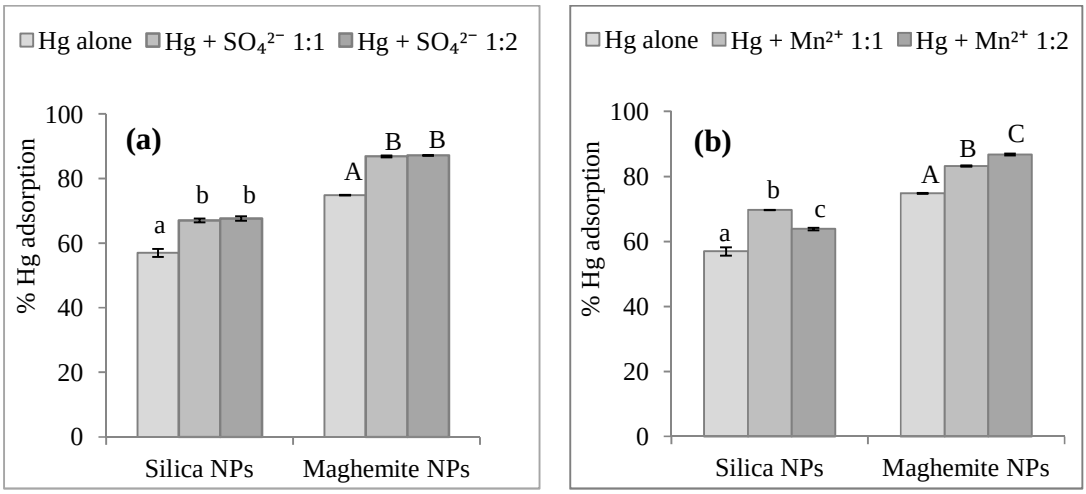

Figure 4.5: The effect of sulphates (a) and manganese ions (b) on adsorption of Hg by silica and maghemite NPs (±SD) at pH 3. Different letters indicate statistically significant differences in adsorption at different treatments; lower case letters for silica and upper case letters for maghemite.

Sulphate-induced adsorption enhancement has been reported previously (Beattie et al., 2008; Qiu et al., 2012). James & Healy (1972) suggested that anions form complexes with metal ions or adsorb to the adsorbent surface, thus reducing Coulombic repulsions e.g. between Hg^{2+} and positively charged maghemite. This then promotes the approach of cations and eventually adsorption. With respect to silica, sulphates likely increased the concentration of adsorbable Hg

by complexing the less adsorbable Hg^{2+} fraction. Higher sulphate concentrations did not however increase adsorption further, possibly due to depletion of Hg^{2+} ions.

As regards manganese, increased adsorption was likely due to an increased drive for diffusion to the adsorbent surface as a result of increased ionic concentrations. Its influence was variable at higher concentrations i.e. double Mn concentrations increased adsorption of Hg to maghemite, but inhibited adsorption to silica (Figure 5b) likely due to the differences in surface charges of the NPs and competition for sorption sites. As the maghemite surface is positively charged at pH 3, adsorption of Mn^{2+} was not favourable and competition for sorption sites was therefore minimal. Silica, on the other hand, is negatively charged at pH 3 and amenable to Mn^{2+} sorption, hence the displacement of $Hg(OH)_2$ at higher Mn^{2+} concentrations.

4.3.5 Effect of adsorbent concentration

The effect of adsorbate concentrations on the efficiency of Hg removal was investigated using 3, 5 and 9 mg L^{-1} NP concentrations. The concentration of adsorbed Hg increased significantly for both NPs under the range of adsorbent concentrations investigated here (Figure 4.6). This trend differs from those observed in studies with Cu, Mn and U where adsorption was lower at 10 mg L^{-1} relative to 5 mg L^{-1} concentrations of the same NPs (Etale et al., 2014). NP aggregation and the consequent diminished access to sorption sites are the most likely explanation for the phenomenon with Cu, Mn and U. In the present study, however, aggregation appears to have has minimal effect, if any, on Hg adsorption to either silica or maghemite. Recent reports have offered some insight into this phenomenon by suggesting that cations can induce aggregation of oppositely charged NPs in aqueous media (Dalai et al., 2014). The apparent low level of aggregation with Hg may therefore be explained by the poor adsorption of Hg^{+} and $HgOH^{+}$ suggested by MacNaughton & James (1974).

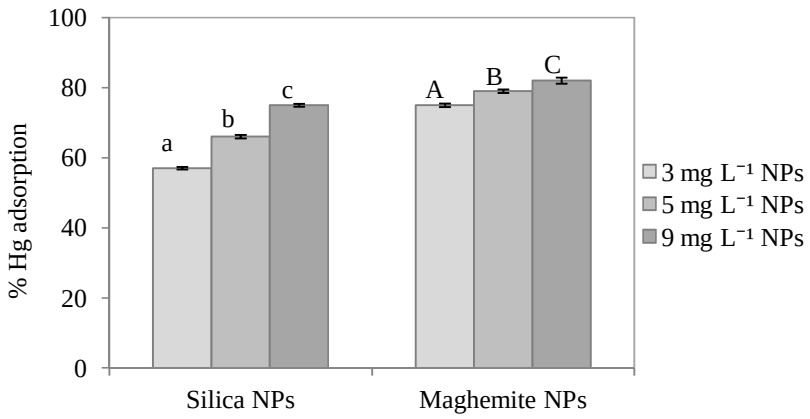

Figure 4.6: The effect of adsorbent concentrations on Hg removal by silica and maghemite NPs (±SD) at pH 3. Different letters indicate statistical differences in adsorption at different NP concentrations; lower case letters for silica and upper case letters for maghemite.

4.3.6 Adsorption isotherms

Mercury adsorption isotherms were investigated at concentrations ranging from 0.1-1.5 mg L^{-1}. The results, as shown in Figure 4.7, indicate that equilibrium adsorbate loading (q_e) increased with Hg concentration. This was due to increased diffusion drive to the adsorbent surface (Ho & Mckay, 2004).

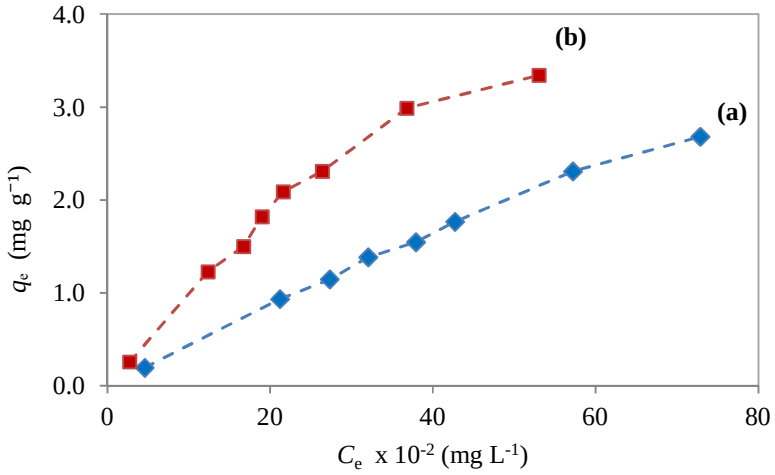

Figure 4.7: The effect of initial Hg concentrations on adsorption efficiency of silica (a) and maghemite (b) NPs

Isotherm data were best fitted by the Freundlich model (Table 4.2), implying that sorption sites in both NPs were energetically heterogeneous, although sites on silica were more heterogeneous. Importantly, despite the higher surface area and negative surface charge of silica NPs, its adsorption capacity (K_F) is only half that of maghemite. It is clear then that maghemite is a more efficient sorbent than silica.

Table 4.2: Isotherm parameters for the adsorption of Hg to silica and maghemite NPs at pH 3 (±0.1) and 25°C.

Adsorbent	Langmuir isotherm			Freundlich isotherm			Temkin isotherm		
	R^2	q_{max} (mg g^{-1})	K_L (L mg^{-1})	R^2	K_F (mg g^{-1}) (L mg^{-1})$^{1/n}$	$1/n$	R^2	A_T(L g^{-1})	b_T(MJ mol^{-1})
Silica	0.68	17.27	0.26	0.99	3.88	0.95	0.88	1.20 x 10^6	454.2
Maghemite	0.77	8.90	1.25	0.98	7.36	0.89	0.93	8.89 x 10^6	454.2

This conclusion is corroborated by the findings of Unob and co-workers (2007) who reported that the adsorption of Cu by iron-oxide coated silica NPs was almost 4.5 times higher than that of uncoated silica, in spite of the latter having a higher surface area i.e. 353 m^2 g^{-1} vs. 236 m^2 g^{-1} for the coated silica. Similar findings were also reported by Gupta et al. (2005) for As and Xu & Axe (2005) for Ni. Collectively, these studies suggest that, factors in addition to a larger surface area and favourable surface charges contribute to adsorbent efficiency. As stated by Kosmulski (2000), the factors behind the lower adsorption capacity of silica, even under favourable conditions, are not fully understood.

Nonetheless, the adsorption capacity of silica NPs used here was higher than that of sulphonated polyethylenimine (Saad et al., 2012) and a Mexican zeolite (Gebremedhin-Haile et al., 2003). That of maghemite was higher than magnetite (Parham et al., 2012) and even thiol-functionalized magnetic beads (Okamoto et al., 2011).

4.3.7 Comparison of NP efficiency

To compare the efficiency of silica and maghemite NPs for Hg adsorption, distribution coefficients, K_d (mL g^{-1}) and adsorption densities Γ (mg m^{-2}) were calculated. K_d values for silica were 1.89, 2.20 and 2.50 mL g^{-1} and those of maghemite were 2.50, 2.64 and 2.73 mL g^{-1} for NP concentrations of 3, 5 and 9 mg L^{-1}, respectively. These K_d values are all >1 x 10^4 mL g^{-1}, indicating that both NPs are exceptional adsorbents.

A clearer distinction in efficiency was made using adsorption density data (Figure 4.8). From this metric, it is evident that maghemite NPs are far more efficient adsorbents in terms of the

metal loading per unit surface area. In addition, the maximum adsorption density of maghemite NPs, based on Freundlich model, is 30 times higher than that of silica i.e. 0.179 and 0.006 mg m^{-2} for maghemite and silica, respectively. This is in spite of the latter having a surface area ~15 times greater. Thus, although they are both exceptional sorbents, maghemite is a more efficient Hg sorbent than silica.

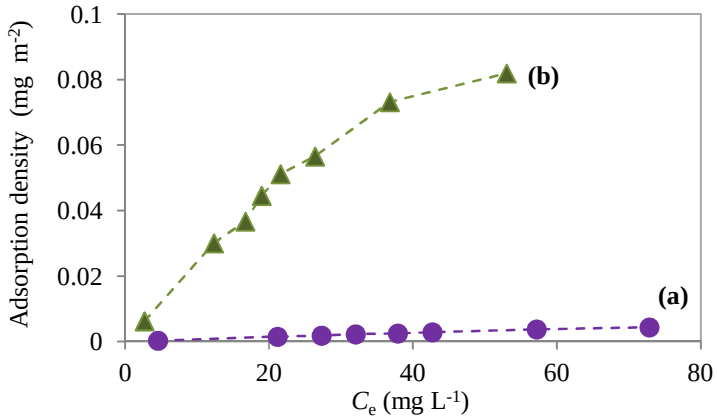

Figure 4.8: Adsorption densities of Hg on silica (a) and maghemite (b) NPs at pH 3

4.3.8 Hg adsorption from AMD-contaminated water

Finally, the performance of silica and maghemite NPs was quantified in AMD-contaminated water collected in the field. One ground water sample (GW) and two surface water samples (SW1 and SW2), (Table 4.3) were used without pH adjustment.

Table 4.3: Characteristics of AMD-contaminated surface and ground water**.**

Sample	pH	$[Hg]_{tot}$ mg L^{-1} (SD)	$[Mn]_{tot}$ mg L^{-1} (SD)	$[SO_4^{2-}]$ mg L^{-1} (SD)
SW1	3.13	0.06 (0.001)	49.74 (0.002)	3112 (5.602)
SW2	2.79	0.14 (0.007)	16.48 (0.006)	2070 (3.984)
GW	5.62	3.02 (0.210)	15.00 (0.140)	1971 (3.102)

Just as with simulated wastewater, Hg removal was significantly higher with maghemite than silica (Figure 4.9), although removal from surface water did not attain efficiencies recorded for simulated wastewater. Adsorption was higher in ground water than surface water, likely due to (i)

higher (>20x) initial Hg concentrations (Table 4.3) hence higher mass transfer, (ii) higher pH and the subsequent favourable speciation of Hg as explained in section 4.3.2 (iii) with respect to silica, less competition for sorption sites from the lower concentrations of manganese. Overall, maghemite was a stronger Hg sorbent than silica even in multi-element solution that is AMD.

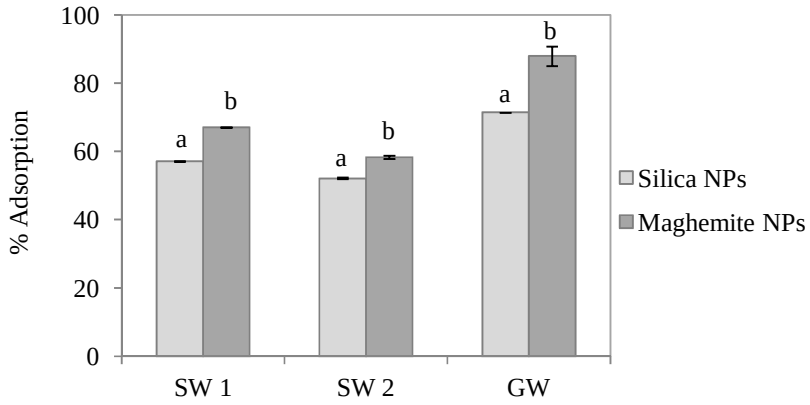

Figure 4.9: Efficiency of Hg removal from AMD-contaminated surface and ground water by silica and maghemite NPs (±SD). Different letters indicate statistically significant differences in adsorption by silica and maghemite from the same water sample.

4.4 Conclusions

The aim of this study was to assess and compare the efficiency of silica and maghemite NPs as adsorbents for the removal of Hg ions from AMD-contaminated water. It is clear that although adsorption to both types of NPs is similar in simulated wastewater and AMD-contaminated surface and ground water, responses to pH and NP concentrations and fit to kinetics and isotherm models, adsorption is faster and more efficient with maghemite than silica NPs under the full range of conditions tested here. For example, 75% of Hg in simulated wastewater was adsorbed by maghemite whereas silica NPs attained only 56% efficiency. Further, adsorption densities were 30 times higher for maghemite despite the fact that silica NPs had a surface area ~15 times greater and were negatively charged at the experimental pH. Clearly therefore, factors besides surface area and charge, influence the adsorption performance of silica and maghemite NPs. Although current knowledge is insufficient for the description of this phenomenon, this work highlights the importance of screening of NP adsorbents as superior physical attributes may not translate to better performance. For the removal of Hg from AMD-contaminated ground and surface water therefore, maghemite will be preferred over silica.

4.5 Acknowledgements

This work was funded by the Global Change and Sustainability Research Institute (GCSRI) of the University of the Witwatersrand. The assistance of Kirstin Olsen with field sampling is gratefully acknowledged.

4.6 References

Aharoni, C. & Ungarish, M. 1977. Kinetics of activated chemisorption. Part 2.-Theoretical models. *Journal of the Chemical Society, Faraday Transactions 1*, 73: 456–464.

Anirudhan, T.S., Divya, L. & Ramachandran, M. 2008. Mercury(II) removal from aqueous solutions and wastewaters using a novel cation exchanger derived from coconut coir pith and its recovery. *Journal of Hazardous Materials*, 157(2-3): 620–7.

Barron-Zambrano, J., Laborie, S., Viers, P., Rakib, M. & Durand, G. 2004. Mercury removal and recovery from aqueous solutions by coupled complexation–ultrafiltration and electrolysis. *Journal of Membrane Science*, 229(1-2): 179–186.

Barrow, N.J. & Cox, V.C. 1992. The effects of pH and chloride concentration on mercury sorption. I. By goethite. *Journal of Soil Science*, 77: 295–304.

Beattie, D.A., Chapelet, J.K., Gräfe, M., Skinner, W.. & Smith, E. 2008. In situ ATR FTIR studies of SO4 adsorption on goethite in the presence of copper ions. *Environmental Science & Technology*, 42(24): 9191–9196.

Brown, G.E. & Calas, G. 2011. Environmental mineralogy – Understanding element behavior in ecosystems. *Comptes Rendus Geoscience*, 343(2-3): 90–112.

Dalai, S., Pakrashi, S., Bhuvaneshwari, M., Iswarya, V., Chandrasekaran, N. & Mukherjee, A. 2014. Toxic effect of Cr(VI) in presence of n-TiO2 and n-Al2O3 particles towards freshwater microalgae. *Aquatic Toxicology*, 146: 28–37.

Dietz, R., Sonne, C., Basu, N., Braune, B., O'Hara, T., Letcher, R.J., Scheuhammer, T., Andersen, M., Andreasen, C., Andriashek, D., Asmund, G., Aubail, A., Baagøe, H., Born, E.W., Chan, H.M., Derocher, A.E., Grandjean, P., Knott, K., Kirkegaard, M., Krey, A., Lunn, N., Messier, F., Obbard, M., Olsen, M.T., Ostertag, S., Peacock, E., Renzoni, A., Rigét, F.F., Skaare, J.U., Stern, G., Stirling, I., Taylor, M., Wiig, Ø., Wilson, S. & Aars, J. 2013. What are the toxicological effects of mercury in Arctic biota? *Science of the Total Environment*, 443(November 2012): 775–90.

Engates, K.E. & Shipley, H.J. 2011. Adsorption of Pb, Cd, Cu, Zn, and Ni to titanium dioxide nanoparticles: effect of particle size, solid concentration, and exhaustion. *Environmental Science and Pollution Research*, 18(3): 386–395.

Etale, A., Tutu, H. & Drake D.C, 2014. Application of maghemite nanoparticles as sorbents for the removal of Cu(II), Mn(II) and U(VI) ions from aqueous solution in acid mine drainage conditions. *Applied Water Science.* DOI: 10.1007/s13201-014-0217-3.

Fidalgo, A. & Ilharco, L.M. 2001. The defect structure of sol-gel-derived silica/polytetrahydrofuran hybrid films by FTIR. *Journal of Non-crystalline Solids*, 283: 144–154.

Fryxell, G.E., Lin, Y., Fiskum, S., Birnbaum, J.C., Wu, H., Kemner, K. & Kelly, S. 2005. Actinide sequestration using self-assembled monolayers on mesoporous supports. *Environmental Science & Technology*, 39(5): 1324–31.

Gebremedhin-Haile, T., Olguín, M.T. & Solache-Ríos, M. 2003. Removal of mercury ions from mixed aqueous metal solutions by natural and modified zeolitic minerals. *Water Air and Soil Pollution*, 148: 179–200.

Gupta, V.K., Saini, V.K. & Jain, N. 2005. Adsorption of As(III) from aqueous solutions by iron oxide-coated sand. *Journal of Colloid and Interface Science*, 288(1): 55–60.

Hahne, H.C.H. & Kroontje, W. 1972. Significance of pH and chloride concentration on behavior of heavy metal pollutants: Mercury(II), cadmium(II), zinc(II), and lead(II). *Journal of Environmental Quality*, 2(4): 444–450.

Ho, Y.S. & Mckay, G. 2004. Sorption of copper(II) from aqueous solution by peat. *Water Air and Soil Pollution*, 158: 77–97.

Houston, M.C. 2011. Role of mercury toxicity in hypertension, cardiovascular disease, and stroke. *Journal of Clinical Hypertension*, 13(8): 621–627.

James, R. & Healy, T. 1972. Adsorption of hydrolyzable ions at the oxide-water interface. III. A thermodynamic model of adsorption. *Journal of Colloid and Interface Science*, 40(1): 65–81.

Jiang, W., Pelaez, M., Dionysiou, D.D., Entezari, M.H., Tsoutsou, D. & O'Shea, K. 2013. Chromium(VI) removal by maghemite nanoparticles. *Chemical Engineering Journal*, 222: 527–533.

Kosmulski, M. 2009. pH-dependent surface charging and points of zero charge. IV. Update and new approach. *Journal of Colloid and Interface Science*, 337: 439–448.

Kosmulski, M. 2000. Sorption of heavy metal cations on silica. In E. Papirer, ed. *Adsorption on silica surfaces*. New York: Marcel Dekker Inc, pp. 399–437.

LeVan, M.D. & Vermeulen, T. 1981. Binary Langmuir and Freundlich isotherms for ideal adsorbed solutions. *Journal of Physical Chemistry*, 85(22): 3247–3250.

López-Antón, M.A., Abad-Valle, P., Díaz-Somoano, M., Suárez-Ruiz, I. & Martínez-Tarazona, M.R. 2009. The influence of carbon particle type in fly ashes on mercury adsorption. *Fuel*, 88(7): 1194–1200.

Low, M.J.D. 1960. Kinetics of chemisorption of gases on solids. *Chemical Reviews*, 60(3): 267–312.

MacNaughton, M.G. & James, R.O. 1974. Adsorption of aqueous mercury (II) complexes at the oxide/water interface. *Journal of Colloid and Interface Science*, 47(2): 431–440.

Mureseanu, M., Reiss, A., Stefanescu, I., David, E., Parvulescu, V., Renard, G. & Hulea, V. 2008. Modified SBA-15 mesoporous silica for heavy metal ions remediation. *Chemosphere*, 73(9): 1499–504.

Naicker, K., Cukrowska, E. & McCarthy, T.S. 2003. Acid mine drainage arising from gold mining activity in Johannesburg, South Africa and environs. *Environmental Pollution*, 122(1): 29–40.

Oehmen, A., Fradinho, J., Serra, S., Carvalho, G., Capelo, J.L., Velizarov, S., Crespo, J.G. & Reis, M.A.M. 2009. The effect of carbon source on the biological reduction of ionic mercury. *Journal of Hazardous Materials*, 165(1-3): 1040–1048.

Okamoto, T., Tachibana, S., Miura, O. & Takeuchi, M. 2011. Mercury removal from solution by superconducting magnetic separation with nanostructured magnetic adsorbents. *Physica C: Superconductivity*, 471(21-22): 1516–1519.

Parham, H., Zargar, B. & Shiralipour, R. 2012. Fast and efficient removal of mercury from water samples using magnetic iron oxide nanoparticles modified with 2-mercaptobenzothiazole. *Journal of Hazardous Materials*, 205-206: 94–100.

Pirrone, N., Cinnirella, S., Feng, X., Finkelman, R.B., Friedli, H.R., Leaner, J., Mason, R., Mukherjee, a. B., Stracher, G.B., Streets, D.G. & Telmer, K. 2010. Global mercury emissions to the atmosphere from anthropogenic and natural sources. *Atmospheric Chemistry and Physics*, 10(13): 5951–5964.

Qiu, H., Zhang, S., Pan, B., Zhang, W. & Lv, L. 2012. Effect of sulfate on Cu(II) sorption to polymer-supported nano-iron oxides: behavior and XPS study. *Journal of Colloid and Interface Science*, 366(1): 37–43.

Ramadan, H., Ghanem, A. & El-rassy, H. 2010. Mercury removal from aqueous solutions using silica , polyacrylamide and hybrid silica – polyacrylamide aerogels. *Chemical Engineering Journal*, 159(1-3): 107–115.

Saad, D.M.G., Cukrowska, E.M. & Tutu, H. 2012. Sulfonated cross-linked polyethylenimine for selective removal of mercury from aqueous solutions. *Toxicological & Environmental Chemistry*, 94(10): 1916–1929.

Sarkar, D., Essington, M.E. & Misra, K.C. 2000. Adsorption of mercury(II) by kaolinite. *Soil Science Society of America Journal*, 64(December): 1968–1975.

Schuster, E. 1991. The behaviour of mercury in the soil with special emphasis on complexation and adsorption processes-A review of the literature. *Water Air and Soil Pollution*, 56(1): 667–680.

Song, B.Y., Eom, Y. & Lee, T.G. 2011. Removal and recovery of mercury from aqueous solution using magnetic silica nanocomposites. *Applied Surface Science*, 257(10): 4754–4759.

Tutu, H., McCarthy, T.S. & Cukrowska, E. 2008. The chemical characteristics of acid mine drainage with particular reference to sources, distribution and remediation: The

Witwatersrand Basin, South Africa as a case study. *Applied Geochemistry*, 23(12): 3666–3684.

Unob, F., Wongsiri, B., Phaeon, N., Puanngam, M. & Shiowatana, J. 2007. Reuse of waste silica as adsorbent for metal removal by iron oxide modification. *Journal of Hazardous Materials*, 142(1-2): 455–62.

Vayssieres, L. 2009. On the effect of nanoparticle size on water-oxide interfacial chemistry. *The Journal of Physical Chemistry C*, 113(12): 4733–4736.

Wittmann, G.T.W. & Förstner, U. 1977. Heavy metal enrichment in mine drainage: III. The Klerksdorp, West Wits and Evander goldfields. *South African Journal of Science*, 73: 23–57.

Wu, S., Li, F., Xu, R., Wei, S. & Li, G. 2009. Synthesis of thiol-functionalized MCM-41 mesoporous silicas and its application in Cu(II), Pb(II), Ag(I), and Cr(III) removal. *Journal of Nanoparticle Research*, 12(6): 2111–2124.

Wu, X.-W., Ma, H.-W., Li, J.-H., Zhang, J. & Li, Z.-H. 2007. The synthesis of mesoporous aluminosilicate using microcline for adsorption of mercury(II). *Journal of Colloid and Interface Science*, 315(2): 555–61.

Xu, Y. & Axe, L. 2005. Synthesis and characterization of iron oxide-coated silica and its effect on metal adsorption. *Journal of Colloid and Interface Science*, 282(1): 11–9.

Xue, X. & Li, F. 2008. Removal of Cu(II) from aqueous solution by adsorption onto functionalized SBA-16 mesoporous silica. *Microporous and Mesoporous Materials*, 116(1-3): 116–122.

4.7 Supplementary information

Supplementary Table 1: Operational specifications for the FI-MH-AAS used for the quantification of mercury

Hg carrier solution	3% (v/v) HCl
Flow rate of carrier solution	70 - 100 mL min^{-1}
Reducing agent	0.2% $NaBH_4$ in 0.05% NaOH
Hg^o carrier gas	Argon
Wavelength (nm)	253.7
Cell temperature	100^oC

5 Synthesis, characterisation and application of amine functionalised silica-carbon hybrid nanoparticles for the adsorptive removal of Cu(II) from acidic solutions

Anita Etale[a] *, Nikita Tavengwa[b], Deanne C. Drake[a], Hlanganani Tutu[b]

[a] School of Animal Plant and Environmental Sciences, [b] Molecular Sciences Institute, School of Chemistry, University of the Witwatersrand, Private Bag X3, WITS 2050, Johannesburg, South Africa.

A novel amine-functionalised inorganic-organic hybrid adsorbent was synthesised for the removal of Cu ions from acidic solutions such as those characterising acid mine drainage (AMD). Synthesis was via a three-step process involving coating of silica nanoparticles (NPs) with carbon, oxidation of the carbon layer and grafting of hexamine to the silica-carbon composites. Transmission electron micrographs revealed that the adsorbent comprised spherical particles in the nanometre range while spectroscopic analyses confirmed the presence of amine, carboxyl and hydroxyl groups. Nitrogen sorption isotherms revealed a considerable decrease in particle area as a result of carbonisation and hexamine grafting. 52% of Cu ions in solution were retained by the adsorbent at pH 3 in a reaction that achieved equilibrium in 45 minutes, and followed the pseudo-second-order kinetics. Metal removal increased with initial concentrations and isotherms were fitted by the Freundlich model which gave an adsorption capacity of 0.016 mmol g^{-1}. Cu removal increased with pH although adsorption at pH 5 was higher than at pH 7 and 9 (62, 57 and 57% respectively). The adsorbent also selectively bound Cu from a multi-elemental solution indicating that it could be applied for the selective removal of Cu from AMD-contaminated waters.

Key words: acid mine drainage, adsorption, carbonisation, organic-inorganic composites

*Corresponding author. Telephone: +27 11 717 6425; Email address: aetale@gmail.com

5.1 Introduction

Nano-structured materials with tailored properties are fundamental to the advancement of technologies including pollution remediation (Valle-Vigón et al., 2013), catalysis (Gupta & Paul, 2011; Wang et al., 2007) and drug delivery (Slowing et al., 2008). These materials, which may be in the form of particles, tubes or sheets are synthesised from organic and inorganic precursors that include semiconductors, metals and metal oxides (Ju-Nam & Lead, 2008). Since their discovery by Mobil researchers, mesoporous silicas have drawn considerable attention because of their unique properties with respect to tuneable pore structures, well defined morphology and porosity (Beck et al., 1992; Mercier & Pinnavaia, 1998). Attention has recently been shifting towards their combination with organic materials because such composite materials often possess qualities superior to those of individual parent materials with respect to adsorption, catalytic properties, hydrophilicity and porosity (Valle-Vigón et al., 2013; Titirici et al., 2007; Yang et al., 2006). Silica-carbon hybrid materials, for example, combine the high surface areas of silica and the easy functionalisability of carbon to produce materials with better pore definition than carbon-only compounds and higher adsorption capacities than silica-only adsorbents (due to chelation by oxygen moieties in phenol, carboxyl and ketone groups in the carbon matrix) (Lu et al., 2005). These functional groups are not only useful for binding cationic contaminants, they can also be used to anchor other functionalities including amine, thiol, sulphate and phosphate groups, thus facilitating target ion specificity (Valle-Vigón et al., 2012).

The aim of this work was to synthesize, characterize and apply amine-functionalized hybrid silica-carbon adsorbents for the removal of Cu from acidic solutions such as those characterizing acid mine drainage (AMD). AMD, which often has a $pH \leq 3$ and high metal and sulphate concentrations, is an increasingly significant challenge in many mining regions globally. In Johannesburg, South Africa, AMD accounts for much of the anthropogenic acidity and metal contamination of ground and surface waters (McCarthy, 2011; Tutu et al., 2008; Durand, 2012). High concentrations of metal ions including Cu have been reported in AMD-contaminated streams and ground water used for animal watering and potable purposes (Naicker et al., 2003). The reported concentrations exceed tolerance limits for most aquatic organisms and the decimation of aquatic life in most stream receiving AMD has been reported (Jooste & Thirion, 1999). The treatment of AMD-contaminated waters is therefore necessary in order to mitigate against negative consequences to both humans and aquatic ecosystems.

The removal of copper from aqueous media by nanoparticles (NPs) has been studied using NPs of various materials including hematite (Grover et al., 2012), selenium (Bai et al., 2011) and titanium (Engates & Shipley, 2011). Lately, NPs with surfaces functionalised by moieties with high affinities for Cu e.g. amine and carboxyl groups are increasingly being applied in order to improve metal removal efficiencies (Aguado et al., 2009; Hao et al., 2010; Lee et al.,

2011; Georgescu et al., 2013; Valle-Vigón et al., 2013; Hu et al., 2012). Lee et al. (2011) for example found that Cu removal by silica NPs increased from 1.5 mg g^{-1} with unfunctionalised NPs to 5.8 mg g^{-1} with amine-functionalised NPs. Most amine functionalised NPs in the literature are prepared by co-condensation or grafting of amine groups to the silica surface via ethoxysilane chains such as the commonly used 3-aminoproyl triethoxysilane (APTES) (Mureseanu et al., 2008; Lee et al., 2011). In this work, amine groups were grafted to the silica surface via a carbon matrix. This functionalisation strategy allows for the inclusion of not only amine groups, but also hydroxyl and carboxyl moieties from the carbon matrix, thus potentially increasing metal uptake. The Cu adsorption efficiency of the synthesised adsorbent was then determined by batch experiments at pH 3.

5.2 Materials and methods

5.2.1 Materials

All metal salts used were of analytical grade or higher. $Cu(NO_3)_2 \cdot 2.5H_2O$ and commercially prepared silica NPs were purchased from Sigma-Aldrich (Schnelldorf, Germany). 2,7 dihydroxynathpthalene (DHN) and hexamine were purchased from Ace chemicals (Johannesburg, South Africa). Deionised water was used for the preparation of Cu stocks and dilutions. The pH of solutions was measured using an Orion Star A211 pH meter (Thermo Scientific) and adjustments made prior to experiments using 0.01 M HNO_3 and 0.01 M NaOH.

5.2.2 Synthesis of amine-functionalized silica-carbon nanoparticle adsorbents

Amine-functionalised silica-carbon (NH-SC) hybrid NPs were prepared by a three step process that involved: (i) carbon-coating of silica NPs resulting in silica-carbon (SC) composites, (ii) oxidation of the carbon layer and (iii) grafting of amine functional groups on SC composites. Carbon-coating was performed using the method reported by Nishihara et al. (2008). Silica NPs (3 g) were added to 6 g of DHN in 100 mL of acetone and the mixture stirred overnight in a covered vessel at ambient temperature. The acetone was then evaporated and the product heated at 300°C for 1 hour under nitrogen. Upon cooling, the SC composite was washed three times with 35 mL acetone to remove unreacted DHN and heated at 450°C for 2 hours. The carbon layer was then oxidized by heating the silica-carbon (SC) composites in concentrated HNO_3 (100 mL) for three hours at 80°C. Particles were retrieved by centrifugation at 2808 *g* for 30 minutes, washed with deionised water until the pH was 5, and dried in an oven at 80°C for 6 hours. Amine functionalisation was performed using hexamine: 1 g of oxidised SC particles was added to 24 g of hexamine dissolved in 40 mL of water and the mixture stirred at 90°C for 24 hours. The product, NH-SC, was retrieved by centrifugation, washed several times with distilled water and oven-dried at 80°C for 12 hours.

5.2.3 Characterisation of the adsorbent

The size of NH-SC particles was determined by TEM using a FEI Tecnai G^2 Spirit TEM operating at an acceleration voltage of 120 kV. Nitrogen adsorption-desorption isotherms were performed on a Micrometrics Tristar 3000 (Georgia, USA) after degassing the sample for 4 hours at 150°C. The BET surface area was determined from analysis of adsorption-desorption isotherms at a relative pressure range of 0.1-1.0. Fourier-transform infrared (FTIR) spectra of NH-SC composites were collected in the 4000-600 cm^{-1} frequency range using a Bruker Tensor 27 IR spectrophotometer (Massachusetts, USA). The carbon content of the adsorbent was quantified by elemental analysis on a Leco SC 632 Analyser (Michigan, USA).

5.2.4 Adsorption studies

Cu adsorption by the NH-SC NPs was quantified in batch experiments using 2 mg L^{-1} Cu solutions. This concentration was selected based on concentrations determined in AMD-impacted surface water (Etale et al. 2014, *in press*). The effects of the following variables on Cu uptake by NH-SC NPs at pH 3 (± 0.1) were quantified (i) amount of adsorbent (3, 5, 7, 10, 15 and 20 mg), (ii) contact time (30 seconds to 1 hour) and (iii) Cu concentrations (0.47-2.87 mg L^{-1}). Adsorption was also quantified at pH 5, 7 and 9 in order to determine adsorbent efficiency in pH-amended mine drainage. Finally, the selectivity of the NH-SC adsorbent for Cu in a multi-element solution consisting of Ag, Cd, Co, Cr, Mn, Pb and Zn was also quantified. Experiments were conducted in triplicate and at ambient temperature (~25°C).

In a typical experiment, 10 mg of the adsorbent was added to a 10 mL sample of pH-adjusted Cu solution in a 40 mL polyethylene terephthalate (PET) jar. The mixture was then shaken at 200 rpm for 60 minutes followed by centrifugation using Amicon ultracentrifugal filters (100 kDa molecular weight cut off; Millipore) to remove the adsorbent. Filtrates were acidified with 3 mL of 1% HNO_3 and their Cu concentrations determined by inductively coupled plasma-optical emission spectrometry (ICP-OES; Spectro Instruments, Kleve, Germany). The adsorption capacity of the adsorbent (q_e) percent adsorption efficiency were calculated using Equations 1 and 2, respectively (Roy and Bhattacharya 2012). C_i and C_e are the initial and equilibrium metal concentrations (mg L^{-1}), m is the mass of adsorbent applied (g) and V is the volume of the solution used (L).

$$q_e = \frac{(C_i - C_e)V}{m} \quad (1)$$

$$\%\ Cu\ removal = \frac{(C_i - C_e)}{C_i} \times 100 \quad (2)$$

5.2.5 Data analyses

Kinetics

Kinetics data were fitted to the pseudo-first-order model (Equation 3) and the pseudo-second-order model (Equation 4) where q_e and q_t are the adsorbent loading capacities (mg g^{-1}) at equilibrium and at time t, respectively (Ho and Mckay 2004). Reaction rate constants (k_1 and k_2) were determined from plots of model equations: k_1 from the slope of the plot of log ($q_e - q_t$) versus t and k_2 from the intercept of t/q_t versus t.

$$\log(q_e - q_t) = \log q_e - \left(\frac{k_1}{2.303}\right)t \tag{3}$$

$$\frac{t}{q_t} = \left(\frac{1}{k_2}\right) + \left(\frac{1}{q_e}\right)t \tag{4}$$

Isotherms

Isotherm data were fitted to equations of the Langmuir and Freundlich models (Equations 5 and 6, respectively) (LeVan & Vermeulen, 1981). The Langmuir model describes monolayer adsorption at energetically homogenous sites while the Freundlich model describes multi-layer adsorption to heterogeneous sites.

$$\frac{C_e}{q_e} = \left(\frac{1}{q_{\max}}\right)C_e + \left(\frac{1}{K_L q_{\max}}\right) \tag{5}$$

$$\log q_e = \left(\frac{1}{n}\right)\log C_e + \log K_F \tag{6}$$

For the Langmuir model, the maximum concentration of metal ions sorbed per unit weight of adsorbent, q_{max}, (mg g^{-1}) and the Langmuir constant for the reaction, $K_{L,}$ were determined from the slope and intercept of a plot of C_e/q_e versus C_e. The energetic heterogeneity of the sorbent surface, $1/n$, and relative capacity of the adsorbent, K_F, in were determined from the slope and intercept of the Freundlich model equation.

5.3 Results and discussion

5.3.1 Adsorbent characterisation

The proposed mechanism for the synthesis of NH-SC hybrid NPs is presented in Scheme 1. A condensation reaction between silanol groups and the hydroxyl groups of the 2,7 dihydroxynaphthalene was the first step of this synthesis strategy. The resulting silica-carbon compound was heated in two steps to fix the adsorbed carbon from DHN (carbonisation). This carbonized composite was then heated in concentrated HNO_3 in order to oxidize the carbon layer and prime it for hexamine uptake, a process which also reduced particle

hydrophobicity. In the final step, amine functionalities from hexamine, a cyclic aliphatic compound, were grafted onto the carbon layer.

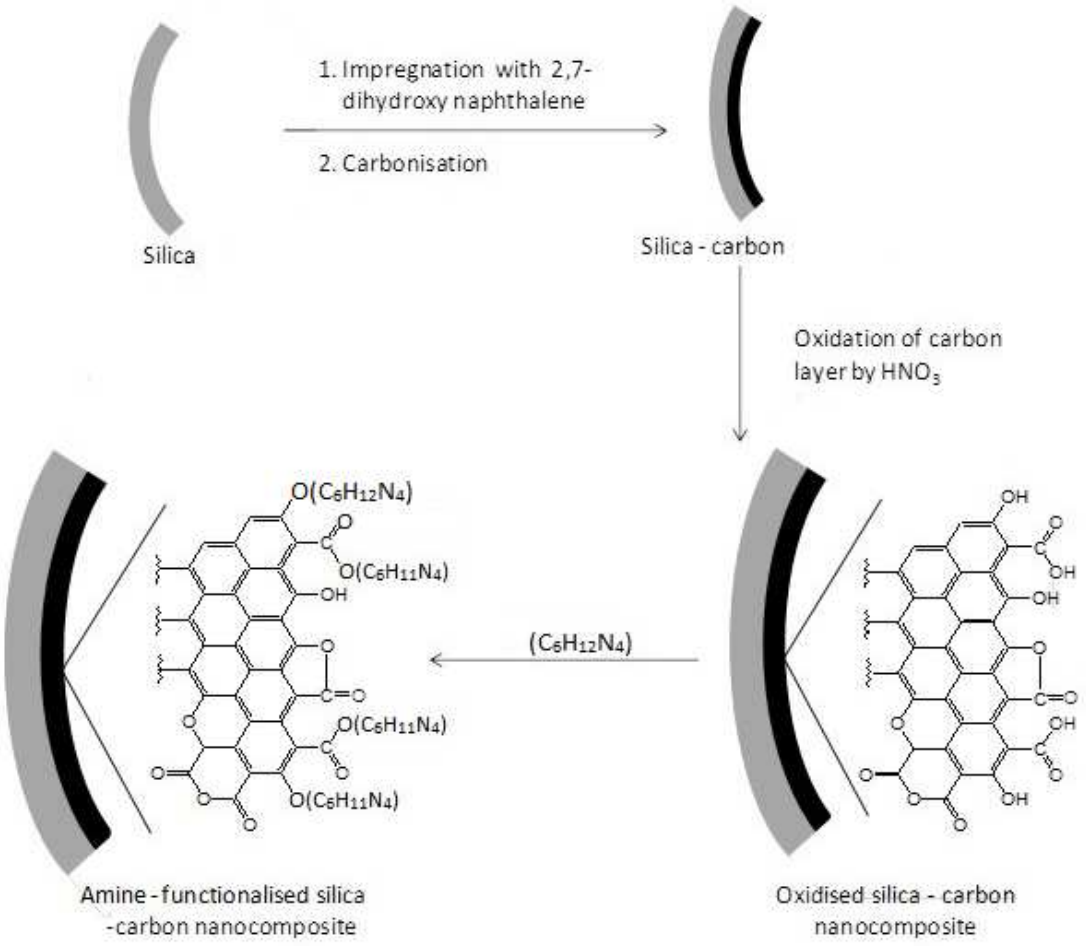

Scheme 1: Proposed synthetic route for the preparation of amine-functionalised silica-carbon hybrid NPs

Transmission electron micrographs (Figure 1) revealed that the synthesised NH-SC adsorbents were nano-sized. These composites were also agglomerated, similar to parent silica NPs (Etale et al., unpublished data). Valle-Vigón et al. (2013) suggested that carbonisation of silica NPs occurred primarily in pores. We surmise that external surface properties of parent silica NPs were largely conserved in the NH-SC particles, hence the tendency for agglomeration, although the nano-scale of the composites may also result in agglomeration due to high surface energies (Waychunas et al., 2005).

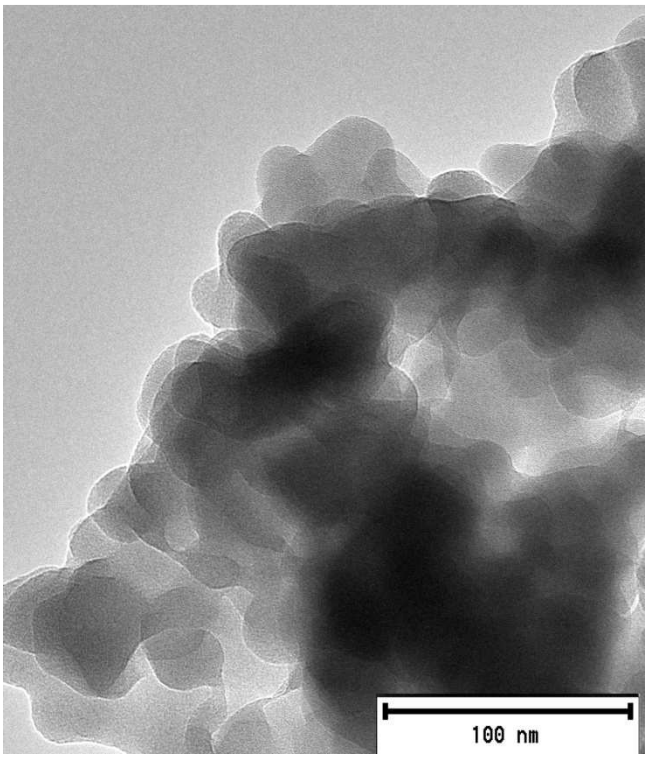

Figure 5.1: TEM image of amine-functionalised silica-carbon hybrid NPs

In contrast, surface area, pore volumes and pore diameters of composites were different from those of the parent silica (Table 5.1). The specific surface area and pore volume of NH-SC adsorbents were approximately 12 and 2.5 times less than those of parent silica. In fact, specific surface area and pore sizes reduced with increasing particle functionalisation i.e. reduction from 612 to 153 $m^2 g^{-1}$ upon carbonization of the silica NPs, followed by a further reduction to 52 $m^2 g^{-1}$ after amine functionalisation. Similar observations were made by Valle-Vigón et al. (2013). These authors reported a reduction in the surface area of SBA-15 silica NPs after carbonisation and oxidation, from 590 to 310 $m^2 g^{-1}$. A greater surface area decrease is reported here i.e. 612 to 153 $m^2 g^{-1}$ which is likely the result of pore clogging by deposited carbon. Clogging was probably exacerbated by the small size of pores. Indeed, with pore diameters of only 4.11 nm, NPs in this study were only half as a large as those in the study by Valle-Vigón (9.5 nm) and therefore more prone to blockages. This hypothesis was confirmed by the hysteresis plot of NH-SC (Figure 5.2) which revealed a reversible type II isotherm characteristic of non-porous adsorbents (Sing et al., 1985).

Table 5.1: Physical properties of silica, oxidised silica-carbon composites and aminated silica-carbon composites.

Sample	S_{BET} ($m^2\ g^{-1}$)	Pore volume ($cm^3\ g^{-1}$)	Pore diameter (nm)	Carbon content (wt. %)	N content (wt. %)[a]
Silica	612	0.63	4.11	-	-
Oxidised silica-carbon	153	0.36	9.41	9.30	-
NH-SC	53	0.26	19.21	21.80	8.32

[a] calculated from C:N ratio in hexamine

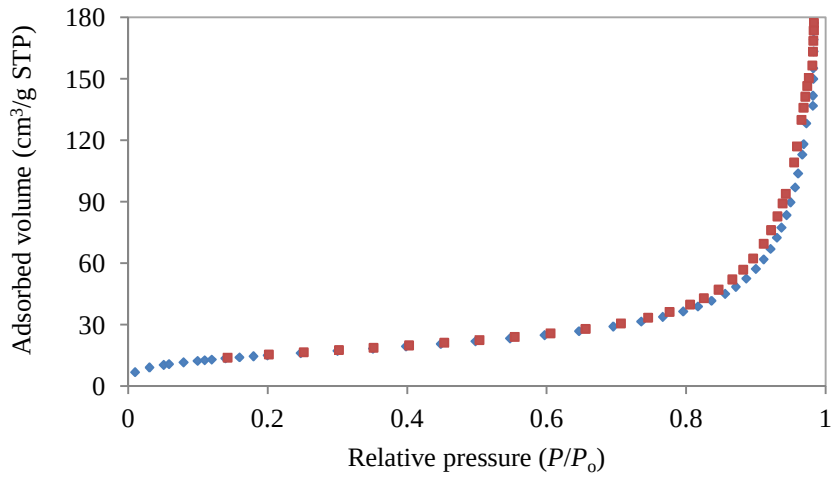

Figure 5.2: Nitrogen adsorption-desorption isotherm for the NH-SC adsorbent.

Functional groups on bare silica and the NH-SC adsorbent were identified from FTIR spectra collected between 4000 and 600 cm^{-1} (Figure 5.3). The spectra of bare silica (a) consisted of bands at 3365 cm^{-1} and 1637 cm^{-1} due to O-H vibrations of adsorbed water as well as the characteristic Si-OH vibration and stretching bands at 1057 and 956 cm^{-1} (Lambert et al., 1987). The attachment of hexamine to the silica matrix was confirmed from the NH-SC spectra (b) by the bands at (i) 809 cm^{-1} which corresponds to N-H wagging (ii) 1370 which corresponds to C-N bonds in the hexamine molecule and (iii) 2954, 2873, 1457 and 1002 cm^{-1} which correspond to stretching, vibration and bending modes of C-H bonds in aliphatic compounds. There was also evidence of the presence of carboxyl groups from COO^- asymmetric stretching vibrations (1607 cm^{-1}) and of hydroxyl groups (697 and 670 cm^{-1}) implying that not all carboxyl and hydroxyl moieties generated during oxidation were aminated.

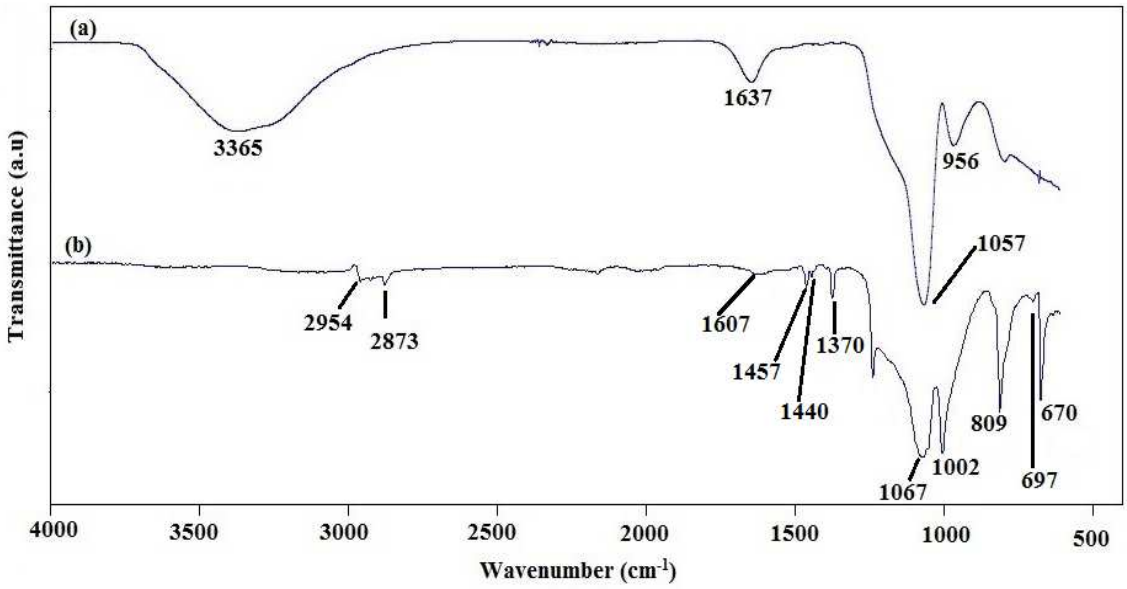

Figure 5.3: FTIR spectra of parent silica NPs (a) and the NH-SC hybrid NPs (b)

5.3.2 Effect of adsorbent concentration

The Cu removal capacity of the NH-SC adsorbent was then investigated. The first step involved quantifying the adsorbent concentration that resulted in optimal Cu uptake. The results of experiments conducted with 3, 5, 7, 10, 15 and 20 mg of the adsorbent showed that Cu uptake increased with adsorbent concentration and was maximal with 10 mg of the adsorbent (Figure 5.4). No increase in metal uptake was recorded with higher adsorbent concentrations; hence 10 mg of the adsorbent was used for subsequent experiments.

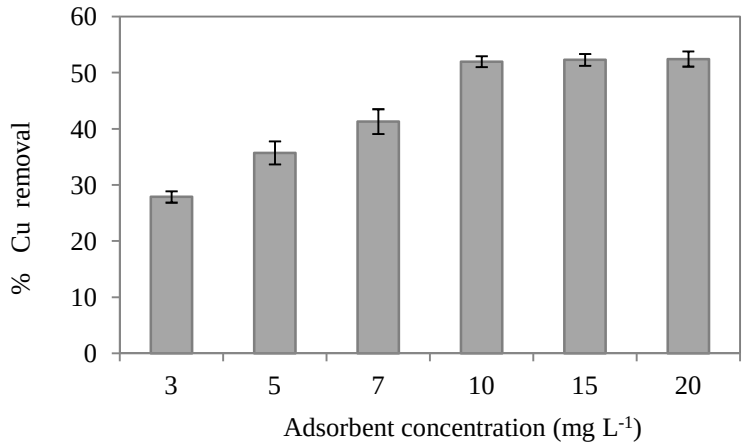

Figure 5.4: The effect of adsorbent concentration on Cu uptake at pH 3. (Experimental conditions: adsorbent mass = 10 mg, contact time = 60 minutes; Cu concentration = 2 mg L^{-1}, sample volume = 10 mL, temperature = ~25°C.)

5.3.3 Effect of contact time

The effect of contact time on Cu adsorption by the NH-SC hybrid NPs was quantified at time intervals ranging from 30, 45, 60, 180, 300, 600, 900, 1800, 2700 and 3600 seconds. Adsorption increased with time from 38% at 30 seconds to 52% after 1 hour (Figure 5.5a). The data also show that reactions attained equilibrium in 45 minutes although the increase in Cu uptake between 15 and 45 minutes was only 2%. Kinetics data were better fitted by the pseudo-second-order model (R^2 = 0.99; Figure 5b) than the pseudo-first-order model (R^2 = 0.943), implying that Cu binding by the adsorbent was by chemisorption (Ho & Mckay, 2004). The rate of the reaction, k_2, was determined as 0.03 mg g^{-1} sec^{-1} and the calculated q_e value of 1.09 mg g^{-1} was close to the experimental value of 1.08 mg g^{-1}.

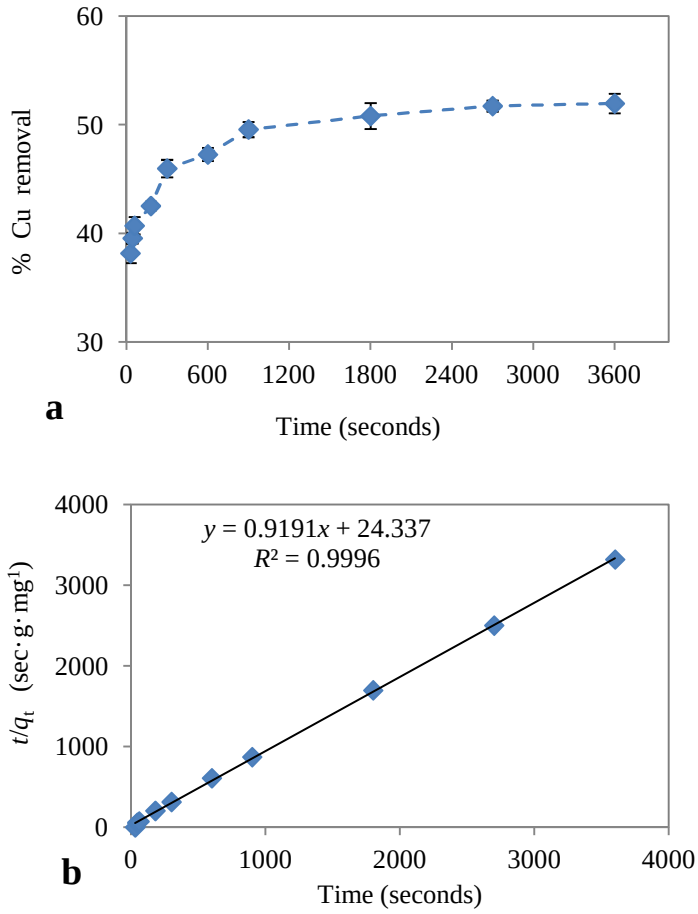

Figure 5.5: (a) The effect of contact time on the uptake of Cu ions by NH-SC hybrid NPs (± SD), and (b) the pseudo-second-order plot for the adsorption. (Adsorbent concentration = 10 mg, Cu concentration = 2 mg L^{-1}, volume of Cu solution = 10 mL, solution pH = 3).

5.3.4 Effect of Cu concentration

The effect of Cu concentrations on the adsorption efficiency of the adsorbent was quantified using metal solutions of the following concentrations: 0.47, 0.53, 0.77, 0.99, 2.09,

2.37 and 2.87 mg L^{-1}. Cu uptake by NH-SC at pH 3 increased with initial concentrations, from 22% in 0.47 mg L^{-1} solutions to 56% in 2.87 mg L^{-1} solutions (Figure 5.6a). These increases are due to the greater diffusion drive to the adsorbent surface at higher metal concentrations (Ho & Mckay, 2004).

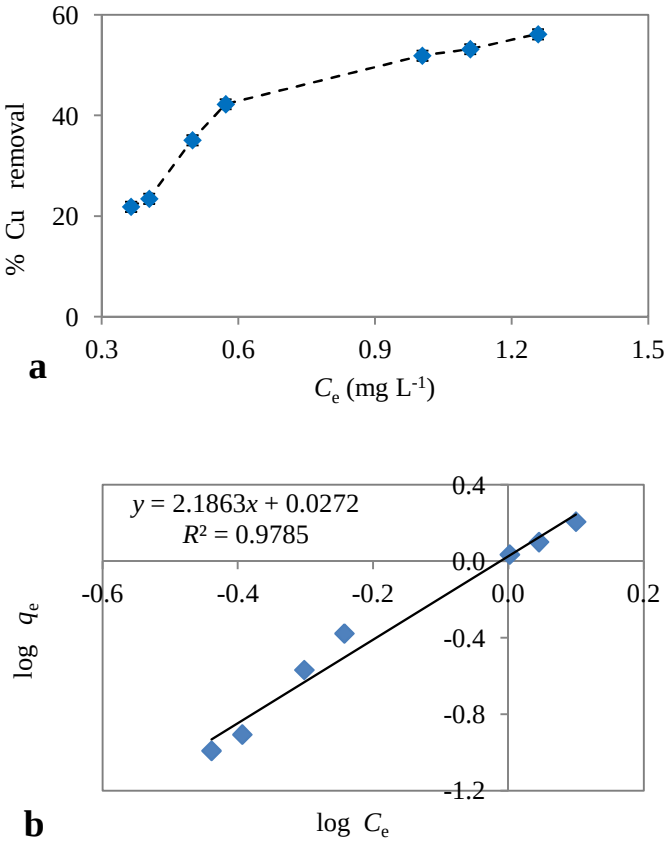

Figure 5.6: (a) The effect of metal concentration on adsorption efficiency of NH-SC hybrid NPs and (b) the linearised Freundlich-model plot of adsorption data. (Adsorbent concentration = 10 mg, Cu solution = 10 mL of 2 mg L^{-1}, solution pH =3).

Isotherm data were better fitted by the Freundlich model (R^2 = 0.98; Figure 6b) than the Langmuir model (R^2 = 0.73), a finding which corroborates the chemisorption conclusion above. This fit to the Freundlich model also implies that adsorbent binding sites were energetically heterogeneous and that Cu ions could have formed more than a single layer on the adsorbent surface. The >1 1/*n* value indicates that Cu uptake was by chemisorption and precipitation (Foo & Hameed, 2010). The adsorption capacity (K_F) of the adsorbent was 1.06 mg g^{-1}. This value was higher than that reported for a fly ash-wollastonite adsorbent i.e. 0.33 mg g^{-1} (Panday et al., 1986) but lower than that of maghemite (4.35 mg g^{-1}) (Etale et al., *in press*) and even unfunctionalised silica (4.06 mg g^{-1}) (Etale et al., unpublished data). The lower adsorption, especially relative to that of bare silica NPs is likely the result of the lower adsorptive surface area of NH-SC (Table 1). Similar findings were reported by Lee et al.

(2011). These authors found that Cu adsorption by amine-functionalised silica NPs decreased with increasing amine chain length due to pore-blocking by longer chains. Adsorption may also be impaired by diminished reactivity of amine sites as a result of (i) hydrogen bonding between adjacent amine groups or (ii) isolation i.e. isolated amine groups tend to be less reactive (Mckittrick & Jones, 2003).

5.3.5 Effect of pH

The adsorption capacity of NH-SC adsorbents was investigated at pH 5, 7 and 9 in order to determine their applicability in pH-amended mine drainage. Cu uptake at these pH levels was higher than at pH 3 (Figure 5.7). The highest adsorption was recorded at pH 5 (62%) while removal at pH 7 and 9 was equal i.e. 57%. These differences may be explained by the pH-related changes in speciation of both Cu and adsorbent functional groups. Cu was present as the free Cu^{2+} ion at pH 3 and 5, and as the insoluble $Cu(OH)_2$ at pH 7 and 9. Despite similar speciation, adsorption was higher at pH 5 relative to pH 3 due to decreased competition for sorption sites from H^+ ions. In addition, fewer amine, hydroxyl and carboxyl functionalities were protonated at this higher pH, thus favouring Cu adsorption. Despite further deprotonation at pH 7 and 9, however, adsorption decreased due to the formation of insoluble $Cu(OH)_2$ specie that were not bound by the NH-SC functionalities. A similar observation was made for Cd adsorption to activated carbon above pH 6 by Ali et al. (2013) - adsorption decreased due to formation of insoluble $Cd(OH)_2$.

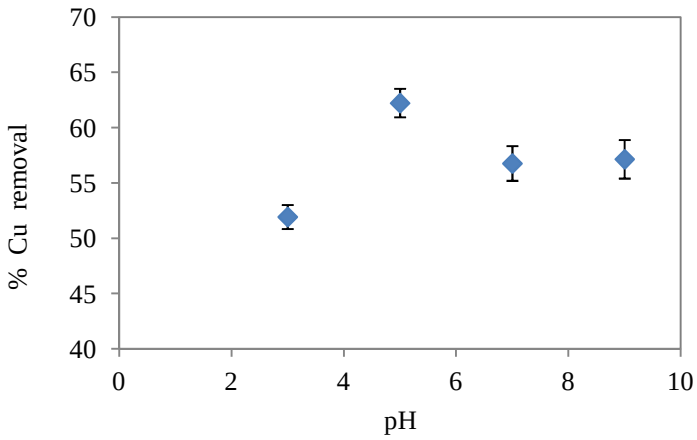

Figure 5.7: The effect of pH in Cu adsorption by NH-SC hybrid NPs. (Adsorbent concentration = 10 mg, Cu concentration = 2 mg L^{-1}, volume of Cu solution = 10 mL).

5.3.6 Selectivity

The selectivity of the synthesised adsorbent for Cu at pH 3 was determined in a multi-element solution of Cd, Co, Cu, Cr, Mn, Pb and Zn. A 10 mL aliquot of a solution containing equimolar concentrations of these ions was reacted with 10 mg of the NH-SC adsorbent. The

results show that ion selectivity was in the order Cu > Pb > Zn > Cr = Mn > Co > Cd (Figure 5.8).

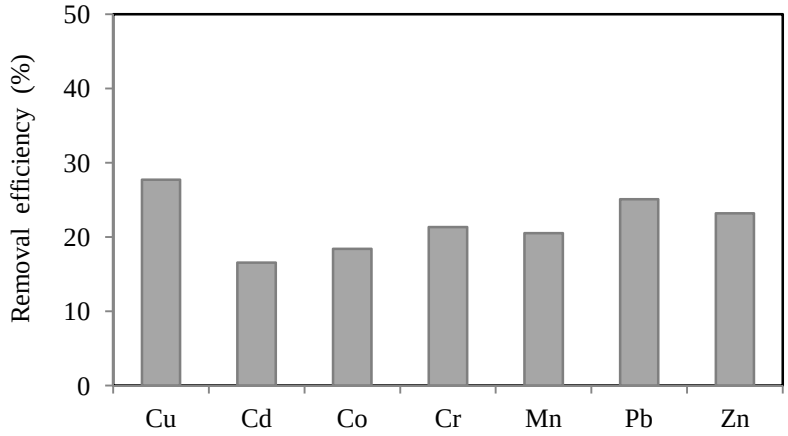

Figure 5.8: The effect of competing ions on Cu adsorption by NH-SC hybrid NPs at pH 3.

The extraction ability of the NH-SC hybrid NPs for the different ions was compared using distribution coefficients, K_d (mL g^{-1}). The higher the K_d value the greater the adsorption capacity of the sorbent for the ion of interest and values ~1 x 10^3 mL g^{-1} indicate good sorption capacity (Fryxell et al., 2005). The results (Table 5.2) show that although NH-SC is a good adsorbent for all the ions tested, its capacity was highest for Cu.

Table 5.2: Distribution coefficients for Cu and other tested metals on the NH-SC adsorbent

Metal ion	K_d (mL g^{-1})
Cu^{2+}	3.89×10^3
Cd^{2+}	2.05×10^3
Co^{2+}	2.20×10^3
Cr^{2+}	2.66×10^3
Mn^{2+}	2.66×10^3
Pb^{2+}	3.33×10^3
Zn^{2+}	2.99×10^3

5.4 Conclusion

Amine-functionalised silica-carbon hybrid NPs were successfully synthesised and applied for the adsorptive removal of Cu from aqueous media. Cu removal was rapid and increased with initial metal concentrations. The fit of kinetic and isothermic data to the pseudo-second-order and Freundlich models, respectively, indicates that Cu binding to the amine, carboxyl

and hydroxyl functional groups of the adsorbent was by chemisorption. Adsorption was greatest at pH 5. Thus, although the pH of AMD-contaminated water is often ≤ 3, it may be worthwhile in practical applications to raise its pH to pH 5 in order to increase Cu removal by this adsorbent. The adsorbent also showed good affinity for Cu in multi-elemental solutions at low pH indicating that it can be applied for the targeted removal of Cu from AMD-contaminated waters. Additional work on desorption, re-use and functionalisation with less bulky amine molecules to minimise pore blocking can improve the efficiency of this adsorbent and allow for wider application.

5.5 Acknowledgements

This work was funded by the Global Change and Sustainability Research Institute (GCSRI) of the University of the Witwatersrand. We appreciate the assistance of Zama Mthabela with carbon analyses.

5.6 References

Aguado, J., Arsuaga, J.M., Arencibia, A., Lindo, M. & Gascón, V. 2009. Aqueous heavy metals removal by adsorption on amine-functionalized mesoporous silica. *Journal of Hazardous Materials*, 163(1): 213–21.

Ali, S.Z., Athar, M., Farooq, U. & Salman, M. 2013. Insight into equilibrium and kinetics of the binding of cadmium ions on radiation-modified straw from *Oryza sativa*. *Journal of Applied Chemistry*, 2013: 1–12.

Bai, Y., Rong, F., Wang, H., Zhou, Y., Xie, X. & Teng, J. 2011. Removal of copper from aqueous solutions by adsorption on elemental selenium nanoparticles. *Journal of Chemical & Engineering Data*, 56: 2563–2568.

Beck, J.S., Vartuli, J.C., Roth, W.J., Leonowicz, M.E., Kresge, C.T., Schmitt, K.D., Chu, C.T.-W., Olson, D.H., Sheppard, E.W., McCullen, S.B., Higgins, J.B. & Schlenker, J.L. 1992. A new family of mesoporous molecular sieves prepared with liquid crystal templates. *Journal of the American Chemical Society*, (14): 10834–10843.

Durand, J.F. 2012. The impact of gold mining on the Witwatersrand on the rivers and karst system of Gauteng and North West Province, South Africa. *Journal of African Earth Sciences*, 68: 24–43.

Engates, K.E. & Shipley, H.J. 2011. Adsorption of Pb, Cd, Cu, Zn, and Ni to titanium dioxide nanoparticles: effect of particle size, solid concentration, and exhaustion. *Environmental Science and Pollution Research*, 18(3): 386–395.

Foo, K.Y. & Hameed, B.H. 2010. Insights into the modeling of adsorption isotherm systems. *Chemical Engineering Journal*, 156: 2–10.

Fryxell, G.E., Lin, Y., Fiskum, S., Birnbaum, J.C., Wu, H., Kemner, K. & Kelly, S. 2005. Actinide sequestration using self-assembled monolayers on mesoporous supports. *Environmental Science & Technology*, 39(5): 1324–31.

Georgescu, I., Mureseanu, M., Cârja, G. & Hulea, V. 2013. Adsorptive removal of cadmium and copper from water by mesoporous silica functionalized with N-(Aminothioxomethyl)-2-thiophen carboxamide. *Journal of Environmental Engineering*, 139(10): 1285–1296.

Grover, V.A., Hu, J., Engates, K.E. & Shipley, H.J. 2012. Adsorption and desorption of bivalent metals to hematite nanoparticles. *Environmental Toxicology and Chemistry*, 433(1): 86–92.

Gupta, P. & Paul, S. 2011. Amorphous carbon-silica composites bearing sulfonic acid as solid acid catalysts for the chemoselective protection of aldehydes as 1,1-diacetates and for N-, O- and S-acylations. *Green Chemistry*, 13(9): 2365.

Hao, Y.-M., Man, C. & Hu, Z.-B. 2010. Effective removal of Cu (II) ions from aqueous solution by amino-functionalized magnetic nanoparticles. *Journal of Hazardous Materials*, 184(1-3): 392–9.

Ho, Y.S. & Mckay, G. 2004. Sorption of copper(II) from aqueous solution by peat. *Water Air and Soil Pollution*, 158: 77–97.

Hu, Z., Zhang, X., Zhang, D. & Wang, J. 2012. Adsorption of Cu^{2+} on amine-functionalized mesoporous silica brackets. *Water, Air, & Soil Pollution*, 223(5): 2743–2749.

Jooste, S. & Thirion, C. 1999. An ecological risk assessment for a South African acid mine drainage. *Water Science and Technology*, 39(10-11): 297–303.

Ju-Nam, Y. & Lead, J.R. 2008. Manufactured nanoparticles: An overview of their chemistry, interactions and potential environmental implications. *Science of the Total Environment*, 400(1-3): 396–414.

Lambert, J.B., Hurvell, H.F., Lightner, D.A. & Cooks, R.G. 1987. *Introduction to organic spectroscopy*. 1st ed. New York: MacMillan publishing company.

Lee, H.W., Cho, H.J., Yim, J.H., Kim, J.M., Jeon, J.K., Sohn, J.M., Yoo, K.S., Kim, S.S. & Park, Y.K. 2011. Removal of Cu(II)-ion over amine-functionalized mesoporous silica materials. *Journal of Industrial and Engineering Chemistry*, 17(3): 504–509.

LeVan, M.D. & Vermeulen, T. 1981. Binary Langmuir and Freundlich isotherms for ideal adsorbed solutions. *Journal of Physical Chemistry*, 85(22): 3247–3250.

Lu, A.-H., Li, W.-C., Muratova, N., Spliethoff, B. & Schüth, F. 2005. Evidence for C-C bond cleavage by H_2O_2 in a mesoporous CMK-5 type carbon at room temperature. *Chemical Communications*, (41): 5184–5186.

McCarthy, T.S. 2011. The impact of acid mine drainage in South Africa. *South African Journal of Science*, 107(5/6): 1–7.

Mckittrick, M.W. & Jones, C.W. 2003. Toward single-site functional materials s preparation of amine-functionalized surfaces exhibiting site-isolated behavior. *Chemistry of Materials*, 15: 1132–1139.

Mercier, L. & Pinnavaia, T.J. 1998. Heavy metal ion adsorbents formed by the grafting of a thiol functionality to mesoporous silica molecular sieves: Factors affecting Hg(II) uptake. *Environmental Science & Technology*, 32(18): 2749–2754.

Mureseanu, M., Reiss, A., Stefanescu, I., David, E., Parvulescu, V., Renard, G. & Hulea, V. 2008. Modified SBA-15 mesoporous silica for heavy metal ions remediation. *Chemosphere*, 73(9): 1499–504.

Naicker, K., Cukrowska, E. & McCarthy, T.S. 2003. Acid mine drainage arising from gold mining activity in Johannesburg, South Africa and environs. *Environmental Pollution*, 122(1): 29–40.

Nishihara, H., Fukura, Y., Inde, K., Tsuji, K., Takeuchi, M. & Kyotani, T. 2008. Carbon-coated mesoporous silica with hydrophobicity and electrical conductivity. *Carbon*, 46(1): 48–53.

Panday, K.K., Prasad, G. & Singh, V.N. 1986. Mixed adsorbents for Cu(II) removal from aqueous solutions. *Environmental Technology Letters*, 7(1-12): 547–554.

Sing, K.S.W., Everett, D.H., Haul, R.A., Moscou, L., Pierotti, R.A., Rouquerol, J. & Siemieniewska, T. 1985. Reporting physisorption data for gas/solid systems. *Pure and Applied Chemistry*, 57(4): 603–619.

Slowing, I.I., Vivero-escoto, J.L., Wu, C.-W. & Lin, V.S.-Y. 2008. Mesoporous silica nanoparticles as controlled release drug delivery and gene transfection carriers. *Advanced Drug Delivery Reviews*, 60: 1278–1288.

Titirici, M.-M., Thomas, A. & Antonietti, M. 2007. Aminated hydrophilic ordered mesoporous carbons. *Journal of Materials Chemistry*, 17(32): 3412.

Tutu, H., McCarthy, T.S. & Cukrowska, E. 2008. The chemical characteristics of acid mine drainage with particular reference to sources, distribution and remediation: The Witwatersrand Basin, South Africa as a case study. *Applied Geochemistry*, 23(12): 3666–3684.

Valle-Vigón, P., Sevilla, M. & Fuertes, A.B. 2013. Carboxyl-functionalized mesoporous silica–carbon composites as highly efficient adsorbents in liquid phase. *Microporous and Mesoporous Materials*, 176: 78–85.

Valle-Vigón, P., Sevilla, M. & Fuertes, A.B. 2012. Sulfonated mesoporous silica–carbon composites and their use as solid acid catalysts. *Applied Surface Science*, 261: 574–583.

Wang, X., Liu, R., Waje, M.M., Chen, Z. & Yan, Y. 2007. Sulfonated ordered mesoporous carbon as a stable and highly active protonic acid catalyst. *Chemistry of Materials*, 19(10): 2395–2397.

Waychunas, G.A., Kim, C.S. & Banfield, J.F. 2005. Nanoparticulate iron oxide minerals in soils and sediments: Unique properties and contaminant scavenging mechanisms. *Journal of Nanoparticle Research*, 7(4-5): 409–433.

Yang, Z., Xia, Y. & Mokaya, R. 2006. Periodic mesoporous organosilica mesophases are versatile precursors for the direct preparation of mesoporous silica/carbon composites, carbon and silicon carbide materials. *Journal of Materials Chemistry*, 16(33): 3417.

6 The effects of silica and maghemite nanoparticles on uptake of Cu(II), Mn(II) and U(VI) from aqueous solutions by a freshwater alga - *Scenedesmus sp.*

Anita Etale[a] *, Hlanganani Tutu[b], Deanne C. Drake[a]

[a] School of Animal Plant and Environmental Sciences, [b] Molecular Sciences Institute, School of Chemistry, University of the Witwatersrand, Private Bag X3, WITS 2050, Johannesburg, South Africa.

The effect of silica and maghemite nanoparticles (NPs) on the sequestration of Cu, Mn and U by *Scenedesmus sp.* was investigated with the aim of quantifying the effect of NPs on phycoremediation efficiency. Metal adsorption was thus quantified in NP-only, algae-only and NP-algae batch treatments. Adsorption in NP-only systems was rapid, attaining equilibrium within 5 minutes. Removal of Cu was higher with maghemite NPs while more Mn and U were removed with silica NPs. Reaction kinetics were better described by the pseudo-second-order rate model and isotherm data were fitted by the Freundlich model. Metal removal in NP-algal systems was significantly higher than in algae-only and NP-only systems. The hypothesis that metal uptake by algae would be enhanced in the presence of NPs due to increased sorption sites availed by NPs was therefore confirmed. NPs also modified algal metal partitioning: extracellular concentrations were higher and intracellular fractions lower in the presence of NPs relative to controls (without NPs). NP agglomeration in metal solutions was quantified in order to determine the potential for NP absorption by algal cells. Results showed that NPs coalesced to form agglomerates 300 (±100) nm in diameter, which were unlikely to be absorbed through algal cell walls. NPs can therefore increase the phycoremediation efficiency of *Scenedesmus sp.* by ~12 - 27% although optimal NP concentrations need to be quantified to avoid NP-induced toxicity to algae and to minimize NP aggregation.

Key words: algae, biosorption, phycoremediation, copper, manganese, uranium.

*Corresponding author. Telephone: +27 11 717 6425; Email address: aetale@gmail.com

6.1 Introduction

The contamination of aquatic systems by metal and radionuclide ions as a result of mining and other anthropogenic activities has elicited increasing concerns globally. This is because excessive metal concentrations are deleterious to both humans and other organisms, extending beyond individual species to entire communities (Niyogi et al., 2002). As such, research is increasingly focused on finding novel and efficient methods for the remediation of metal-contaminated water, not only to avert toxicity in ecosystems but also to meet the growing human demand for water.

Various techniques including chemical precipitation, reverse osmosis, nanofiltration, adsorption and ion exchange are currently applied for the removal of metal ions from contaminated water (Kurniawan et al., 2006). The high costs of some of these conventional technologies has, however, spurred interest in lower cost technologies that make use of plants (phytoremediation) and algae (phycoremediation). These are relatively new approaches to the treatment of metal-contaminated water that exploit the potential of algae and higher plants to accumulate metal ions in their biomass (Rai, 2009). The use of microalgae e.g. *Scenedesmus sp.* for phycoremediation is particularly attractive due to their large surface area to volume ratios. These organisms also possess and high-affinity metal binding functionalities on their cell walls *viz.* hydroxyl, sulphydryl, carboxyl and amino groups that enable microalgae to bind up to 10% of their biomass as metals (Monteiro et al., 2008; Rajamani et al., 2007).

The adsorptive removal of metal ions from contaminated water is also of considerable interest due to the ease of the adsorption process and the availability of a wide range of adsorbents. In keeping with recent advances in nanoscience, nanoparticles are increasingly investigated as adsorbents for the remediation of metal-contaminated water. Because of their high reactivities and relatively large surface areas, nanoparticles (NPs) sequester contaminants more efficiently than larger adsorbents, while also generating smaller volumes of contaminated wastes (Engates & Shipley, 2011). Various types of NPs have been investigated including maghemite (Tuutijärvi et al., 2009), hematite (Grover et al., 2012), zero-valent iron (Wilkin & McNeil, 2003), silica (Mureseanu et al., 2008), alumina (Kim et al., 2004) and titania (Giammar et al., 2007).

The aim of this study was to explore the combined use of NPs and algae for the remediation of metal contaminated water. Based on the high efficiency of both these adsorbents, metal removal should be enhanced relative to NP-only or algae-only systems due to biologically mediated uptake, higher sorptive surface areas and the high reactivity of NPs. Recent evidence also points to a reduction in the toxicity of metal ions to algae in the presence of NPs (Hartmann et al., 2010; Yang, Miao, et al., 2012; Yang, Li, et al., 2012; Dalai et al., 2014). As such, besides increasing

sorptive surface areas and the efficiency of phycoremediation, NPs may also increase the viability of algae in remediation systems.

Cu, Mn and U are common metal contaminants in freshwater bodies receiving wastewater from mining and industrial effluent. Their uptake by *Scenedesmus sp.,* an easily cultured freshwater green microalga with a high metal removal capacity (Zhang et al., 1997; Knauer et al., 1997; Knauer et al., 1999; Monteiro et al., 2008; Terry & Stone, 2002) was studied in the presence and absence of silica and maghemite NPs in order to determine the influence of NPs on metal removal by *Scenedesmus sp.* The influence of NPs on the partitioning of metal ions between extracellular and intracellular fractions of algal cells was also quantified. The information generated from this study, besides informing the optimization of phycoremediation, may also be applied for delineating the potential effects of NPs on algae-contaminant interactions, especially in light of the expected increase of anthropogenic NPs in the environment (Wilson Centre, 2014). They also provide insights into the transport of metals within natural environments in which metals, NPs and algae are important components.

6.2 Materials and methods

6.2.1 Materials

Analytical grade $Cu(NO_3)_2 \cdot 2.5\ H_2O$ and $Mn(NO_3)_2 \cdot H_2O$ (Sigma Aldrich; Schnelldorf, Germany) and $UO_2(NO_3)_2 \cdot 6H_2O$ (Ace Chemicals; Johannesburg, South Africa) were used for experiments. Commercially prepared silica and maghemite NPs were purchased from Sigma Aldrich. A starter culture of *Scenedesmus sp*. was acquired from a stock isolated from a fresh water source in Johannesburg.

All metal solutions, NP suspensions and culture media were prepared using deionised water. NP suspensions were prepared by 30-minute sonications in a water bath. This was done immediately before use to minimise losses through particle settling and adhesion to container walls. Metal solutions were prepared one day in advance to allow for equilibration. The pH of metal solutions was adjusted to pH 6.5 using 0.01 M NaOH. This pH was chosen as it was found to be favourable for the survival of the algae.

6.2.2 Algal culturing

Algae were cultured in modified Bold's Basal media (Supplementary information) in 250 mL Erlenmeyer flasks at 25 ±1°C and with continuous bubbling with air. Light (150 μmol photons/m^2/s) was provided in a 18:6-h light:dark cycle by cool white fluorescent lamps and the pH of cultures was pH maintained at 6-8. All glassware and plastic ware were soaked overnight in

0.2 M HNO_3 and rinsed three times with deionised water before culturing. Glassware and culture media were sterilized by autoclaving at 121°C for 15 minutes before use.

6.2.3 Particle characterization

The primary particle size of NPs was determined by a Tecnai G^2 Spirit transmission electron microscope at an acceleration of 120 kV. NPs were suspended in deionised water, sonicated in a water bath for 30 minutes and placed on lacey copper grids to dry before analysis. The specific surface area, pore volume and pore sizes of particles were determined using a Micrometrics Tristar 3000 (Micrometrics Instruments, USA) following N_2 adsorption-desorption for 4 hours at 150°C. Particle phase (crystalline or amorphous) was determined by X-ray diffraction (XRD) using a Bruker D8 diffractometer (Cu-$K\alpha$).

In order to understand the state of particles in test media, their hydrodynamic sizes in metal solutions were determined by dynamic light scattering (DLS) using a Zetasizer NanoZS (Malvern Instruments, UK). Measurements were taken as soon as NPs were dispensed into metal solutions, t_o, and after 4 hours (t_4; the experimental duration of adsorption reactions). Thus, 3 mg of NPs were suspended in 1 L of deionised water and sonicated for 30 minutes. An aliquot of this suspension (10 mL) was then dispensed into a 50 mL polyethylene terephthalate (PET) jar containing 10 mL metal solution and light scattering readings taken immediately (10-15 seconds lag-time) and after 4 hours. The hydrodynamic sizes of NPs after the 30-minute sonications in deionised water were also determined.

6.2.4 Metal uptake studies

The first step in studying the effect of NPs on algal metal uptake was the investigation of NP-metal interactions. Thus, the kinetics and isotherms of Cu, Mn and U adsorption by NPs were investigated at pH 6.5 (± 0.2). This was followed by quantification of metal adsorption by algae alone and eventually by algae in the presence of NPs.

Adsorption of Cu, Mn and U by silica and maghemite NPs

Adsorption kinetics were determined at reaction durations ranging from 10 seconds to 1 hour using 1.42, 3.30 and 0.99 mg/L of Cu, Mn and U, respectively. Isotherms were studied at concentrations ranging from 0.66-5.41 mg/L for Cu, 1.36-5.65 mg/L for Mn and 0.55-1.57 mg/L for U. Ten millilitres of NP suspension (3 mg/L) was added to each metal ion solution in a polyethylene terephthalate (PET) jar and allowed to react for 5, 10, 15, 30, 45, 60, 300, 600, 900, 1800, 2700 and 3600 seconds. Isotherm experiments were conducted for 60 minutes. All experiments were conducted in duplicate and at ambient temperature (~25°C).

At the end of the incubations, NPs were separated from mixtures using 100 kDa Amicon ultracentrifugal filters at 2,808 *g* for 30 minutes. Filtrates were acidified with 3% HNO_3 and their metal concentrations (non-adsorbed fraction) determined by inductively coupled plasma-optical emission spectrometry (ICP-OES; Spectro Instruments, Kleve, Germany). Metal removal was quantified by mass balance calculations. Nanoparticle metal loading at a given time, q_t (mg/g) and at equilibrium, q_e (mg/g), were calculated using Equations 1 and 2, respectively. C_i and C_e are the initial and equilibrium metal ion concentrations (mg/L), m is the mass of adsorbent (g) and V is the volume of adsorbent solution used (L).

$$q_t = \frac{(C_i - C_e)V}{m} \quad (1)$$

$$q_e = \frac{(C_i - C_e)V}{m} \quad (2)$$

Kinetics data were fitted to the pseudo-second order model ($q_t=q_e$ (1-exp(-kt))) (Ho & Mckay, 2004) and isotherm data to the Freundlich adsorption isotherm ($\log q_e=1/n \times \log C_e + \log K_F$) (LeVan & Vermeulen, 1981). Data fit was determined by linear regression.

Metal uptake by Scenedesmus sp. in the presence and absence of NPs

Experiments were then conducted to investigate the effects of NPs on metal adsorption by *Scenedesmus sp*. Metal uptake by algae was quantified at initial metal concentrations varying from 0.66 - 1.42 mg/L for Cu, 1.36 - 3.30 mg/L for Mn and 0.55 - 0.99 mg/L for U, in the presence or absence of silica and maghemite NPs. Cu and U concentrations were selected based on average concentrations in AMD-contaminated surface water from Johannesburg (Etale et al., 2014) but those of Mn were lower than field concentrations to prevent toxicity.

Algal cells in the exponential growth phase were harvested by centrifugation for 20 minutes at 2,808 *g* and 4°C. The supernatant was discarded and the algal pellet rinsed twice with deionised water and re-suspended in deionised water. One millilitre of harvested cells (1.69×10^8 cells/mL) were then added to 10 mL metal ion solutions in PET jars simultaneously with 10 mL of silica or maghemite NP suspensions (3 mg/L in deionised water). Control experiments i.e. without NPs were also conducted under the same conditions. Experiments were conducted in triplicate, at pH 6.5 (± 0.2), for 4 hours. They were run for this duration due to the rapid rate of metal adsorption by both NPs (as determined in the treatments run in the presence of NPs alone, as well as in previous experiments; *personal observation*) and by algae (Monteiro et al., 2008). This short duration also obviates pH increments due to CO_2 depletion by photosynthesis (Vogel et al., 2010).

At the end of the exposure period, algae or algae-NP pellets were separated from the aqueous fraction as in NP-only experiments. Aqueous fractions were acidified using 3% HNO_3 and their metal concentrations (un-adsorbed metal fraction) determined by ICP-OES.

Determination of extracellular and intracellular metal concentrations of Scenedesmus sp.

In order to quantify both absorbed (intracellular) and surface adsorbed (extracellular) metal concentrations, algal pellets (from controls) and algal-NP pellets (from treatments with NPs) were processed following the method described by Franklin et al. (2000). Briefly, the pellets were re-suspended in 10 mL of 0.02 M ethylenediaminetetraacetic acid di-sodium salt (EDTA), shaken for 60 seconds and centrifuged (2,808 *g*) for 20 minutes at 4°C. The supernatant, considered the extracellular or surface-adsorbed metal fraction, was then decanted, acidified with 3% HNO_3 and analysed for metal concentrations by ICP-OES. The pellet (intracellular contents) was then digested by the addition of 2 mL concentrated HNO_3 and the digest made up to 10 mL with deionised water. An aliquot of un-exposed algae was processed in the same manner in order to facilitate the calculation of actual adsorbed and absorbed concentrations by mass balance.

6.2.5 Statistical analyses

Variations in agglomerate size with metal concentrations, and algal metal uptake in the presence and absence of NPs were analysed for significant differences ($p < 0.05$) based on results of a one-way analysis of variance with Tukey's *post hoc* comparisons. The relationship between intracellular and extracellular metal concentrations was analysed by the Pearson correlation test. Statistical analyses were conducted using SAS (version 9.2).

6.3 Results

6.3.1 Particle characterization

The primary particle size of silica NPs was determined to be in the < 20-50 nm range while that of maghemite NPs as in the < 10-80 nm range (Figure 6.1). The specific surface area of silica NPs was however, much higher than that of maghemite, likely due to its greater pore volume (Table 6.1). X-ray diffractograms (Supplementary Information) showed that silica NPs were amorphous while maghemite NPs were crystalline.

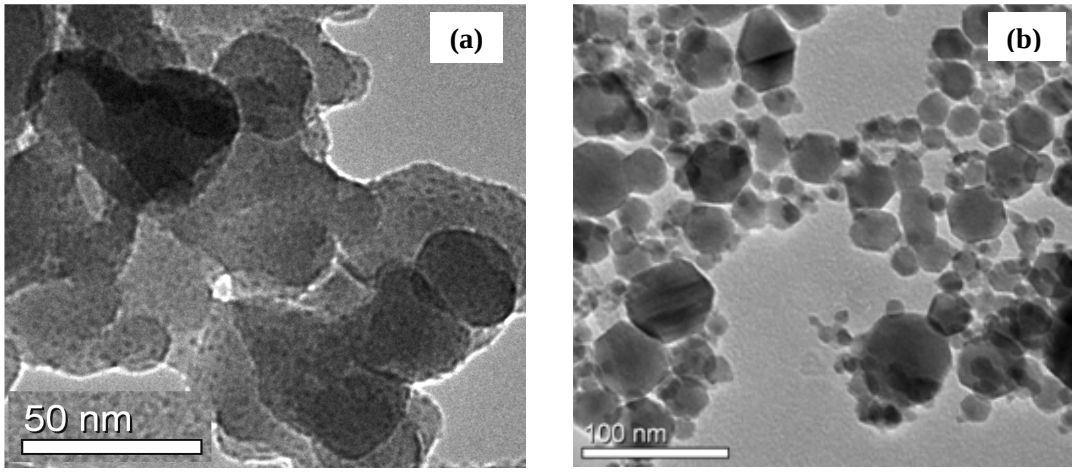

Figure 6.1: Transmission electron micrographs of silica (a) and maghemite (b) NPs

Table 6.1: Structural properties of silica and maghemite NPs as determined by N_2 sorption experiments.

Material	Surface area ($m^2 g^{-1}$)	Pore size (nm)	Pore volume ($cm^3 g^{-1}$)
Silica	611.71	4.12	0.63
Maghemite	40.84	11.27	0.11

Light scattering measurements revealed that both silica and maghemite NPs agglomerated considerably in water (no metal), attaining hydrodynamic diameters of 280 and 283 nm, respectively (Figure 6.2).

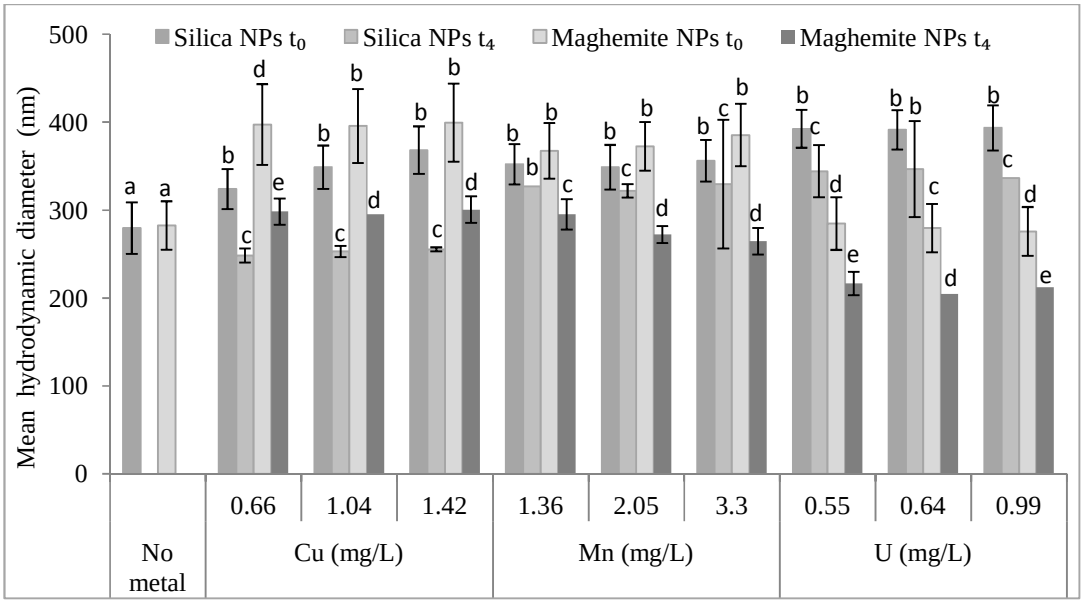

Figure 6.2: Silica and maghemite particle size in the absence of metal ions and in the presence of various concentrations of Cu, Mn and U. t_o values correspond to aggregate diameters immediately NPs were added to metal solutions, and t_4 to diameters after 4 hours. Initial NP concentrations were 3 mg/L and data are mean ± standard deviation (n = 3). Different letters above columns within a concentration indicate statistically significant differences (p <0.05) in the mean hydrodynamic size of NP agglomerates within that particular concentration.

Four observations were made based on the light scattering data. First, NP agglomerates were significantly larger (p < 0.05) in metal solutions than in deionised water. For example, in 1.42 mg/L Cu solutions, Si NPs had a mean hydrodynamic diameter of 368 (±27) nm but only 280 (±29) nm in deionised water. Second, although agglomerate sizes of both NP types were comparable in deionised water, in metal solutions, maghemite NP agglomerates were in some cases larger than those of silica. The third observation was that NP agglomerate sizes were significantly lower after the 4-hour incubation (t_4) compared to t_o. Lastly, although the presence of metal ions increased NP agglomerate sizes (relative to in deionized water), there was no additional increase in agglomerate size with further increases in metal concentrations. Dalai et al. (2014) reported similar observations for titania NPs i.e. that although NP hydrodynamic sizes were greater in the presence of Cr(VI) ions than in their absence, increasing metal concentrations from 0.5 - 1 mg/L did not significantly increase the hydrodynamic size of titania agglomerates.

NPs agglomerate in solution due to (i) inherent properties such as high surface energies and (ii) solution characteristics including pH, temperature, ionic strength and the nature of cations in solution (Guzman et al., 2006; Piccapietra et al., 2012). Divalent cations like Cu^{2+}, Mn^{2+} and

UO_2^{2+} enhance NP agglomeration by decreasing the Debye length of the NP hydration sheath. This leads to less electrostatic repulsion and the domination of attractive forces between particles, hence agglomeration (Navarro et al., 2008). Solution pH also affects agglomerate formation; particles in solutions with a pH close to their pH_{PZC} (pH at which particle charge equals zero) coalesce due to reduced repulsive surface charges. As such, in the present study, maghemite NPs with a pH_{PZC} of 6.3 (Vayssieres, 2009) agglomerated more than those of silica (pH_{PZC} of 2-3 (Kosmulski, 2009)).

Time-related decreases in agglomerate size were likely the result of incomplete adsorption at t_o i.e. immediately after introducing NPs to metal solutions. With time, metal ions experienced the full attractive force of the NP surface and were held closer, resulting in slightly smaller agglomerates at t_4. Nonetheless, the particle size distribution for both NP types was narrow (data not shown) and hydrodynamic diameters were all in the range of 300 (± 100) nm. At this size, it is unlikely that NPs traversed algal membranes which have a threshold of only 20 nm (Navarro et al., 2008). Thus, unless membranes were breached e.g. by reactive oxidative species (ROS) (Hartmann et al., 2010), NPs were likely localized on the external algal surface. Nevertheless, the effect of such localization on metal uptake by algae extended beyond extracellular uptake as will be shown in the following sections.

6.3.2 NP metal adsorption

The adsorption of Cu, Mn and U to silica and maghemite NPs was rapid and equilibrium was attained within 5 minutes (Figure 6.3). Slightly more Cu was adsorbed by maghemite than silica i.e. 65 versus 62% but Mn and U were more efficiently adsorbed by silica i.e. 65 versus 61% for Mn and 68 versus 65% for U. Rapid adsorption is characteristic of adsorption to NPs and has been reported previously for various NPs (Mureseanu et al., 2008; Hartmann et al., 2010; Grover et al., 2012; Yang, Li, et al., 2012) and is simply the result of a greater number of atoms and reactive surface features like kinks and edges located at the surface of particles (Brown et al., 1999). Kinetics data for all three ions to both NP types were fitted by the pseudo-second order model ($R^2 \geq 0.99$) (Table 6.2).

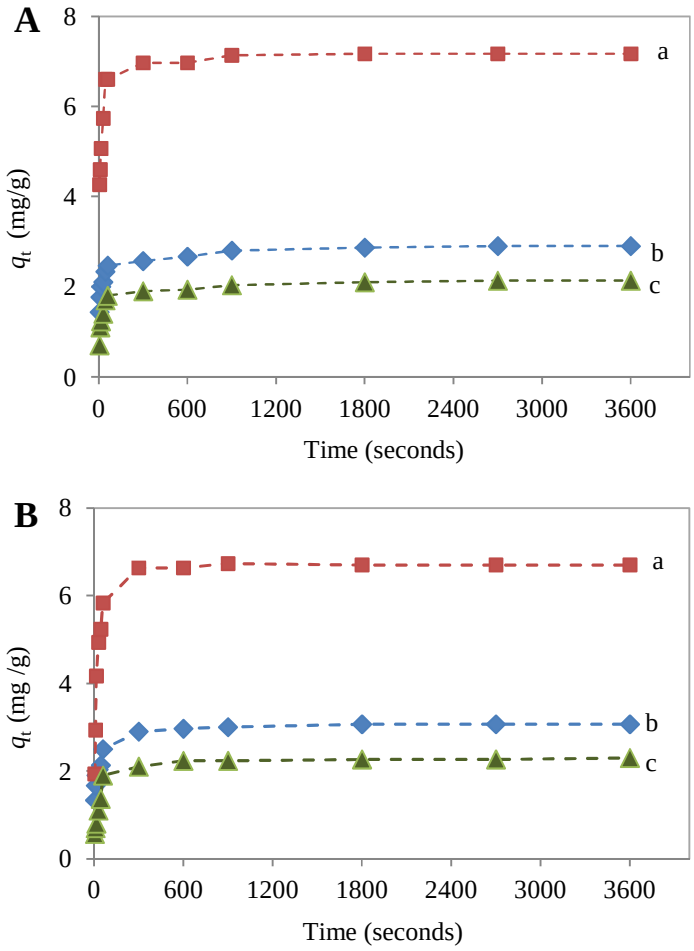

Figure 6.3: Adsorption kinetics of Mn (a), Cu (b) and U (c) to silica (A) and maghemite (B) nanoparticles at pH 6.5. Data are mean ± standard deviation (n = 2).

Isotherm studies showed that metal adsorption by NPs increased with initial concentrations and data were best fitted by the Freundlich model (Table 6.2). 1/n values for Cu and U were >1, implying that removal of these ions at the test pH was via both adsorption and precipitation (Foo & Hameed, 2010). This is explained by the fact that these two ions existed primarily in the insoluble forms i.e. CuO and $UO_2(OH)_2.H_2O$ (schoepite). On the other hand, Mn which existed in solution only as the hydrated ion was removed by adsorption alone. Based on K_F values, adsorption affinities of ions for both NP types were in the order Cu > U > Mn. In comparison with studies conducted at similar pH, silica's capacity for U binding was higher than that reported for tin oxide NPs at pH 6 (4.42 mg/g) by Nilchi et al. (2013) but maghemite's capacity for Cu was lower than that of maghemite nanotubes (111 mg/g), likely due to the higher surface area of the nanotubes (Roy & Bhattacharya, 2012).

Table 6.2: Kinetic and isotherm parameters obtained after fitting adsorption data to the pseudo-second order kinetics model and the Freundlich isotherm model.

NP type	Metal	Pseudo-second order model			Freundlich model		
		R^2	q_e (mg g^{-1})	k_2 (g mg^{-1} sec^{-1})	R^2	K_F (mg g^{-1}) (L $mg^{-1})^{1/n}$	$1/n$
Silica	Cu	1	2.91	0.018	0.99	8.74	1.77
	Mn	1	7.18	0.020	0.99	3.77	0.99
	U	0.99	2.24	0.064	0.99	7.98	1.26
Maghemite	Cu	0.99	3.08	0.022	0.99	10.13	1.62
	Mn	1	6.73	0.017	0.95	3.68	0.96
	U	0.99	2.15	0.032	0.99	9.91	1.18

6.3.3 Modification of algal metal removal by NPs

The influence of NPs on removal of Cu, Mn and U from solution by algal cells was assessed in terms of (i) total removed concentrations (ii) extracellular (bound to cell walls) and intracellular partitioning.

Effect on total metal removal

The algal cellular content of all three ions increased with initial concentrations of Cu, Mn and U. Further, metal content was significantly higher in the presence of NPs than in their absence ($p < 0.05$) (Figure 6.4). For instance, for 1.42, 3.30 and 0.99 mg/L solutions of Cu, Mn and U, respectively, algal metal content in the absence of NPs was 4.71, 9.98 and 3.64×10^{-9} µg/cell for Cu, Mn and U, respectively. However, these concentrations increased to 6.94, 14.2 and 4.11×10^{-9} µg/cell, in the presence of silica NPs and 7.40, 13.4 and 4.02×10^{-9} µg/cell in the presence of maghemite NPs. Notably metal uptake by algae in the presence of the two NPs followed trends suggested by isotherm calculations (Table 6.2) i.e. Cu uptake was higher with maghemite than silica, while Mn and U uptake were higher with silica than maghemite.

Metal removal in NP-algal systems was higher than in NP-only or algae-only systems due to the greater number of sorption sites in NP-algal systems (Dalai et al., 2014; Yang, Miao, et al., 2012; Yang, Li, et al., 2012). However, the observed metal removal efficiencies did not match expectations based on uptake in NP-only and algae-only systems even though such expectations would not be unreasonable considering their individual adsorption efficiencies. For example, while maghemite NPs and algae took up 65% and 56%, respectively, of Cu from 1.42 mg/L solutions, only 85% was taken up in NP-algae systems. Similarly, 65% of Mn was adsorbed by

silica NPs and 51% was taken up by algae from 3.30 mg/L solutions, but only 73% was removed by the NP-algal system.

A number of factors may be responsible for such outcomes, including the sequestration of NPs by the cell wall and exopolymeric substances (EPS) before metal adsorption to the NPs was complete. Reinhardt (2004), showed that these polysaccharide-rich anionic colloids (EPS) produced by algae in response to high metal concentrations also induce NP aggregation. Nevertheless, compared to algae-only systems, removal efficiencies in NP-algal systems were >20% higher for Cu and Mn and >10% higher for U. Such an increase represents a significant gain and makes a case for the combined use of NPs and algae. Successful operations will, however, hinge on determining the optimal NP concentration as concentrations that are too high can reduce efficiencies due to (i) diminished sorptive surface areas as a result of NP aggregation, (ii) algal membrane damage by ROS resulting in cell death, (iii) reduced nutrient uptake and impeded photosynthesis due to encapsulation of cells by particles (Hartmann et al., 2010). In addition, it is recommended that where treatment is done in batch systems, NPs are first introduced into metal solutions and given a chance to adsorb metal ions before algae are introduced into the treatment system. This would counter ‘premature’ sequestration of NPs by EPS and algal cell walls which we think curtailed NP and overall adsorption efficiency in this study.

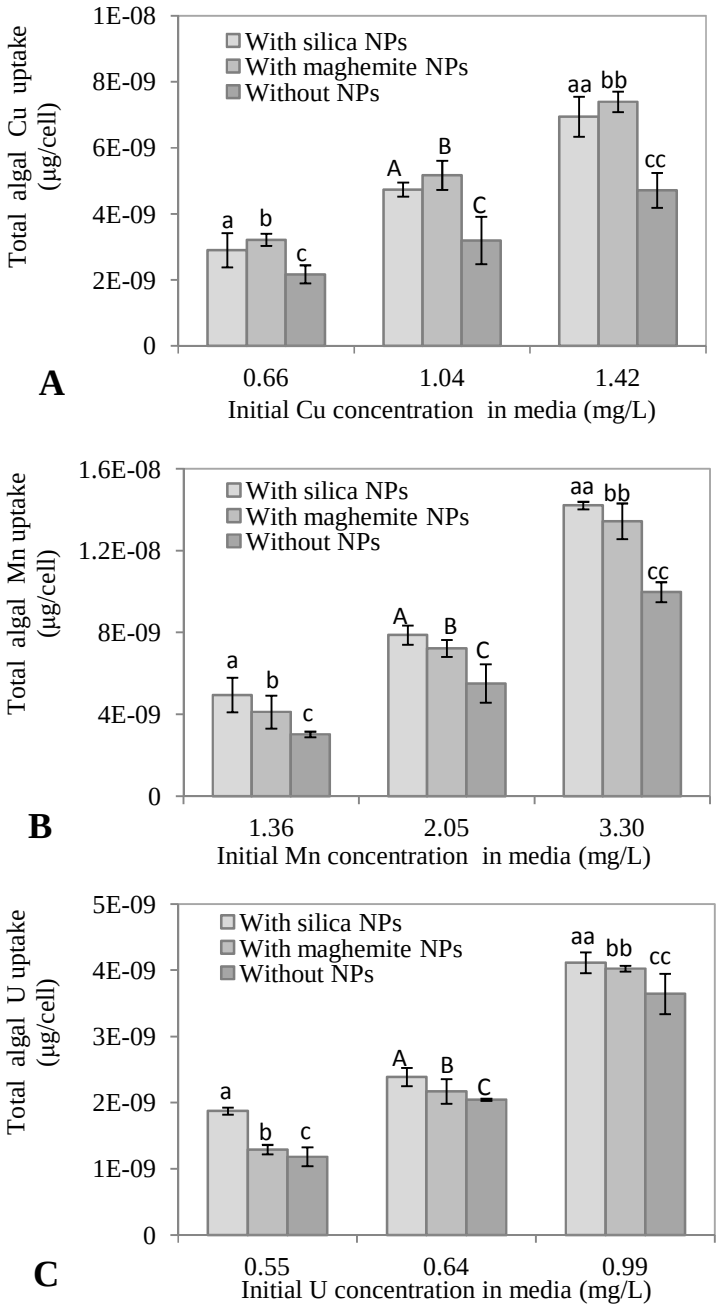

Figure 6.4: Removal of Cu (A), Mn (B) and U (C) by *Scenedesmus sp.* in the presence and absence of silica and maghemite NPs after 4 hours. Data are mean ± standard deviation (n = 3). Different letters above columns within a concentration indicate statistically significant differences (p <0.05) in the means of total algal metal content as a result of the different treatments.

Effect of NPs on algal metal partitioning

Assessments of the effects of NPs on algal-metal partitioning are essential because not only do they facilitate an understanding of modifications in algal-metal interactions brought about by NPs, they may also provide some information for the prediction of physiological responses. In this study, we observed that although both extracellular and intracellular concentrations increased with solution metal concentrations, the former were significantly higher in the presence of NPs (Figure 5). For example, at an initial U concentration of 0.99 mg/L, mean extracellular U concentrations were 3.79×10^{-9} ($\pm 7.39 \times 10^{-11}$) μg/cell in the presence of silica NPs, 3.62×10^{-9} ($\pm 4.75 \times 10^{-11}$) μg/cell in the presence of maghemite NPs, but only 3.17×10^{-9} ($\pm 2.66 \times 10^{-10}$) μg/cell in controls. Intracellular concentrations on the other hand, were not significantly different in the presence and absence of NPs, except for U (Figures 5 A(ii), B(ii), C(ii)). However, there were no correlations between extracellular and intracellular algal metal concentrations, except for a weak correlation in U ($r = 0.54$; $p = 0.004$).

Concerning the effects of individual NPs, extracellular Cu concentrations were significantly higher from solutions containing silica than maghemite NPs while the opposite was true for Mn and U. Taken together, these results suggest that (i) except for U, NPs did not affect intracellular metal uptake (ii) extracellular uptake followed trends seen in metal removal using NPs only and (iii) the additional metal uptake due to the presence of NPs was localized to external surfaces of algal cells and that, as a result, intracellular uptake was reduced.

With respect to metal removal by algae in the absence of NPs, our findings are consistent with other studies of green algae, including Cu and U uptake by *Chlorella sp.*(Franklin et al., 2000), Cu uptake by *Scenedesmus subspicatus* (Ma et al., 2003) as well as Zn and Cu accumulation by *Chlorella pyrenoidosa* and *Scenedesmus obliquus* (Zhou et al., 2012). The addition of NPs, however, changed uptake dynamics. In their presence, extracellular metal concentrations were higher and intracellular fractions lower, relative to controls. This can be explained both by the rapid metal complexing action of NPs which reduced the bioavailable fraction for intracellular uptake, and the fact that metal-laden NP agglomerates were too large to go through algal cell wall pores (5-20 nm; (Navarro et al., 2008). Thus, unless cell membranes are damaged e.g. by reactive oxidative species (Hartmann et al., 2010), or NPs were internalised by other mechanisms such as in *Ochromonas danica* where CdTe quantum dots were internalised by macropinocytosis (Wang et al., 2013), intracellular metal uptake by algae is likely to be reduced in the presence of NPs.

Concentrations in extracellular matrices, on the other hand, are likely to increase due to the localisation of metal-laden NPs on external surfaces of algae. We note, however, that these concentrations may have been overestimated because they were a combination of ions (i) adsorbed to algal surfaces and exudates, (ii) adsorbed to NPs, in turn bound to algal surfaces, and

(iii) adsorbed to unbound NPs but precipitated on algal surfaces over the duration of the experiment or during the first centrifugation cycle. Although this last fraction should not be included in extracellular concentrations, there was no way of eluting it separately from the actual algal-bound fraction. Nevertheless, this technicality is not relevant to remediation operations where higher total sequestration is the primary consideration.

NPs modify extracellular and intracellular metal uptake in various ways, the most obvious being the depletion of the bioavailable metal pool by adsorption. A few other mechanisms analogous to those facilitated by organic matter are also plausible. (i) The adsorption of NPs to algal cells, for instance, may increase the population of negatively charged sites on algal cell walls, and subsequently, cation uptake (Slaveykova et al., 2003). (ii) NPs may form ternary surface complexes linking metal ions to algal functional groups, thus increasing the adsorption of ions that have a low affinity for algal binding sites but a high affinity for NPs (Lamelas & Slaveykova, 2007). (iii) NPs may also disrupt algal membranes via oxidative action, allowing access for metal-laden NPs (Hartmann et al., 2010).

To our knowledge, silica and maghemite NP effects on metal uptake by algae have not been reported in peer-reviewed literature, and so the results presented here are novel. Furthermore, most studies to date have been conducted on multicellular organisms like daphnids and fishes e.g. Zhang et al. (2007), Tan et al. (2012), which have different modes of metal uptake than algae. Nonetheless, the findings reported here are comparable to those using the more commonly studied titania NPs (Hartmann et al., 2010; Yang, Miao, et al., 2012; Yang, Li, et al., 2012). Yang and co-workers, for example, reported reduced intracellular Cd^{2+} concentrations in *Chlamydomonas reinhardtii* in the presence of bare titania NPs (Yang, Li, et al., 2012) and polyacrylate-coated titania NPs (Yang, Miao, et al., 2012).

For the treatment of AMD-contaminated waters, factors including pH, metal concentrations and sulphates need also to be considered. Our previous studies have shown ferric, manganese and sulphate ions to increase metal adsorption to NPs (Etale et al. 2014). These ions may therefore also increase the efficiency of remediation systems combining NPs and algae. However, these factors (pH, metal ions) also affect the viability of algae. The pH of mine drainage for example (pH 2-5) may induce physiological stress and affect the metal uptake efficiency of algal cells, although some studies have shown aquatic species to be more tolerant to low pH than metal ions. Nonetheless, we surmise that the addition of NPs prior to introduction of algae may counter, to some extent, metal toxicity to algae.

Finally, concerning the correlation between intracellular and extracellular U concentrations and the significant effect of NPs on the former (Figure 6.5 C(ii)), the interpretation of this result

requires knowledge on the speciation of the test ions at the experimental pH. At pH 6.5, U existed largely as the uncharged $UO_2(OH)_2.H_2O$ species (schoepite), alongside a smaller fraction of charged polymeric species such as UO_2OH^+, $(UO_2)_3(OH)_5^+$ and $(UO_2)_2(OH)_3CO_3^-$ (Franklin et al., 2000). Unlike ions, uncharged species easily traverse biological membranes (Vigneault et al., 2000), hence the correlation between extracellular and intracellular U concentrations. This transport was, however, decreased in the presence of NPs because of the additional surface areas for schoepite deposition. The same rationale explains the significantly lower intracellular fraction with silica relative to maghemite i.e. the higher surface area of the former provided greater depositional surface areas for schoepite.

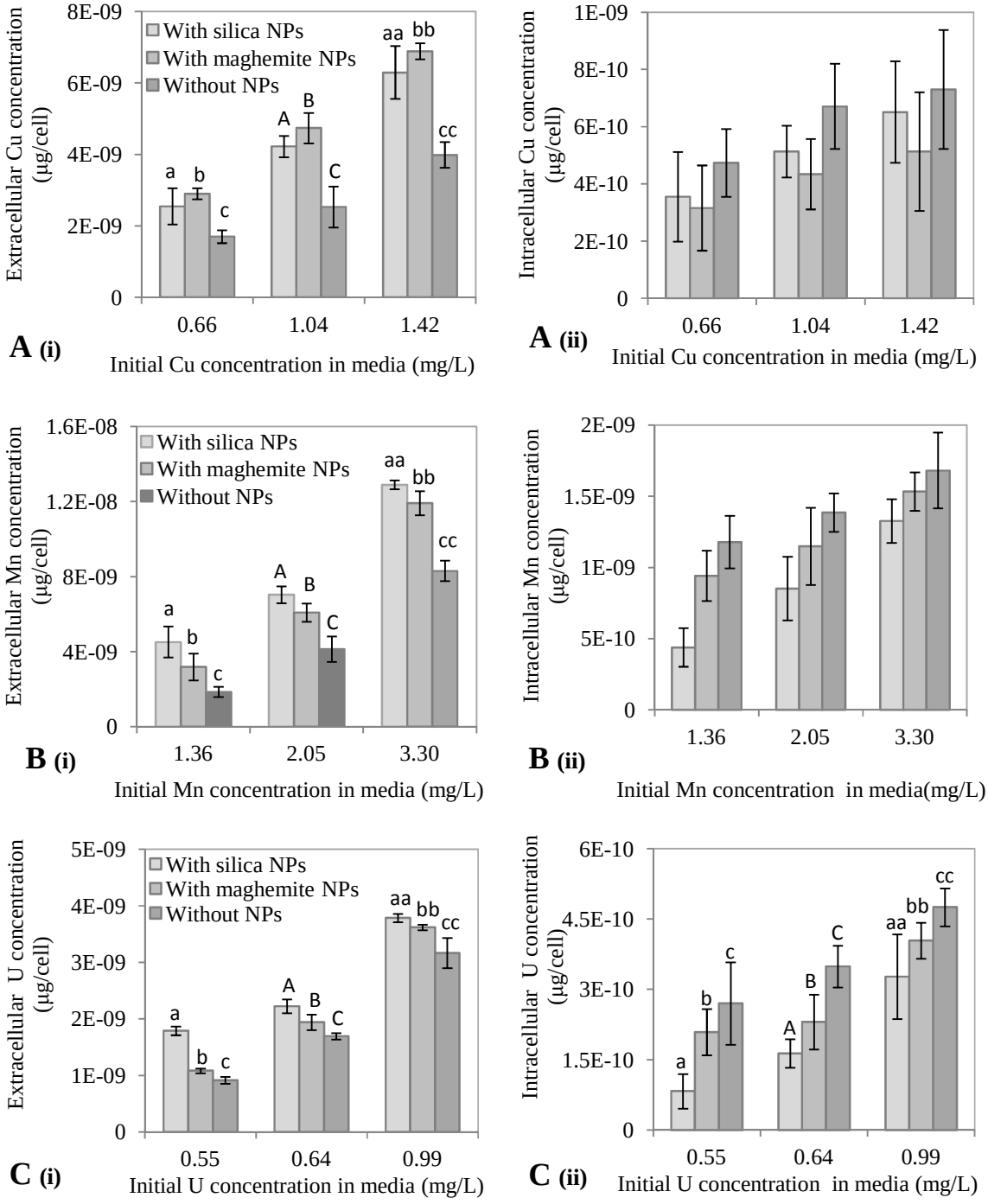

Figure 6.5: Extracellular (i) and intracellular (ii) concentrations of Cu (A), Mn (B) and U (C) of *Scenedesmus sp.* cells in the presence and absence of silica and maghemite NPs. Legends in (i) are for both graphs in the set and data are mean ± standard deviation (n = 3). Different letters above columns within a concentration indicate statistically significant differences (p <0.05) in the means of intracellular or extracellular metal concentrations of algal cells.

6.4 Conclusions

Although silica and maghemite NPs aggregated considerably in metal solution, the adsorption of Cu, Mn and U in NP-only treatments was a rapid and efficient process. For all three ions, uptake in NP-algal systems was higher than in NP-only or algae-only systems due to the higher sorptive surface area in the NP-algal system. Notably, these increases mirrored trends in NP-only experiments. Thus, Cu removal was higher with maghemite than silica NPs in both NP-alone and NP-algal systems, while Mn and U removal were greater with silica than maghemite.

NPs also influenced the partitioning of metal ions between extracellular and intracellular spaces of *Scenedesmus sp.* cells. Metal concentrations in extracellular matrices were higher in the presence of NPs while intracellular concentrations were lower. Although it was not the objective of this study to investigate the toxicity of metal ions to *Scenedesmus sp.*, qualified inferences may be made from these data as some studies have shown metal toxicity to be related to intracellular metal fractions in algae. If *Scenedesmus sp.* behaves in a similar manner, the inclusion of silica or maghemite NPs in phycoremediation systems using this alga will likely increase its viability by reducing its intracellular metal uptake. These data therefore suggest that a combination of NPs and algae for phycoremediation can improve the efficiency of operations both by increasing removed metal fractions and by protecting algal cells from metal toxicity. Further work is, however, needed to determine optimal parameters with respect to NP concentrations that (i) will not be inhibitory to algal growth and performance e.g. by inhibiting photosynthesis through encapsulation of algal cells, or (ii) result in aggregation sufficient to negate the effects of additional sorption surface areas. Information on whether NP-bound metal ions become bioavailable to the alga with time is also necessary.

6.5 Acknowledgements

Funding for this study was provided by the Global Change and Sustainability Research Institute of the University of Witwatersrand. We are indebted to Prof. Stuart Sym for the starter culture, access to his culturing facility and for helpful comments on the manuscript, to Mr. Sipho Mhlambi for identifying the algal specie and to Dr. Lisa Du Toit for help with light scattering measurements.

6.6 References

Brown, G.E., Henrich, V.E., Casey, W.H., Clark, D.L., Eggleston, C., Felmy, A., Goodman, D.W., Grätzel, M., Maciel, G., McCarthy, M.I., Nealson, K.H., Sverjensky, D.A., Toney, M.F. & Zachara, J.M. 1999. Metal oxide surfaces and their interactions with aqueous solutions and microbial organisms. *Chemical Reviews*, 99(1): 77–174.

Dalai, S., Pakrashi, S., Bhuvaneshwari, M., Iswarya, V., Chandrasekaran, N. & Mukherjee, A. 2014. Toxic effect of Cr(VI) in presence of n-TiO_2 and n-Al_2O_3 particles towards freshwater microalgae. *Aquatic Toxicology*, 146: 28–37.

Engates, K.E. & Shipley, H.J. 2011. Adsorption of Pb, Cd, Cu, Zn, and Ni to titanium dioxide nanoparticles: effect of particle size, solid concentration, and exhaustion. *Environmental Science and Pollution Research*, 18(3): 386–395.

Etale, A., Tutu, H. & Drake D.C, 2014. Application of maghemite nanoparticles as sorbents for the removal of Cu(II), Mn(II) and U(VI) ions from aqueous solution in acid mine drainage conditions. *Applied Water Science.* DOI: 10.1007/s13201-014-0217-3.

Foo, K.Y. & Hameed, B.H. 2010. Insights into the modeling of adsorption isotherm systems. *Chemical Engineering Journal*, 156: 2–10.

Franklin, N.M., Stauber, J.L., Markich, S.J. & Lim, R.P. 2000. pH-dependent toxicity of copper and uranium to a tropical freshwater alga (*Chlorella sp.*). *Aquatic Toxicology*, 48(2-3): 275–289.

Giammar, D.E., Maus, C.J., Xie, L. & Louis, S. 2007. Effects of particle size and crystalline phase on lead adsorption to titanium dioxide nanoparticles. *Environmental Engineering Science*, 24(1): 85–95.

Grover, V.A., Hu, J., Engates, K.E. & Shipley, H.J. 2012. Adsorption and desorption of bivalent metals to hematite nanoparticles. *Environmental Toxicology and Chemistry*, 433(1): 86–92.

Guzman, K.A.D., Finnegan, M.P. & Banfield, J.F. 2006. Influence of surface potential on aggregation and transport of titania nanoparticles. *Environmental Science & Technology*, 40(24): 7688–7693.

Hartmann, N.B., Von der Kammer, F., Hofmann, T., Baalousha, M., Ottofuelling, S. & Baun, A. 2010. Algal testing of titanium dioxide nanoparticles--testing considerations, inhibitory effects and modification of cadmium bioavailability. *Toxicology*, 269(2-3): 190–7.

Ho, Y.S. & Mckay, G. 2004. Sorption of copper(II) from aqueous solution by peat. *Water Air and Soil Pollution*, 158: 77–97.

Kim, Y., Kim, C. & Yi, J. 2004. Arsenic removal using mesoporous alumina prepared via a templating method. *Environmental Science and Technology*, 38(3): 924–931.

Knauer, K., Behra, R. & Sigg, L. 1997. Adsorption and uptake by the green alga *Scenedesmus subspicatus* (Chlorophyta). *Journal of Phycology*, 33: 596–601.

Knauer, K., Jabusch, T. & Sigg, L. 1999. Manganese uptake and Mn(II) oxidation by the alga *Scenedesmus subspicatus*. *Aquatic Sciences*, 61(1): 44–58.

Kosmulski, M. 2009. pH-dependent surface charging and points of zero charge. IV. Update and new approach. *Journal of Colloid and Interface Science*, 337: 439–448.

Kurniawan, T.A., Chan, G.Y.S., Lo, W.-H. & Babel, S. 2006. Physico–chemical treatment techniques for wastewater laden with heavy metals. *Chemical Engineering Journal*, 118(1-2): 83–98.

Lamelas, C. & Slaveykova, V.I. 2007. Comparison of Cd(II), Cu(II), and Pb(II) biouptake by green algae in the presence of humic acid. *Environmental Science and Technology*, 41(11): 4172–4178.

LeVan, M.D. & Vermeulen, T. 1981. Binary Langmuir and Freundlich isotherms for ideal adsorbed solutions. *Journal of Physical Chemistry*, 85(22): 3247–3250.

Ma, M., Zhu, W., Wang, Z. & Witkamp, G.J. 2003. Accumulation, assimilation and growth inhibition of copper on freshwater alga (*Scenedesmus subspicatus* 86.81 SAG) in the presence of EDTA and fulvic acid. *Aquatic Toxicology*, 63(3): 221–228.

Monteiro, C.M., Castro, P.M.L. & Malcata, F.X. 2008. Use of the microalga *Scenedesmus obliquus* to remove cadmium cations from aqueous solutions. *World Journal of Microbiology and Biotechnology*, 25(9): 1573–1578.

Mureseanu, M., Reiss, A., Stefanescu, I., David, E., Parvulescu, V., Renard, G. & Hulea, V. 2008. Modified SBA-15 mesoporous silica for heavy metal ions remediation. *Chemosphere*, 73(9): 1499–504.

Navarro, E., Baun, A., Behra, R., Hartmann, N.B., Filser, J., Miao, A.-J., Quigg, A., Santschi, P.H. & Sigg, L. 2008. Environmental behavior and ecotoxicity of engineered nanoparticles to algae, plants, and fungi. *Ecotoxicology*, 17(5): 372–86.

Nilchi, A., Dehaghan, T. & Garmarodi, S. 2013. Kinetics, isotherm and thermodynamics for uranium and thorium ions adsorption from aqueous solutions by crystalline tin oxide nanoparticles. *Desalination*, 321: 67–71.

Niyogi, D.K., Lewis, W.M. & McKnight, D.M. 2002. Effects of stress from mine drainage on diversity, biomass, and function of primary producers in mountain streams. *Ecosystems*, 5: 554–567.

Piccapietra, F., Sigg, L. & Behra, R. 2012. Colloidal stability of carbonate-coated silver nanoparticles in synthetic and natural freshwater. *Environmental Science & Technology*, 46(2): 818–25.

Rai, P.K. 2009. Heavy metal phytoremediation from aquatic ecosystems with special reference to macrophytes. *Critical Reviews in Environmental Science and Technology*, 39(9): 697–753.

Rajamani, S., Siripornadulsil, S., Falcao, V., Torres, M., Colepicolo, P. & Sayre, R. 2007. Phycoremediation of heavy metals using transgenic microalgae. In R. Leon, A. Galvan, & E. Fernandez, eds. *Transgenic microalgae as green cell factories*. Landes Bioscience and Springer Science + Business Media, pp. 99–109.

Reinhardt, A. 2004. *Contrasting roles of natural organic matter on colloidal stabilization and flocculation in freshwaters*. PhD thesis, University of Geneva.

Roy, A. & Bhattacharya, J. 2012. Removal of Cu(II), Zn(II) and Pb(II) from water using microwave-assisted synthesized maghemite nanotubes. *Chemical Engineering Journal*, 211-212: 493–500.

Slaveykova, V.I., Wilkinson, K.J., Ceresa, A. & Pretsch, E. 2003. Role of fulvic acid on lead bioaccumulation by *Chlorella kesslerii*. *Environmental Science & Technology*, 37(6): 1114–21.

Tan, C., Fan, W.-H. & Wang, W.-X. 2012. Role of titanium dioxide nanoparticles in the elevated uptake and retention of cadmium and zinc in *Daphnia magna*. *Environmental Science & Technology*, 46(1): 469–76.

Terry, P.A. & Stone, W. 2002. Biosorption of cadmium and copper contaminated water by *Scenedesmus abundans*. *Chemosphere*, 47(3): 249–55.

Tuutijärvi, T., Lu, J., Sillanpää, M. & Chen, G. 2009. As(V) adsorption on maghemite nanoparticles. *Journal of Hazardous Materials*, 166(2-3): 1415–1420.

Vayssieres, L. 2009. On the effect of nanoparticle size on water-oxide interfacial chemistry. *The Journal of Physical Chemistry C*, 113(12): 4733–4736.

Vigneault, B., Percot, A., Lafleur, M. & Campbell, P.G.C. 2000. Permeability changes in model and phytoplankton membranes in the presence of aquatic humic substances. *Environmental Science & Technology*, 34(18): 3907–3913.

Vogel, M., Günther, A., Rossberg, A., Li, B., Bernhard, G. & Raff, J. 2010. Biosorption of U(VI) by the green algae *Chlorella vulgaris* in dependence of pH value and cell activity. *Science of the Total Environment*, 409(2): 384–95.

Wang, Y., Miao, A.-J., Luo, J., Wei, Z.-B., Zhu, J.-J. & Yang, L.-Y. 2013. Bioaccumulation of CdTe quantum dots in a freshwater alga *Ochromonas danica*: A kinetics study. *Environmental Science & Technology*, 47: 10601–10610.

Wilkin, R.T. & McNeil, M.S. 2003. Laboratory evaluation of zero-valent iron to treat water impacted by acid mine drainage. *Chemosphere*, 53(7): 715–25.

Wilson Centre. 2014. Project on emerging nanotechnologies (2014). Consumer products inventory. http://www.nanotechproject.org/cpi 10 June 2014.

Yang, W.-W., Li, Y., Miao, A.-J. & Yang, L.-Y. 2012. Cd^{2+} toxicity as affected by bare TiO_2 nanoparticles and their bulk counterpart. *Ecotoxicology and Environmental Safety*, 85: 44–51.

Yang, W.-W., Miao, A.-J. & Yang, L.-Y. 2012. Cd^{2+} toxicity to a green alga *Chlamydomonas reinhardtii* as influenced by its adsorption on TiO_2 engineered nanoparticles. *PloS One*, 7(3): e32300.

Zhang, X., Luo, S., Yang, Q., Zhang, H. & Li, J. 1997. Accumulation of uranium at low concentration by the green alga *Scenedesmus obliquus* 34. *Journal of Applied Phycology*, 9: 65–71.

Zhang, X., Sun, H., Zhang, Z., Niu, Q., Chen, Y. & Crittenden, J.C. 2007. Enhanced bioaccumulation of cadmium in carp in the presence of titanium dioxide nanoparticles. *Chemosphere*, 67(1): 160–166.

Zhou, G.-J., Peng, F.-Q., Zhang, L.-J. & Ying, G.-G. 2012. Biosorption of zinc and copper from aqueous solutions by two freshwater green microalgae *Chlorella pyrenoidosa* and *Scenedesmus obliquus*. *Environmental Science and Pollution Research*, 19(7): 2918–2929.

Supplementary Information 1: Bold's Basal formula

250 mg $(NH_4)_2SO_4$ was dissolved in 800 mL of millipure water and the following solutions added:

10 mL of 25 g/L $NaNO_3$

10 mL of 7.5 g/L $MgSO_4 \cdot 7H_2O$

10 mL of 2.5 g/L NaCl

10 mL of 7.5 g/L $K_2HPO_4 \cdot 3H_2O$

10 mL of 17.5 g/L KH_2PO_4

10 mL of 2.5 g/L $CaCl_2 \cdot 2H_2O$

6 mL of a trace-element solution containing the following salts in 1 L

97 mg $FeCl_3 \cdot 6H_2O$

41 mg $MnCl_2 \cdot 4H_2O$

5 mg $ZnCl_2 \cdot 6H_2O$

2 mg $CoCl_2 \cdot 6H_2O$

4 mg $Na_2MoO_4 \cdot 2H_2O$

The solution was then made up to 1 L and autoclaved at 15 psi for 15 minutes.

Modified from: Pollio A, Cennamo P, Ciniglia C, De Stefano M, Pinto G & Huss VAR (2005) *Chlamydomonas pitschmanii* Ettl, A little known species from thermoacidic environments. Protist **156**: 257-302. (http://www.ccap.ac.uk/media/recipes/ABM.htm)

Supplementary Information 2: Powder X-ray diffractograms of maghemite (a) and silica (b) NPs

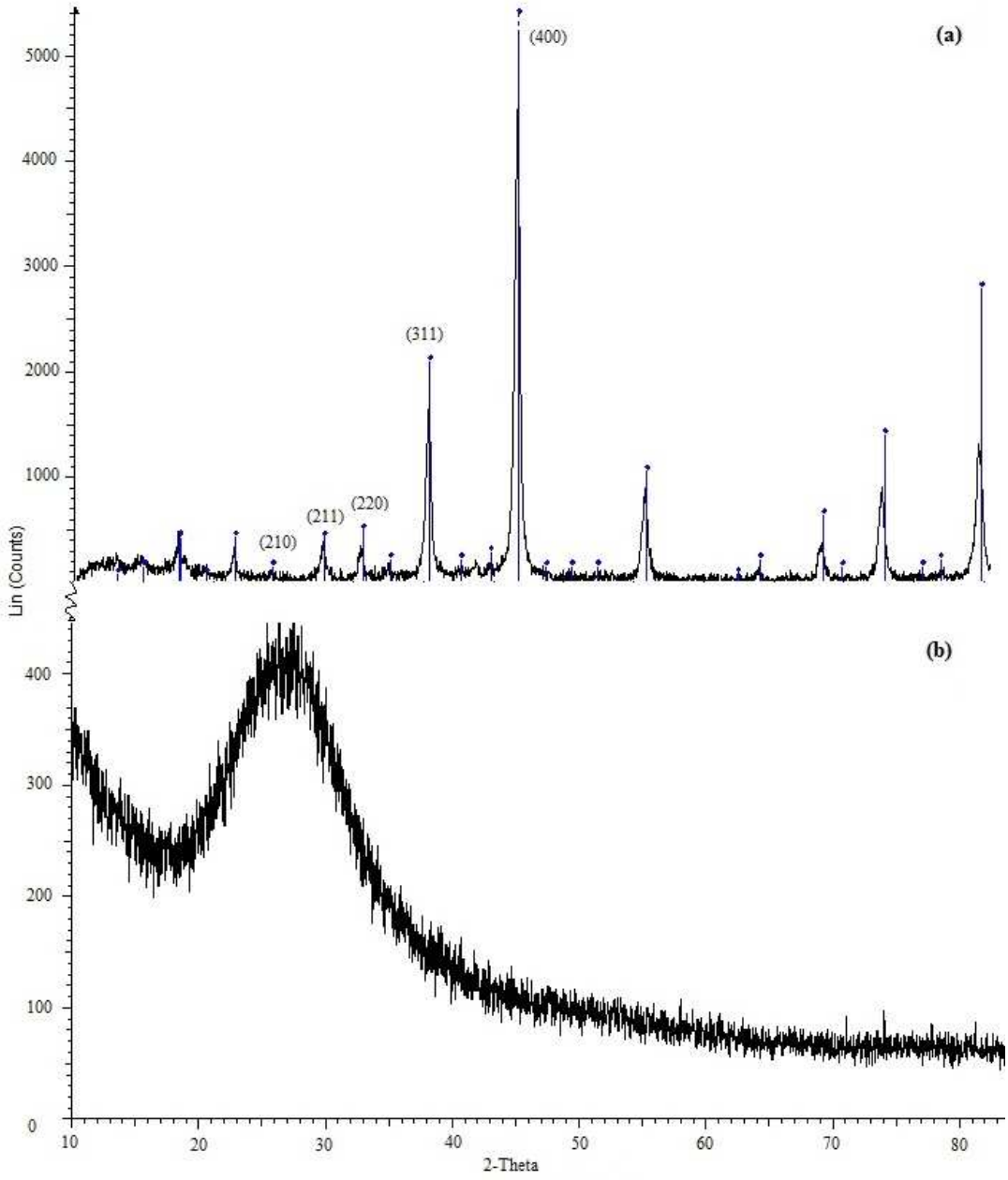

7 Summary and outlook

A number of findings have been made in this research with respect to (i) NP-metal interactions in AMD conditions (ii) the effect of functionalisation on NP adsorption efficiency and (iii) the effect of NPs on metal uptake by a freshwater green alga, *Scenedesmus sp.* This final chapter of the thesis presents a summary of these and suggestions for future research.

7.1 NP-metal interactions

The systematic approach applied in this study revealed that silica and maghemite NPs can indeed be applied for the adsorptive removal of Cu, Mn, Hg and U ions from AMD-contaminated water. The effects of investigated factors affecting metal adsorption by NPs at pH 3 can be summarized thus:

Contact time: All test ions were rapidly adsorbed from solution and equilibria were attained within 5 minutes. Kinetics data were best fitted by the pseudo-second-order model implying that adsorption of ions was via chemical bonding (chemisorption). The removal efficiencies of Cu, Mn, Hg and U at pH 3 were 52, 56, 56 and 49%, respectively with silica and 56, 52, 75 and 50%, respectively with maghemite NPs. Thus, except for manganese, adsorption efficiencies of test ions were higher with maghemite than with silica NPs.

Metal concentrations: Metal uptake increased with solution metal concentrations and isotherms were best described by the Freundlich model implying that sorption sites on both types of NPs were energetically heterogeneous. Based on 1/*n* values, the removal of Cu, Mn and Hg was by adsorption while that of U was by both adsorption and precipitation. K_F values showed that adsorption affinities were in the order Mn > Cu > Hg > U for silica NPs and Hg > Cu > Mn > U for maghemite NPs. Cu and Hg isotherms were also well fitted by the Temkin isotherm, implying that the heat of adsorption for the binding of these ions decreased linearly with increasing adsorption due to adsorbate interactions.

Ferric, manganese and sulphate ions: The presence of these ions increased adsorption by >10%. The adsorption of Hg from simulated wastewater, for example, increased from 75 to 83% and 87% in the presence of manganese and sulphate ions, respectively. Sulphate-induced adsorption increases likely involved lowering of the energy barrier for the approach of cations to the adsorbent surface through:

i. the formation of metal-sulphate complexes in solution;

ii. the binding of sulphate ions by the adsorbent thus altering its surface electrical properties; and
iii. the formation of ternary surface complexes.

In the case of manganese, increased adsorption was likely due to a greater drive for diffusion of ions to the adsorbent surface. However, Cu adsorption was inhibited in solutions with a >1 Mn:Cu ratio. We surmise that these ions bind to similar sites on both NP types resulting in competition where Mn concentrations are high.

pH: Adsorption was also investigated at pH 5, 7 and 9 in order to quantify process efficiency in pH-amended mine drainage. The removal of test ions was found to increase with pH e.g. removal of Cu by silica NPs increased from 52% at pH 3 to 94 and 99% at pH 7 and 9, respectively. Similarly, U removal increased from 49% at pH 3 to 77% at pH 7 and 9, and Hg removal was highest at pH 5 and 7 (68% with silica NPs and 82% with maghemite NPs). In contrast, Mn removal increased by only ~6% across the test pH range (55 - 61%). Increases in metal removal were attributed to hydrolysis at higher pH. Thus, Mn removal did not increase considerably due to the late hydrolysis of this ion (above pH 9).

These results imply that adsorption efficiencies of NPs can be increased by raising the pH of mine drainage. However, conventional methods of achieving this such as addition of lime lead to the production of large volumes of toxic sludge that present disposal challenges. Some options to circumvent this while still achieving satisfactory reductions in solution metal concentrations include:

i. increasing the concentration of NPs although this has to be balanced with the need to minimize agglomeration which reduces adsorption efficiency due to decreased access to sorption sites and NP cost considerations;
ii. successive absorption until acceptable concentrations are achieved; and
iii. surface modification of NPs by functional groups with high affinity for target metal ions e.g. functionalisation with amine groups to increase Cu uptake.

In these ways, the need for an additional pH-amendment step can be negated, the additional cost of lime eliminated and toxic waste volumes minimized.

NP concentrations: Unlike bulk adsorbents, increases in NP concentrations do not always increase metal uptake because of the tendency of NPs to agglomerate in order to reduce their high surface energies. Agglomeration, which increases with NP concentrations due to particle

proximity and higher incidence of collisions during Brownian motion, reduces accessibility of NP sorption sites thereby decreasing adsorption efficiencies. This phenomenon was seen in this study, with metal uptake increasing when NP concentrations increased from 3 to 5 mg L^{-1} but decreasing when the NP concentration was decreased further to 10 mg L^{-1}. This means that optimal NP concentrations have to be established under specific conditions, as higher concentrations may not necessarily result in greater process efficiencies.

Further research should also examine the effect of NP sizes on adsorption efficiencies. Although smaller NPs offer larger surface areas, they also tend to aggregate more than larger particles and metal removal efficiencies may well be greater with slightly larger NPs. Indeed, some studies have shown that larger particles showed greater adsorption efficiencies when adsorption results were surface area normalised (Giammar et al., 2007).

Nonetheless, it must be borne in mind that a high sorptive surface area is not the sole determinant of adsorption efficiency as was demonstrated by the comparative study with Hg i.e. Hg removal efficiency was 75% with maghemite and 56% with silica NPs, despite the latter having a surface area ~15 times greater. Other material properties therefore determine the efficiency of adsorbents, hence the need for detailed investigations before use.

The effect of temperature: Metal removal by NPs increased with temperature. Mn adsorption to silica, for instance, increased from 54 to 61% as temperatures increased from 293 - 310 K, indicating that adsorption was an endothermic process. $\Delta G°$ values were negative while those of $\Delta H°$ and $\Delta S°$ were positive, implying that adsorption was spontaneous, endothermic and thermodynamically favourable.

Application to field samples: The adsorption of test ions from AMD-contaminated surface and groundwater samples followed trends in simulated waste water e.g. more Hg was adsorbed by maghemite than silica. However, removal did not attain efficiencies recorded in simulated wastewater, likely due to competition from other ions in AMD. Competition between Cu and Mn was also stronger in field samples due to the much higher Cu:Mn ratios, particularly in surface water. Nevertheless, the fact that Mn can be removed is significant as Mn removal from wastewaters is generally harder to accomplish due to the late hydrolysis of the ion i.e. while Cu can be removed by raising the pH of solutions to above 5, Mn hydrolysis only happens above pH 9, necessitating the use of copious amounts of lime and creating large sludge volumes. The use of NPs therefore circumvents one of the major challenges associated with the more commonly used chemical precipitation approach.

It is clear from this work that optimization of the adsorption process hinges on NP concentrations and solution pH. Additional research is therefore required to determine optimal NP concentrations and finding suitable ways of increasing solution pH. As NPs are still relatively expensive adsorbents, research to quantify their re-use would be valuable for the scale-up of this remediation option.

On the other hand, concerns over the ecotoxicological effects of NPs in aquatic environments necessitates their immobilisation e.g. in permeable reactive barriers (PRBs). Furthermore, PRBs also facilitate the use of NPs for large-scale clean-up operations and their re-use (after elution of adsorbed ions) hence cost-effectiveness. The design and appraisal of PRBs is therefore one way through which the use nanotechnologies for AMD treatment may be advanced. At R37/g, maghemite NPs were twice as expensive as those of silica (R18/g). Based on their adsorption efficiencies for the test metals, silica NPs are cost-effective for the removal of Cu, Mn and U where differences in removal efficiencies for the two NP types were only 3-4%. For Hg, however, the ~20% higher removal efficiency with maghemite than silica NPs makes the former a more cost effective option for the removal of this ion.

NPs as transport vectors for metals in the environment: The findings of this study also reveal the potential of silica and maghemite, as naturally-occurring adsorbents in contaminated environments, to remove metals from water. As such, the findings provide some insight into the processes involving partitioning of metals between the liquid and solid phases of contaminated systems. Consequently, besides macro particles like clay and sand that are more widely reported in literature, NPs are also important in the removal, transport and subsequent fate of metal ions in contaminated systems.

7.2 The effect of NP functionalisation on adsorption efficiency

The effect of functionalisation on adsorption efficiency of silica NPs was quantified by the adsorption of Cu using amine-functionalised silica-carbon (NH-SC) hybrid NPs. This adsorbent was prepared by grafting hexamine onto a carbon layer deposited on silica NP surfaces by reaction with 2,7-dihydroxynaphthalene followed by carbonisation at 400°C. Cu removal by this adsorbent was only 52%, similar to the efficiency of bare / unfunctionalised silica NPs, despite the presence of high affinity amine groups in the former. This paradox was solved by the results of N_2 sorption experiments which revealed that sorption surface areas of NH-SC NPs were greatly reduced as a result of the functionalisation process. These functionalised NPs had a surface area ~12 times less than that of unfunctionalised NPs likely due to pore blockage by carbon and hexamine molecules. Nevertheless, this adsorbent shows promise based on the fact that it was

able to remove the same concentration of Cu with 12 times less surface area. Further research should therefore look into ways of functionalisation that result in minimal surface area reduction.

7.3 The effect of NPs on metal uptake by *Scenedesmus sp.*

The effect of NPs on metal uptake by *Scenedesmus sp.* was examined with the hypothesis that removal would be greater in NP-algae treatments relative to NP-only or algae-only treatments due to the higher surface areas available in that (NP-algae) treatment. This hypothesis was confirmed by results which showed metal uptake in NP-algal systems to be 12-27% higher than in NP-only or algae-only systems. Notably, these increases traced trends in NP-only experiments e.g. Cu removal was higher with maghemite than silica NPs in both NP-alone and NP-algal systems, while Mn and U removal were greater with silica than maghemite.

NPs also influenced the partitioning of metal ions between extracellular (bound to cell wall) and intracellular spaces of *Scenedesmus sp.* cells. Relative to controls (no NPs), extracellular metal concentrations were higher and intracellular concentrations lower in treatments containing NPs. This was likely because although NPs adsorbed metal ions, they formed large aggregates that could not traverse cellular membranes and were thus localised on the external surfaces of algal cells. The rapid NP adsorption also reduced the bioavailable metal fraction, hence the decrease in intracellular fractions.

The approach employed here i.e. combining NPs and algae to enhance remediation efficiency, has not been described previously in peer-reviewed literature. As such, much remains unknown and work is required to address a number of questions e.g. regarding the longer-time bioavailability and toxicity of NP-bound metals, optimal NP concentrations, as well as operational factors such as removal/harvesting of NPs and algae at the end of adsorption cycles. This latter concern may also be addressed by PRBs through the immobilisation of algae and NPs on polymers.

In conclusion, the use of NPs for the remediation of AMD-contaminated water and for the enhancement of phycoremediation shows promise. It is expected that new production techniques and market competition will moderate the cost of NPs and allow for the adoption of nanotechnology in AMD treatment.

7.4 Reference

Giammar, D.E., Maus, C.J., Xie, L. & Louis, S. 2007. Effects of particle size and crystalline phase on lead adsorption to titanium dioxide nanoparticles. *Environmental Engineering Science*, 24(1): 85–95.

8 Appendix

Scientific meetings at which work detailed in this thesis have been presented:

A. Etale, D. C. Drake & H. Tutu (2013). The use of nanoparticles for remediation of mine drainage contaminated water. *9th IWA International Conference on Water Re-use*, 27-31 October 2013, **Windhoek, Namibia. [Poster**].

A. Etale, D. C. Drake & H. Tutu (2013). Metal contamination of aquatic systems: Might nanoparticles be complicit? *International Conference on Challenges in Aquatic Sciences*, 15-21 March 2013, **Keelung, Taiwan. [Oral].**

A. Etale, D. C. Drake & H. Tutu (2012). Sequestration of copper (II) ions by silica nanoparticles. *Assaf Young Scientists' Conference*, 16-18 October 2012, **Pretoria, South Africa. [Poster].**